2011

RNA in Forensic Science: Novel Techniques for Biological Evidence

Stephanie T. Young
West Virginia University

RNA in Forensic Science: Novel Techniques for Biological Evidence

Stephanie T. Young

Dissertation submitted to the
Eberly College of Arts and Sciences
at West Virginia University
in partial fulfillment of the requirements
for the degree of

Doctor of Philosophy
in
Biology

Clifton P. Bishop, Ph.D., Chair
Stephen P. DiFazio, Ph.D.
Jed H. Doelling, Ph.D.
David A. Ray, Ph.D.
Jeffrey D. Wells, Ph.D.

Department of Biology

Morgantown, WV
2011

Keywords: Forensic Science, RNA, Postmortem Interval, Reverse Transcription Real-Time PCR, Tissue Identification, Molecular Beacons

ABSTRACT

RNA in Forensic Science: Novel Techniques for Biological Evidence

Stephanie T. Young

The techniques currently utilized for collecting biological evidence at the scenes of violent crimes such as murder, rape, and kidnapping are employed simply to preserve evidence for future DNA analysis. Although DNA is extremely useful in forensic casework, biological samples possess yet another valuable molecule, RNA. The use of RNA in forensic analysis of samples is currently on the rise. In the past, RNA was thought to degrade much too quickly to be of any benefit to the forensic community. The work presented in this dissertation seeks to demonstrate otherwise. While true that RNA is not as stable as DNA, its rate of degradation in *ex vivo* specimens has been found to be a function of the size and species of the molecule, as well as predictable in certain biological fluids and tissues. The first objective of this research was to determine if the size-dependent, predictable decay of RNAs could be utilized as an indicator of postmortem interval (PMI), or time since death. A method to efficiently isolate and correctly quantify RNA from tooth pulp was established. By quantifying the remaining molecules of a large versus a small section of β-actin mRNA from aging tooth pulp from deceased pigs, and the postmortem alterations in pulp color, a relationship between these factors and PMI was established. Previous studies had indicated that rate of RNA decay may be a temperature-dependent process. It was determined that the degradation rate of RNA could be better described by the accumulation of temperature to which pigs were exposed, rather than time in days. This analysis led to a simple mathematical equation into which measurable variables can be placed to find the number of accumulated degree days (ADD) that have passed since death with 95% confidence. The resulting method can provide reliable estimates of PMI that surpass the amount of time following death in which current estimators, primarily forensic entomology, can reliably produce an estimate of time since death. We have also developed a novel technique to determine the body fluid type of biological stains found at the scene of violent crimes. This technique makes use of fluorescently labeled probes known as molecular beacons (MBs) to identify tissue-specific RNAs in a confirmatory assay. Importantly, it has the potential to be made portable to a crime scene and does not involve the use of PCR. It was successfully demonstrated that the MBs designed for experimentation release a signal only in the presence of RNA extracted from one of three tissues: blood, saliva, or semen. By determining if a potential piece of evidence should be collected or left behind at the scene as not pertinent to the crime at hand, this technique has the potential to reduce DNA backlog among crime laboratories.

ACKNOWLEDGEMENTS

This dissertation would not have been possible if it were not for my advisor, Clif Bishop. His guidance, encouragement, and enthusiasm have made the projects held within this dissertation a joy on which to work. Clif cultivated a sense of family in our laboratory that further fostered collaboration, creativity, and independent thought; an atmosphere that greatly enhanced my graduate school experience. Thank you for your time, your patience, and your stories shared.

To my committee, Steve DiFazio, Jed Doelling, David Ray, and Jeff Wells, I want to express my deepest gratitude for your hours and ideas shared. Your advice and support has allowed me to strengthen my research skills, as well challenged the way I think about scientific problems. From providing insightful suggestions and papers, to supplying the field site on which my preliminary studies were performed, thank you for taking the time to help me obtain my goals and further my career.

Over the years, I have had the opportunity to work with many wonderful graduate students, inquisitive undergraduate researchers, and one awesome technician. From trouble-shooting during lab meetings to their friendship outside of the department, I would like to thank my lab mates: Kristen, Bia, Tiffany, Swati, and Ashley. Cooperation and a genuine sense of encouragement always ran high in the Bishop lab. For assistance with field work, I am immensely grateful to all of our undergraduate researches for their time spent and interest in my work. As for our tech, Regina, I will always appreciate the time and energy that you put forth to assist with my projects. Your experience and advice is as invaluable as your friendship.

I would like to share my appreciation for many with whom I work within the Biology Department at West Virginia University. To the wonderful staff of our department, Mickey, Diana, Judy, Pat, Wendy, and Katrina, know that everything that you have done for me is much appreciated. I would also like to acknowledge the faculty of our department, who at one time or another, were all unofficial committee members, especially Dr. Letha Sooter. I thank you all for your kindness. I would like to thank all of the graduate students as well, a select few who without our daily shenanigans I think I would have lost my sanity: Ezgi, Marissa, Mohna, Christine, Anne, Michelle, Sara, John, and Ryan.

Finally, I would like to thank my family and friends outside the department for their support and constant encouragement, especially my parents. Your love and kind words have made this difficult process much easier. It has been a long journey, but I never felt as if I were in this alone. There are no words strong enough to describe how much I appreciate you!

TABLE OF CONTENTS

LIST OF TABLES

LIST OF FIGURES

ABBREVIATIONS

ADD	Accumulated Degree Days
ADH	Accumulated Degree Hours
ANOVA	Analysis of Variance
cDNA	Complementary DNA
Ct	Cycle Threshold
DMPO	5,5-dimethyl-l-pryrroline-N-oxide
EPR	Electron Paramagentic Resonance
GAPDH	Glyceraldehyde-3-Phosphate Dehydrogenase
Tm	Melting Temperature
mRNA	Messenger RNA
mtDNA	Mitochondrial DNA
MB	Molecular Beacon
NC	Negative Control
NIJ	National Institute of Justice
NMD	Nonsense Mediated Decay
PBS	Phosphate Buffered Saline
PMI	Postmortem Interval
QD	Quantum Dot
QDMB	Quantum Dot-modified Molecular Beacon
qPCR	Quantitative Real-Time PCR
qRT-PCR	Quantitative Reverse Transcription Real-Time PCR
RFU	Relative Fluorescence Unit
ROS	Reactive Oxygen Species
RNA	Ribonucleic Acid
rRNA	Ribosomal RNA

Chapter One: Introduction

DNA versus RNA

It is the stability of DNA that leads to its usefulness in forensic casework. DNA can be extracted from evidentiary tissue samples and provide useful DNA profiles for extended periods of time. Sir Alec Jeffreys provided evidence of this when nuclear DNA was extracted from 13 year-old femur bone that provided an STR profile strong enough to identify Joseph Mengele, an Auschwitz physician known as the "Angel of Death" [1]. More recently, nuclear DNA from 38,000 year-old Neanderthal fossils was extracted and sequenced using pyrosequencing to determine evolutionary relatedness to modern *Homo sapiens* [2, 3]. Mitochondrial DNA (mtDNA) has shown a tendency to persist longer than nuclear DNA. Large fragments of mtDNA have been extracted and sequenced from 5,500 year-old human bone [4] and from ~47,000 year-old woolly mammoth tissue [5].

To date biological samples found at the scene of a crime that may have been left days, weeks, or months prior to sample collection, a molecule less stable than DNA would be required. RNA, a single-stranded nucleic acid molecule, possess this characteristic. In addition to its reduced stability relative to DNA, RNA will also be present in greater abundance within a sample than DNA. For most genes, each nucleated cell will contain two copies of the DNA encoding for the gene, whereas 100s to 1,000s of copies of the same RNA molecule for the gene may be present. Because RNA is made from a DNA template, one can exploit species-specific polymorphisms to create species-specific assays, thus eliminating common sources of contaminating nucleic acids in the environment. RNA is also a strong candidate for forensic study due to improved methods of co-isolation of both DNA and RNA from the same sample material [6, 7]. One biological sample presented to a crime laboratory as evidence can undergo one isolation procedure, yet yield both DNA and RNA for separate analyses.

RNA Degradation

The two forms of RNA of interest for our experiments are messenger RNA (mRNA) and ribosomal RNA (rRNA). In humans, programmed *in vivo* degradation of many mRNAs is accomplished through deadenylation (or removal of the poly-A tail) followed by 3' to 5' transcript degradation, through nonsense mediated decay (NMD), or through RNA interference (RNAi). Although no direct degradation pathway has yet been identified in humans, rRNA seems to have high stability as compared to mRNA. This is most likely due to the molecule's nucleic acid structure being protected by associated proteins.

Even though the degradation of RNA molecules *in vivo* has been extensively studied, the degradation of RNAs found in biological samples *ex vivo* remains a mystery. A controversy remains as to if 3' to 5' or 5' to 3' degradation occurs in dried samples at all. In the case of bloodstains, it is thought that once the samples are completely dry, enzymatic activity of RNases should cease. Through past experimentation, we see that it is more likely that degradation within these stains have no common directionality, but seemingly occurs in a random manner [S. Anderson, personal communication]. The degradation itself, in actuality, may not be random. Rather, a particular base pair, or combination of base pairs, may be more susceptible to degradation than others. The probability that such nucleotide combinations are present would increase as the length of the molecule under observation increases. Thus, the likelihood of a break is expected to be a function of the length of the portion of RNA studied.

We believe that free radicals may be involved in the degradation of RNA within dried biological samples. Free radical accumulation can occur without the presence of water and has been known to cause damage to nucleic acids [8, 9]. Due to the high oxygen content of blood, one group of free radicals, reactive oxygen species (ROS), are known to be constantly produced in red blood cells [10]. [See Appendix A for preliminary data on free radical accumulation within bloodstains.]

Current Use of RNA in Forensic Science

Several groups have begun experimentation leading to the use of RNA in the identification of body fluids [11-19], in the determination of time since deposition of biological materials [20-22], in determination of the age of an individual whom has left behind a biological stain [23], and in PMI estimation [24-25]. Many of these studies have analyzed the presence/absence of particular species of RNA or have attempted to measure degradation of particular RNAs to find predictable patterns.

Postmortem Interval

Previous work in our laboratory has focused on estimating the age of a bloodstain that has been left behind at the scene of a violent crime [21, 22]. We are currently interested in determining if the same techniques that measure RNA degradation within *ex vivo* bloodstains can be employed to measure degradation of RNA contained within postmortem bodily tissues to determine postmortem interval (PMI), or time since death.

Described in further detail below, currently accepted indicators of PMI include visual identification of the stages of tissue decomposition due to cell autolysis and putrification, temperature of the body at the time the body is recovered, the presence/absence of the

stiffening of the limbs, biochemical changes within certain bodily remains, and the presence/absence of forensically significant insect species on or around the body.

Decomposition can be greatly affected by temperature and other environmental factors such as exposure to rainfall, humidity or lack thereof, composition of the surface on which the body is laid or buried, and presence of scavengers [26]. Although defined stages of death and decomposition do exist, there are many factors that must be taken into consideration when using this visual method of PMI determination, therefore exact time of death is difficult to predict. Scientific investigations continue to reveal factors that may influence the rate of decomposition. Rodriguez and Bass noted that burial underground can slow the decomposition process in comparison to those bodies left upon the surface or in direct sunlight [27]. This subjective estimation of tissue decomposition relies on personal experience, and due to the fact that environmental conditions can vary drastically, continued research is needed to make this indicator of PMI more accurate.

After death, body temperature will slowly begin to acclimate to ambient temperature. This process, known as algor mortis, can be used alone to determine PMI [28], but its measurement is usually combined with the presence/absence of body stiffening, or rigor mortis. These two indicators can accurately estimate PMI for a period of 2-48 hours after death depending on ambient weather conditions [29].

Biochemical means of estimating PMI have also been studied in the past. Most techniques look for biomarkers, or recognizable byproducts of cell autolysis and putrification, such as oxalic acid, that change in concentration within human organs after death [30]. The increase of potassium ions within the inner eye fluid was first established in 1963 as a potential indicator of time since death. Sturner declared that this method was an accurate indicator of PMI up to 104 hours after death ±9.5 hours [31]. Over the years this claim has been disputed and many groups have worked to strengthen the discriminatory power of this indicator either through increased experimentation or attempts to provide better statistical analysis of previous data [32-36].

Finally, forensic entomology as an estimator of PMI is held in high esteem among the forensic community. This technique exploits the temperature-dependant life cycles of insects attracted to a body after death. Although there are several forensically significant insect orders, the carrion flies of order Diptera are most often used for PMI estimation due to their quick colonization of a corpse [37]. With a combination of information regarding environmental conditions and life stage of species present, a carefully calculated estimation of PMI can be given. Again, this method also has its limitations. Diptera remain with a decomposing body until the point of skeletonization (no flesh is found) [38]. This can take

varied amounts of time depending on several factors including temperature, weather conditions such as rain, amount of sunlight, and surface upon which the body is found.

Real-Time Reverse Transcription PCR

The method that we propose to estimate the age of a biological sample is conceptually similar to carbon-14 dating. In radiocarbon dating, an estimation of age is determined after considering the relative ratio of radioactive carbon (^{14}C) to non-radioactive carbon (^{12}C). As an organism lives and grows, it incorporates ^{14}C into its system at a fixed ratio of ^{14}C to ^{12}C until it reaches a concentration that is similar to atmospheric conditions. When the organism dies, the unstable ^{14}C begins to decay while ^{12}C remains stable. A comparison of these two forms of carbon (unstable versus stable) can be used to estimate the time frame in which the specimen lived due to known amounts of ^{14}C within the atmosphere over historical time [39]. With our method, estimation of age can be considered after a comparison of the degradation of two differently sized portions of RNA, one being more labile than the other. At the time of death, two differently sized, non-overlapping, regions of the same RNA molecule, one large (301 bp) and one small (71 bp), should be present in approximately equal amounts. Based merely on size, the larger region of the molecule will be more susceptible to degradative environmental forces and will therefore decay more quickly than will the smaller region of the same molecule (**Figure 1**). If we can compare the rates of degradation of these regions over time, a large (unstable) portion compared to a small (stable) portion, we can make an estimate *ex vivo* age.

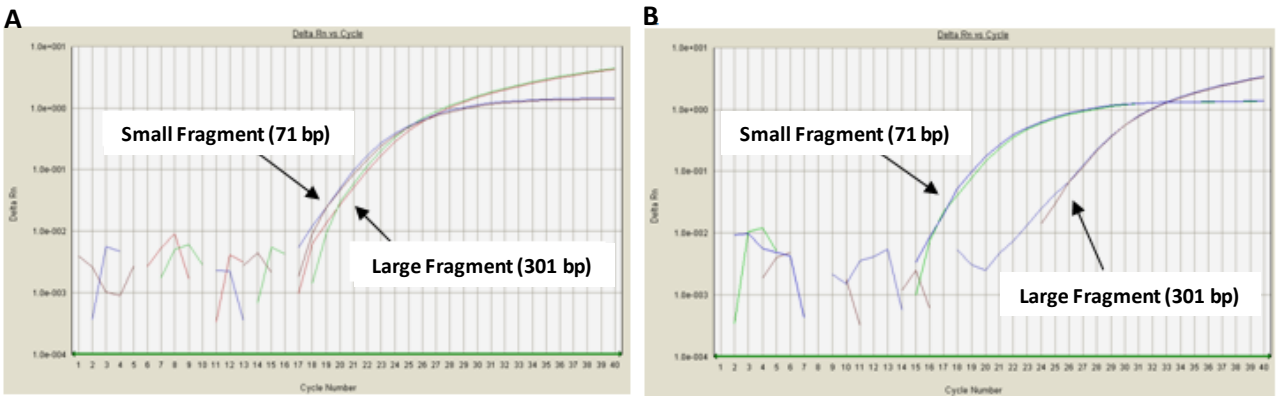

Figure 1: Raw data of Real-Time PCR on cDNA isolated from pig tooth pulp. The remaining RNA molecules of a small (71 bp) region of β-actin mRNA is compared to a separate, large (301 bp) region of the same mRNA at (A) day 0 and at (B) day 56. The greater the amount of starting material present, the fewer the number of cycles required to reach exponential phase. Therefore, the above illustrates a greater loss of the large mRNA region by day 56 as compared to fresh samples.

To obtain a relative measure of the change in unstable to stable RNA, we have employed multiplexed quantitative Real-Time Reverse Transcription Polymerase Chain Reaction (qRT-PCR). After extraction of total RNA using a TRI-Reagent-based method, the RNA is then reverse transcribed to double-stranded complimentary DNA (cDNA). The cDNA is then used as template for a Real-Time PCR reaction. Real-Time PCR is much like traditional PCR in the way that it is designed to exponentially amplify selected sections of DNA, but is different in the way that Real-Time PCR gives visual documentation of how much product is actually being produced through each amplification cycle. This is accomplished through the use of fluorescently labeled probes that release a light signal as each new strand is created. The signal is captured and recorded by the machine. By incorporating Real-Time probes labeled with fluorescent reporter molecules of different wavelengths, both the small and large portions of the RNA molecule can be viewed in the same reaction tube (i.e., a multiplexed assay).

qRT-PCR results for a given sample are recorded in the form of a cycle threshold (Ct) value. As amplification proceeds, three stages are seen: lag phase, exponential amplification phase, and finally a stationary phase. The Ct value designates the number of cycles where amplification, and therefore amount of fluorescence, exceeds initial background noise seen in lag phase and is indicative of the concentration of template cDNA used in the reaction. Once Ct values for both the large and the small RNA regions have been determined, the two are compared by using the equation: $2^{-\Delta Ct}$ [40]. This allows for a direct comparison between the

two differently sized regions while taking into account the logarithmic nature of PCR amplification.

Biological Stain Identification

One universal presumptive test can be used to discover the presence of the three most commonly found biological stains at the scene of a crime. Blood, semen, and saliva can all be presumptively identified under an alternative light source [41-43]. After a stain has been identified using presumptive testing, a battery of confirmatory tests can be run to determine the tissue type for the stain. Blood is easily distinguishable from the two others based on morphological differences, but multiple confirmatory tests exist to be sure that a darkened, red stain is actually blood. Confirmatory tests for blood include identification of blood cells under a microscope [41], crystal tests such as the Teichman and Takayama tests [42, 44], and ultraviolet absorption tests [43]. Semen is usually confirmed by either the presence of Christmas Tree stained sperm cells in the sample [45] or by the presence of prostate-specific antigen (PSA) which will provide a positive result even with aspermatic males [46]. At present, there are no reliable confirmatory tests available for the identification of saliva. Presumptive tests for saliva seek to determine the presence of specific enzymes, such as amylase, but cannot be made conclusive due to the presence of amylase in other body secretions such as breast milk and sweat [46].

Novel techniques for more sensitive confirmatory tests for biological stains have been described in the literature, many of which are based on tissue-specific mRNAs [11-13, 17, 19] or micro-RNAs [18]. Although the use of RNA in these specific techniques is promising, they utilize techniques such as PCR which must occur within a full laboratory setting.

To determine the type of body fluid in a piece of biological evidence, we propose the use of alternatively-spliced RNAs that are blood-, saliva-, and semen-specific, as well as the use of fluorescently-labeled probes known as Molecular Beacons (MBs). Although we are not the first to use RNA for tissue identification, our protocol holds several advantages over existing methods. Our technique provides a single test for the confirmation of blood, saliva, and/or semen within a sample that does not require PCR, can be performed in a short amount of time, and has the potential to be made portable to the scene of a crime.

Alternatively Spliced RNAs

Although the number is frequently debated, the human genome has been estimated to contain approximately 26,383 to 39,114 protein-coding genes [47]. Estimates of gene number had plagued scientists for quite some time because these estimates could not explain the

amount of variation or number of proteins found within the human proteome. In 1978, Walter Gilbert proposed a mechanism in which one gene can be transcribed, then subsequently translated into more than one protein. The process of multiple protein creation from one gene lies within the introns that are normally spliced out of RNA before protein creation. The sequence of nucleotides within the RNA directs the splicing machinery. If different splicing machinery is present in different cells types, then differently spliced mRNAs result in differences in polypeptides derived from the same gene [48].

Since the time of its discovery, scientists have studied the occurrence of alternative splicing in different tissue types. The use of micoarrays in splicing experimentation has led to a conservative estimate that 74% of human genes are likely to undergo alternative splicing at one point in time during development [49]. In 2002, the use of expressed sequence tags (ESTs) identified 667 tissue-specific splice variants [50]. Since that time, many databases have been compiled that contain alternatively spliced RNAs by tissue type and pathology: the UCLA Bioinformatics Community Site ASAP database, the Institut Universitaire d'Hematologie FastDB database [51-52], the Alternative Splicing Gallery [53], and the European Bioinformatics Institute's Alternative Splicing and Transcript Diversity 1.1 database, among others.

Molecular Beacons

First described in 1996 by Tyagi and Kramer, MBs are single-stranded nucleic acid probes that possess the ability to give a fluorescent signal when bound to a target nucleic acid with a complimentary sequence. This is due to a conformational change that occurs upon target binding (**Figure 2**). The probe sequence of the MB (usually 15-35 nucleotides in length) is flanked on either side by a series of nucleotides of complementary sequence (usually 5-7 nucleotides in length). One end of the MB has an attached fluorophore, while the other end is bound to a quencher molecule. When the MB is not in the presence of its target, the probe takes on a secondary hairpin shape that keeps the fluorophore in close vicinity to the quencher molecule. Little-to-no fluorescence can be detected when the MB is held in this conformation. When the target molecule is present, the secondary hairpin structure is opened and the beacon binds its target. In this "open" conformation, the fluorophore is no longer in close proximity to the quencher molecule and an increase in fluorescence can be measured. The amount of fluorescence quantified in a reaction is therefore indicative of the amount of template present in a sample [54].

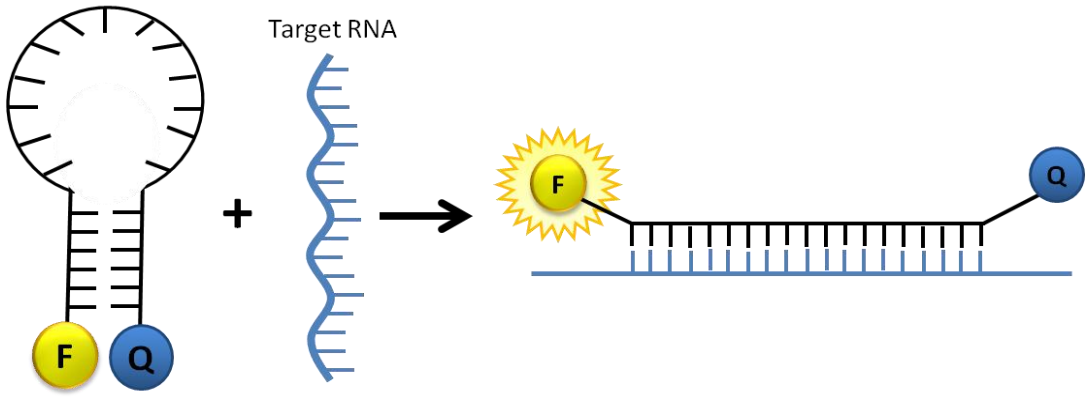

Figure 2: Structure and fluorescence of a MB in a "closed" and "open" confirmation. When a MB is not in the presence of its target nucleic acid, it maintains a "closed" hairpin shape in which the emitted signal of the fluorophore (F) is quenched by the close proximity of the quencher molecule (Q). Upon introduction of the target nucleic acid, here an RNA with a complementary nucleic acid sequence, the MB probe "opens" and binds to the target. Upon binding, the distance between the fluorophore and the quencher is great enough that increased fluorescence can be detected.

Depending upon desired application, MBs can be designed to incorporate different types of emission molecules (depending upon required amount of light emission) or to contain fluorophores of different emission spectra/color if multiple target nucleic acid detection is needed within a single sample. High or low copy number targets within a given sample may require a different fluorescence detection procedure. Specialized MBs have been effectively used to detect migration, localization, and relative quantity of specific RNA molecules within single living cells [55-59]. Sokol *et al.* reported that they were able to visually track RNA of the *vav* protooncogene within cells as long as 10 copies of the RNA molecule were present [55]. Others have reported that the use of more powerful varieties of emission molecules may be needed for detection of low copy number RNAs within a single cell, examples being Alexa Fluor fluorophores [59], quantum dots [60], duel FRET MB [57], and conjugated MBs [reviewed in 61].

We are interested in detecting RNAs isolated from biological fluids without the use of PCR. To do so, we have used an approach similar to that used for MB detection of low copy number RNAs, in which the fluorophore attached to the MB must be exceptionally intense. The fluorophore of choice was that of a quantum dot (see below). Joong H. Kim was the first to attach a quantum dot to a MB for use in detecting a complementary DNA sequence using amide chemistry [60]. Instead of amide chemistry, we have chosen a linkage strategy that utilizes the interactions of biotin and streptavidin proteins.

Quantum Dots

Quantum Dots (QDs), first synthesized in the 1980's by Alexei Ekimov, are semiconductor nanoparticles/nanocrystals that due to their intense fluorescence, can be used in place of traditional fluorophores in a variety of biological applications [62]. QDs are composed of a core of CdSe atoms that provide the particle its fluorescent properties. The size of the CdSe core is responsible for the emission wavelength, whereas increasing the size of the core, increases the QDs emission wavelength [63]. Surrounding this core is a shell of ZnS molecules. This protective shell adds stability to the nanocrystal while in solution. These nanoparticles have several properties that make them candidates for use in scientific research applications in which more commonly used fluorophores such as FAM or Texas Red would not have been applicable. QDs have been found to fluoresce much more intensely than traditional fluorophores. The extinction coefficients (used to determine the intensity, or brightness, of a fluorophore) for FAM and Texas Red are 74,850 M^{-1} cm^{-1} and 136,000 M^{-1} cm^{-1} respectively [64]. The extinction coefficients for QDs with emission wavelength of 525 nm to 800 nm can range between 710,000 M^{-1} cm^{-1} and 12,600,000 M^{-1} cm^{-1} [65]. As well as enhanced brightness, QDs are extremely resistant to photobleaching. The absorption range for QDs is quite broad, while the emission wavelength remains narrow [66]. This makes experimentation in which several QDs are used at once much easier than dealing with the "cross-talk" of using multiple traditional fluorophores.

Note: Each chapter was written as a publishable manuscript, and therefore some sections may be repetitive.

Chapter 2: Optimizing the Extraction of DNA-Free RNA from Porcine Dental Pulp

Introduction

The ability to efficiently isolate and correctly quantify ribonucleic acid (RNA) from biological samples is shaping the fields of biological, biomedical, and forensic sciences. The advent of quantitative Real-Time Reverse Transcription Polymerase Chain Reaction (qRT-PCR) has supplied an extremely sensitive technique to quantify multiple RNAs from a variety of tissues in a relatively short amount of time.

RNA is of interest for forensic science due to several of the molecule's unique qualities. First, RNA is found in high abundance within cells. Most RNAs from transcribed genes will be found in multiple copies within each nucleated cell, as opposed to two copies of its DNA counterpart. RNA is less stable than DNA and its degradation has been found to be predictable in *ex vivo* biological samples. The sequence of RNA is determined by a DNA template, therefore like DNA, polymorphisms can be exploited to make assays species-specific, including human-specific. Human-specificity appeals to forensic science when the species of origin of a particular biological sample is of interest or debate. For most applications, primers and probes that are designed to be human-specific can reduce the probability of amplifying any contaminating nucleic acids from the environment along with the human amplicon of interest. Due to alternative splicing events, some mRNAs are only found in certain tissues [48]. This allows for the design of assays in which target RNAs that can provide additional information about the type of biological material present, as well as its quantity.

Several groups have begun investigating the use of RNA in the identification of body fluids [11-19], in the determination of time since deposition of biological materials [20-22], in determination of the age of an individual from whom a biological stain was derived [23], and in Postmortem Interval (PMI) estimation [24, 25]. Many of these studies are analyzing the presence/absence of particular species of RNA or are attempting to measure degradation of particular RNAs to find predictable patterns.

Biomedical science has recently focused on screening for the detection of abnormal RNAs or RNA concentrations for diagnostic purposes. These screens usually target the presence of alternatively spliced RNAs or significant increases/decreases in normal transcript levels. A large portion of this research concentrates on cancer diagnosis. Li *et al.* has shown four normal transcripts in saliva that are elevated 3.5 fold in 91% of individuals who have oral cancer [67]. Similarly, the presence of cytokeratin 19 RNA in peripheral blood samples has been suggested as a screen for breast cancer relapse following chemotherapy treatment [68]. Expression levels of RNAs have also been used for less severe illnesses as well. The expression of platelet genes

in peripheral blood samples has lead to better diagnostic techniques for patients who suffer from migraine headaches, as opposed to the more severe symptoms of chronic migraine [69].

It can be seen that in both forensic and medical applications, correct detection, amplification, and quantification of RNA is imperative for proper analysis and application of results from qRT-PCR. To accurately quantify, one must be sure the extraction protocol, as well as all downstream applications of qRT-PCR are optimized.

Previous work in our laboratory has focused on the use of detecting RNA degradation to estimate the time since deposition, or age, of a bloodstain that has been left behind at the scene of a crime [21, 22]. We are currently interested in determining if the same techniques that measure RNA degradation within *ex vivo* bloodstains can be employed to measure degradation of RNA contained within postmortem bodily tissues (in particular, dental pulp) to determine PMI, or time since death.

With our method, estimation of PMI can be determined after a comparison of the degradation of two differently sized portions of RNA, one being more labile than the other. At the time of death, two differently sized, non-overlapping, regions of the same RNA molecule, one large (301 bp) and one small (71 bp), should be present in approximately equal amounts. Due to death at a tissue level, no further transcription should occur, and over time, the RNA remaining in the tissue should degrade. Based merely on size, the larger region of the RNA molecule will be more susceptible to degradative environmental forces and will therefore decay more quickly than will the smaller region of the same molecule. By comparing the rates of degradation of these regions over time, a large (unstable) portion compared to a small (stable) portion, we can make an estimate of PMI.

The tissue that was chosen for our analysis was dental pulp obtained from a porcine model system. An isolation protocol that extracts DNA-free RNA was desired. No such technique was available in the preliminary stages of our experimentation, therefore a DNase treatment was applied to any sample in which DNA was observed. One benefit of removing residual DNA from RNA isolates is that it reduces the need for qRT-PCR primers that are RNA-specific. If primers for Real-Time PCR cannot be designed to be RNA-specific, one can assume that if the sample is free of DNA, then the only template for these primers will be the intended RNA molecule. Primers and probes for some RNAs, however, cannot be made RNA-specific due to the absence of useful exon-exon boundaries. In these instances, both RNA and contaminating DNA could be quantified, which is not desirable.

RNA samples are routinely screened for DNA contamination and, in preliminary studies, consequently treated with Ambion TURBO DNA-free DNase. RNA isolates from tooth pulp, unlike earlier analyses with blood, yielded higher than average levels of DNA contamination.

Such treated samples unexpectedly produced high Ct values, which are indicative of low RNA quantities, even when fresh pulp was used and Ct values were anticipated to be low. Other young samples not treated with DNase continued to produce lower Ct values.

It was thought that perhaps the loss of signal in qRT-PCR due to DNase was tissue-specific. Our laboratory had a great deal of previous experience isolating RNA from dried bloodstains and had never noticed a reduction in Ct values as was seen in dental pulp after DNase treatment. To determine if the effects were tissue-specific, RNA isolates from both blood and dental pulp would be tested for their response to DNase treatment.

As well as tissue specificity, it was important to determine whether differently sized amplicons in a multiplex reaction would be affected equally by DNase treatment. As we have hypothesized that differently sized portions of RNA will degrade at different rates due to random environmental insults, it was thought that larger amplicons may be more greatly affected by DNase than small, thus skewing estimates of PMI using our proposed method when DNase treatments are applied.

Although some commercially available DNase treatments may have no effect on RNA quality, it is an additional step within a protocol that lengthens the amount of time RNA isolations take to perform, as well as increasing the cost of the assay. To determine if another, more recently developed RNA isolation technique could make the use of DNase unnecessary, several isolation techniques were tested on tooth pulp to determine which would yield the most RNA, while simultaneously isolating the least residual DNA.

The objective of this work is to determine the effects of a commercial DNase treatment on RNA samples obtained from both porcine tooth pulp and human blood, as well as to find an optimized protocol for isolation of DNA-free RNA suitable for downstream qRT-PCR applications.

Methods

Sample Collection

Teeth were extracted from a freshly slaughtered pig's head obtained from Emerick Meat & Packing (Hyndman, PA). Each tooth was removed using a hammer, chisel, and pliers. The intact teeth were frozen at -80^{o}C until RNA isolation was performed. To gain access to the dental pulp, the frozen teeth were placed in a ceramic mortar and struck with a pestle. Forceps were used to remove a small amount of dental pulp from the exposed pulp chamber.

Blood samples were obtained from healthy human volunteers by finger prick. Ten microliters of fresh blood was transferred from the volunteer's finger to a sterile 1.5 ml eppendorf tube. Isolation of RNA was performed immediately. Blood samples were obtained with a protocol approved by the West Virginia University Institutional Review Board for Protection of Human Research Subjects.

RNA Isolations from Porcine Tooth Pulp and Human Blood for DNase Treatment

A small amount of dental pulp was added to a 1.5 ml tube containing 1 ml TRI-Reagent (Molecular Research Center, Inc., Cincinnati, OH). The pulp was then manually homogenized and the samples incubated at room temperature for 5 minutes. One hundred microliters of 1-bromo-3-chloropropane (Molecular Research Center, Inc.) were added and the tube mixed by vortex for 15 seconds. Tubes were then centrifuged for 15 minutes at 16,099 x g. All centrifugations were performed at 4^{o}C. The top, aqueous layer was removed and transferred to a new, RNase-free 1.5 ml tube (Fisher Scientific, Pittsburgh, PA). Five hundred microliters of cold isopropanol were added to each tube, the tubes inverted several times to mix, and incubated at room temperature for 8 minutes. After the incubation period, the tubes were centrifuged for 8 minutes at 16,099 x g. The supernatant was removed and the RNA pellet washed with 1 ml 75% ethanol. Again, samples were centrifuged for 5 minutes at 6,289 x g. The supernatant was removed and the RNA pellets allowed to air dry under the hood for 5 minutes. Each pellet was rehydrated with the addition of 80 μl nuclease-free water (Fisher Scientific) and incubation at 55^{o}C for 10 minutes. Three replicate samples were performed using this RNA isolation technique.

Ten mircoliters of fresh blood were transferred from the volunteer's finger to a sterile 1.5 ml eppendorf tube containing 200 μl nuclease-free water, 750 μl TRI-Reagent, and 3 μl polyacryl carrier (Molecular Research Center, Inc.). The samples were mixed briefly by vortex and incubated at room temperature for 10 minutes. After addition of 100 μl 1-bromo-3-chloropropane, the samples were again mixed by vortex for 15 seconds and incubated at room temperature for 3 minutes. The tubes were then centrifuged for 15 minutes at 16,099 x g. All

centrifugations were performed at 4°C. The aqueous layer was transferred to a new, RNase-free 1.5 ml tube. Five hundred microliters of cold isopropanol were added to each tube, the tubes inverted several times to mix, and incubated at room temperature for 7 minutes. After the incubation period, the tubes were centrifuged for 8 minutes at 16,099 x g. The supernatant was removed and the RNA pellet washed with 1 ml 75% ethanol. Again, samples were centrifuged for 5 minutes at 16,099 x g. The supernatant was removed and the RNA pellets allowed to air dry under the hood for 5 minutes. Each pellet was rehydrated with the addition of 80µl RNase-free water and incubation at 55°C for 10 minutes. Three replicate samples were performed using this RNA isolation technique.

DNase Treatment of RNA Samples

RNA isolates were each divided so that half would be treated with Ambion's TURBO DNA-free DNase (Austin, TX) according to the manufacturer's protocol, and the other half not. Thirty-five microliters of each sample were stored at -20°C until reverse transcription.

Various Methods of RNA Isolation from Porcine Tooth Pulp

Additional RNA isolations on porcine dental pulp were performed using TRI-Reagent, Tri-Reagent BD (Molecular Research Center, Inc.), TRI-Reagent RT (Molecular Research Center, Inc.), PerfectPure RNA Cell &Tissue Kit (5 Prime, Inc., Gaithersburg, MD), SurePrep TrueTotal RNA Purification Kit (Fisher Scientific), and the SV Total RNA Isolation System (Promega, Madison, WI). Three replicate samples were processed for each method, including three additional replicates for optional DNase treatments if mentioned in the protocol. Permutations to the manufacturer's protocol are listed below for each method performed.

For TRI-Reagent isolation, a small amount of dental pulp was added to a 1.5 ml tube containing 1 ml TRI-Reagent. The pulp was then manually homogenized and the samples incubated at room temperature for 5 minutes before the addition of 1-bromo-3-chloropropane.

Isolations performed with TRI-Reagent RT began with the addition of pulp to a glass tissue grinder containing 350 µl TRI-Reagent RT. The tissue was ground until no substantial pulp masses remained. The homogenate was transferred to a 1.5 ml tube containing 650 µl TRI-Reagent RT. Samples were incubated at room temperature for 5 minutes. To pellet any remaining tissue, the samples were centrifuged for 10 minutes at 16,099 x g. All centrifugations were performed at 4°C. Taking care not to disturb the cell pellet at the bottom of the tube, approximately 950 µl of the homogenate was removed and transferred to a new 1.5 ml tube before the addition of 4-bromoanisole (Molecular Research Center, Inc.).

RNA isolated by the 5 Prime PerfectPure RNA Cell & Tissue kit was obtained using the manufacturer's tissue protocol, which includes a homogenization step. Whenever a choice was given regarding g-force, centrifugation at 15,000 x g was selected. The protocol was performed both with and without the optional DNase treatment on replicates of three samples each.

While employing the Fisher SurePrep TrueTotal RNA Purification Kit, RNA isolates were extracted using a slightly modified version of the manufacturer's protocol for animal tissues. The alteration introduced was to grind the tissue in 200 μl of lysis solution before bringing the total volume of lysis solution to 600 μl. This step replaces grinding the tissue in liquid nitrogen in a mortar and was chosen due to the very small amount of pulp used for extraction. The protocol was performed both with and without the optional DNase treatment on replicates of three samples each.

RNA was isolated from dental pulp by Promega's SV Total RNA Isolation System following the manufacturer's protocol for small tissue samples. It should be noted that this protocol contains a DNase treatment that is not optional. Three replicate isolations were performed using this protocol.

qPCR Screen for Genomic DNA Contamination in RNA Samples

To determine the relative amount of residual DNA within the RNA isolates obtained through various methods, quantitative Real-Time PCR (qPCR) utilizing DNA-specific primers and probe was utilized. All primer and probe sequences used for qPCR were developed using Applied Biosystems Primer Express Software version 3.0 (Foster City, CA). The sequences of these primers and probes can be found in **Table 1**. For porcine tooth pulp, PGAP71 primers amplify a 71bp non-transcribed region of the porcine glyceraldehyde-3-phosphate dehydrogenase gene. A master mix was created so that each reaction contains 12.5 μl Applied Biosystems TaqMan Universal PCR Master Mix, PGAP71 forward and reverse primers at 200 nM, PGAP71 VIC-labeled probe at 250 nM, and 2.75 μl nuclease-free water. Five microliters of the RNA isolate was combined with 20 μl master mix in a thin-walled PCR tube (Applied Biosystems). Samples were run in an Applied Biosystems 7300 Real-Time PCR System under the following conditions: 1 cycle at 50^{o}C for 2 minutes, 1 cycle at 95^{o}C for 10 minutes, and 40 cycles at 95^{o}C for 15 seconds followed by 60^{o}C for 1 minute. Each sample was run in duplicate. A positive control was included in each run that contained 20 μl master mix and 5 μl either porcine or human DNA. Negative controls were 20 μl master mix and 5 μl nuclease-free water, and 25 μl nuclease-free water. Amplification resulting in Ct values below 35 in our RNA isolates is indicative of residual DNA contamination.

Reverse Transcription of RNA Isolates

After screening for genomic DNA contamination, all RNA isolates were reverse transcribed for downstream qRT-PCR quantification of RNA in the form of cDNA. Applied Biosystems' TaqMan Gold Reverse RT-PCR kit was used to make a master mix with final concentrations: 1X TaqMan buffer A, 2.5 μM random hexamers, 5.5 mM magnesium chloride, and 500 μM each dATP, dCTP, dGTP, and dTTP. 57 μl of the reverse transcription mix was combined with 35 μl of RNA isolate, 2 μl of RNase inhibitor (0.8 U), and 2.5 μl of Multiscribe reverse transcriptase (3.25 U). The samples were then pulse centrifuged and placed into a Techne Touchgene Gradient thermocycler (Burlington, NJ) and run under the following conditions: 25°C for 10 minutes, 48°C for 30 minutes, 95°C for 5 minutes.

Multiplex qRT-PCR Quantification of DNase or No DNase Treated RNA

For RNA samples from blood or tooth pulp, either DNase treated or not, multiplex Real-Time PCR reactions utilizing RNA-specific primers were performed. The sequences of these primers can be found in **Table 1**.

For porcine tooth pulp cDNA, the primer and probe combinations of PBA 71 and PBA301 were used in multiplex reactions. PBA71 primers amplify a 71 bp portion of porcine β-action mRNA. PBA301 primers amplify a 301 bp portion of porcine β-actin mRNA that is separate from that amplified by PBA71. Concentrations of PBA71 used in Real-Time PCR are 100 nM both forward primer and reverse primer and 250 nM VIC-labeled probe. Concentrations of PBA301 used are 1100 nM both forward primer and reverse primer and 250 nM FAM-labeled probe.

For human blood cDNA, the primer and probe combinations of BA4 and BAA were used in multiplex reactions. BA4 primers amplify an 89 bp segment of human β-actin mRNA. BAA primers amplify a separate, 301 bp portion of human β-actin mRNA. The concentrations for BA4 were forward primer at 100 nM, reverse primer at 125 nM, and the VIC-labeled probe at 250 nM. The concentrations for BAA were forward primer at 900nM, reverse primer at 800nM, and the FAM-labeled probe at 250 nM.

A master mix was created so that each reaction contains 12.5 μl Applied Biosystems TaqMan Universal PCR Master Mix, the specified concentration of forward, reverse, and probe for either reactions amplifying cDNA from porcine tooth pulp or human blood, and nuclease-free water to bring the final volume of each reaction to 20 μl. Five microliters of the RNA isolate was combined with 20 μl master mix in a thin-walled PCR tube. Samples were run in duplicate in an Applied Biosystems 7300 Real-Time PCR System under the following conditions: 1 cycle at 50°C for 2 minutes, 1 cycle at 95°C for 10 minutes, and 40 cycles at 95°C for 15 seconds followed by 60°C for 1 minute. A positive control was included in each run that

contained 20 μl master mix and 5 μl either porcine or human cDNA respectively. Negative controls were 20 μl master mix and 5 μl nuclease-free water, and 25 μl nuclease-free water.

Table 1: Real-Time PCR primers and probes used to detect RNA and DNA contamination in RNA isolates from porcine tooth pulp or human blood. The DNA-specific primers and probe were designed from the porcine GAPDH gene sequence. RNA-specific primers and probes for tooth pulp and blood were designed to amplify porcine or human β-actin RNA respectively.

Name	Size Amplified (bp)	Specificity	Primer/Probe Sequence
PGAP71 (Pulp)	71	DNA-Specific	FP: 5'-GGCTGACTTGGACCAGGAAAG-3' RP: 5'-CCCTTCAAGTGAGCCTGCAG-3' Probe (VIC): 5'-AAGCCCGGGTGTCTGACTGCTCC-3'
PBA71 (Pulp)	71	RNA-Specific	FP: 5'-TCGCCGCCGGTCTACA-3' RP: 5'-GCCGTTGTCGACCACGAG-3' Probe (VIC): 5'-CGCCATGGATGACGATATTGCTGC-3'
PBA301 (Pulp)	301	RNA-Specific	FP: 5'-ACCGACTACCTCATGAAGATCCTG-3' RP: 5'-GCACTTCATGATGGAGTTGAAGG-3' Probe (FAM): 5'-CTGCCCGACGGCCAGGTCATC-3'
BA4 (Blood)	89	RNA-Specific	FP: 5'-TCATTCCAAATATGAGATGCATTGT-3' RP: 5'-GGACTGGGCCATTCTCCTTAG-3' Probe (VIC): 5'-AAGTCCCTTGCCATCCTAAAAGCCACC-3'
BAA (Blood)	301	RNA-Specific	FP: 5'-CTTCAACACCCCAGCCATGT-3' RP: 5'-CTCTTGCTCGAAGTCCAGGG-3' Probe (FAM): 5'-CTGTGCTATCCCTGTACGCCTCTGGC-3'

Singleplex qRT-PCR Quantification of RNA Isolated with Various Methods

To quantify the amount of RNA extracted from porcine tooth pulp through multiple extraction methods, singleplex Real-Time PCR utilizing RNA-specific PBA71 primers and probe were used. A master mix was created so that each reaction contains 12.5 μl Applied Biosystems TaqMan Universal PCR Master Mix, PBA71 forward and reverse primers at 100 nM, PBA71 VIC-labeled probe at 250 nM, and 6.38 μl nuclease-free water. Five microliters of the RNA isolate was combined with 20 μl master mix in a thin-walled PCR tube (Applied Biosystems). Samples were run in an Applied Biosystems 7300 Real-Time PCR System under the following conditions: 1 cycle at 50°C for 2 minutes, 1 cycle at 95°C for 10 minutes, and 40 cycles at 95°C for 15 seconds followed by 60°C for 1 minute. A positive control was included in each

run that contained 20 μl master mix and 5 μl porcine cDNA. Negative controls were 20 μl master mix and 5 μl nuclease-free water, and 25 μl nuclease-free water.

Data Analysis

After amplification using qRT-PCR, Ct values were acquired for both DNA-specific and RNA-specific primer/probe pairs for all sample types. The Ct values were obtained by placing the horizontal threshold within the phase of the exponential growth above any background noise seen in early amplification cycles. Relative quantification analysis of the data was performed using Applied Biosystems Sequence Detection Software Version 1.3. The data were exported into Microsoft Excel (Microsoft Corporation, Redman, WA) for further analysis. Once in Excel, the average Ct value for each set of samples was determined along with the standard error.

Due to possible Real-Time machine error of +/- 0.5 Ct, all samples were run in duplicate, and then duplicates were analyzed for differences in Ct value. Any duplicate samples that gave Ct values outside the range of +/- 0.5 Ct would be removed from analysis. This potential machine error was also the basis for the horizontal line drawn along the bar graph of **Figure 3**. This line is indicative of reported RNA loss due to DNase treatment that can be contributed to machine error alone.

To determine if there was differential loss of cDNA after DNase treatment between two differently sized amplicons, a 71 bp to a 301 bp (human) and an 89 bp to a 301 bp (porcine) segment of β-actin mRNA, in a multiplex reaction, Ct values of the same amplicon were compared before and after treatment with DNase. This analysis was performed on samples of human blood as well as porcine tooth pulp that underwent RNA isolation using TRI-Reagent. The Ct values obtained from the samples where no DNase treatment was used were subtracted from the same sample after treatment with Ambion's TURBO DNA-free DNase using the manufacturer's protocol. This measure of DNase minus no DNase (Ct_{DNase}-$Ct_{No\ DNase}$) provided the number of Ct values gained after DNase treatment, and thus a measure of the RNA/cDNA lost due to this treatment.

To show how differential effects of DNase, based on amplicon size, can affect downstream data analysis, the common statistic of ΔCt was applied to average Ct values from our DNase and No DNase treated samples. This data conversion exploits the difference in Ct value between two amplicons in a multiplex reaction. Here, the ΔCt refers to the Ct value of the large amplicon minus the Ct value of the small amplicon (Ct_{large}-Ct_{small}).

To simplify the quantitation of RNA and DNA found in RNA isolates from the various isolation procedures, singleplex qRT-PCR was utilized in place of a multiplex reaction. Only one Ct value was obtained for each DNA and RNA in each sample. High Ct values are indicative of a low concentration of starting template material in qRT-PCR. The opposite is also true, low Ct values indicate a high amount of starting material. To combat this counterintuitive data, a calculation of 40-Ct was used. Forty being the number of cycles used in amplification, 40-Ct then shows high values as having a high amount of starting material and low 40-Ct values as having a low amount of starting material. To make a comparison of the amount of RNA versus the amount of DNA extracted by each isolation technique, a ratio of these values was analyzed. The ratio of Ct values obtained for RNA to DNA (RNA/DNA), after the subtraction of each Ct value from 40, yields high values for isolation techniques that extract high RNA and low DNA. Low values obtained through the comparison show isolation techniques that isolate high RNA concentrations, but also co-isolate high levels of DNA.

Statistical Analysis

Two-way Analysis of Variances (ANOVAs) were utilized to compare the results from multiplex Real-Time PCR followed by subsequent Tukey-Kramer multiple comparison procedures. To determine if there was a differential loss of cDNA based on size of the amplicon and/or tissue type, Ct values in the form of DNase-no DNase were used as the experimental unit measured. Effects in the ANOVA model were tissue type (either blood or pulp), amplicon size (either 71/89 bp or 301 bp) and tissue type crossed with amplicon size. Determination of whether there was an effect of DNase treatment on final qRT-PCR analysis used ΔCt as the experimental unit. Effects in this two-way ANOVA were tissue type (either blood or pulp), treatment type (either DNase treatment or no DNase treatment), and tissue type crossed with treatment type. All experimental units were compared using $\alpha = 0.05$.

A one-way ANOVA and subsequent Tukey-Kramer HSD multiple comparison procedure were performed on Ct values from porcine tooth pulp samples extracted using the various isolation protocols to determine if there was a difference in the amount of nucleic acid extracted between techniques. All isolation techniques were compared to each other to determine which isolated the most RNA and contained the least DNA contamination. The ratio of RNA to DNA (RNA/DNA) 40-Ct values were the experimental unit compared and the level of significance was determined using $\alpha = 0.05$.

Results

Effect of DNase on RNA Samples from Dental Pulp and Blood

Multiplex qRT-PCR analysis allows for control and experimental RNAs to be assayed in the same reaction. To determine the effect that DNase treatment may have on multiple RNA targets of different lengths in the same reaction, RNA samples were divided and half treated with DNase, while the other half was not. Two differently sized, yet distinct amplicons of β-actin mRNA were analyzed for both porcine tooth pulp (a 301 bp and a 71 bp region) as well as human blood (a 301 bp and a 89 bp region). Two-way ANOVA results of cDNA loss due to DNase treatment for the larger and smaller amplicon in each multiplex qRT-PCR are shown in **Figure 3**. There was a significant difference in the loss of cDNA between the small and large amplicons in both tissue types after treatment with DNase ($F=78.1747$, $p=<0.0001$). This loss was greater in the large amplicons from both tissues. The difference seen in cDNA loss by size of amplicon was not influenced by tissue type ($F=0.3599$, $p=0.5528$), therefore the effect of DNase on isolated RNA is not tissue-specific.

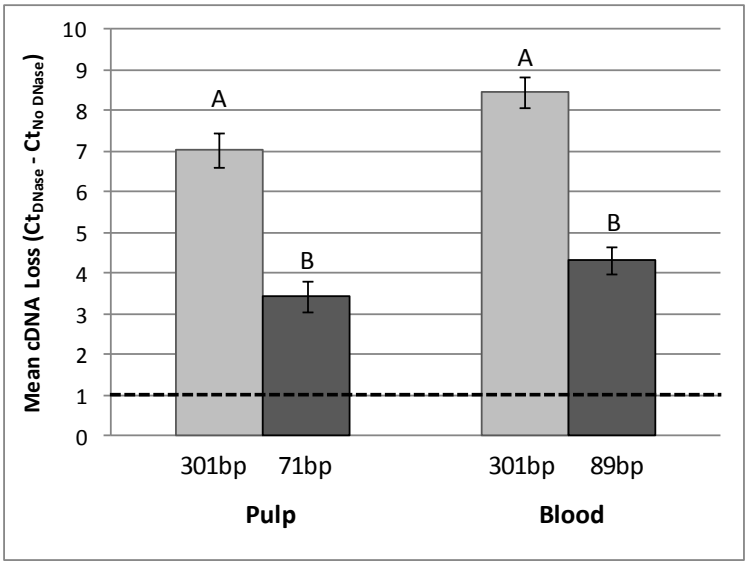

Figure 3: Average cDNA loss after DNase treatment as a function of the size of the RNA in a multiplex assay. Human blood and porcine pulp samples were divided in half after RNA isolation. After treating one half of each sample with DNase and reverse transcribing, the resulting cDNA was amplified in a multiplex Real-Time PCR reaction (a 301 bp and 71 bp region for pulp or a 301 bp and 89 bp region for blood). The loss of cDNA after DNase treatment based on size of the portion of the molecule amplified is shown. The dashed line signifies the range of error that can be attributed to the Real-Time machinery (+/- 0.5 Ct value); therefore indicating that values of RNA loss above this line cannot be attributed to machine error. The error bars indicate standard error where n=12. Means associated with the same letter are not significantly different (Tukey-Kramer HSD).

Ct values for small and large amplicons were obtained and a ΔCt analysis was applied to samples treated with DNase and those that were not. These results can be seen in **Figure 4**. There is a significant difference in the ΔCt values obtained for the two different tissue types (F=51.9739, p=<0.0001). This is to be expected as the amount of starting material (β-actin mRNA) found in various types of tissues differs. Results indicate that there is a significant difference in the calculated ΔCt between samples that were DNase treated versus not DNase treated (F=108.7998, p=0.0001). The ΔCt increases after DNase treatment in both pulp and blood. Although both the large and the small amplicons are affected by DNase, the rise in ΔCt is due to a greater loss of the larger amplicon than the small. This observed increase of ΔCt in all DNase treated samples is not influenced by tissue type (F=0.5009, p=0.4842).

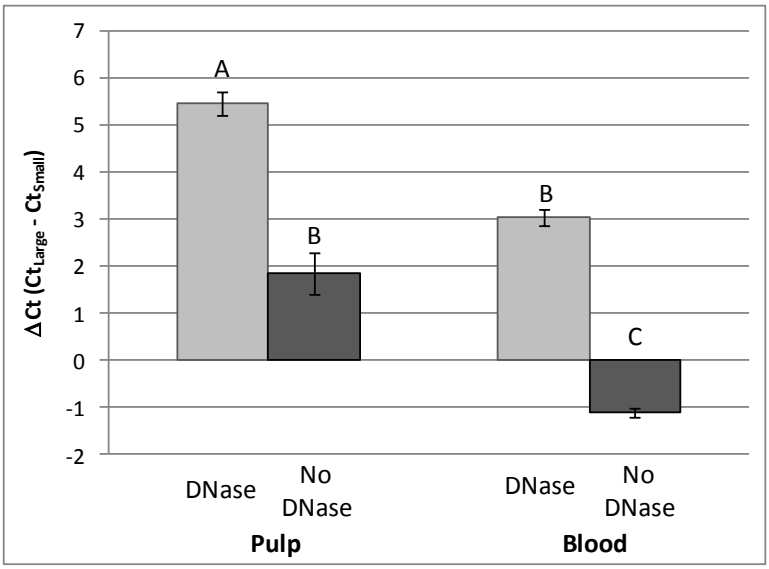

Figure 4: Average Change in ΔCt before and after DNase treatment. Human blood and porcine pulp samples were divided in half after RNA isolation. After treating one half of each sample with DNase and reverse transcribing, the resulting cDNA was amplified in a multiplex Real-Time PCR reaction (a 301 bp and 71 bp region for pulp or a 301 bp and 89 bp region for blood). The comparison of the ΔCt of samples either DNase treated or not DNase treated is shown. The error bars indicate standard error where n=12. Means associated with the same letter are not significantly different (Tukey-Kramer HSD).

Comparison of Various RNA Isolation Methods

Six RNA isolation techniques were used to isolate total RNA from porcine dental pulp in hopes that one would provide a high yield of RNA, while reducing the amount of contaminating residual DNA seen in previous samples. Three of the methods tested were one-step, monophase solutions containing phenol and guanidine thiocyanate: TRI-Reagent, TRI-Reagent BD, and TRI-Reagent RT. The remaining three methods were affinity-based spin column kits. Two of these kits, from 5Prime and Fisher, have optional DNase treatments. The final kit, from Promega, utilizes a DNase treatment that is required in the manufacturer's protocol. The ratio depicting the amount of RNA to DNA (RNA/DNA) isolated using these methods is found in **Figure 5**. Although significant differences existed between the amount of RNA/DNA extracted from dental pulp using these methods ($F=10.4815$, $p=<0.0001$), all techniques extracted high levels of the β-actin mRNA target. High DNA concentrations were found in isolates from both the 5Prime and Fisher kits, as seen by the relatively low ratio values obtained from analysis. There was no significant difference in RNA/DNA quantity found between samples isolated using these two kits with or without the optional DNase treatments (Tukey-Kramer HSD). Although the Promega kit isolated the least amount of contaminating DNA among all of the spin column kits tested, these levels are still considered to be above background (having a Ct value below 35) and would interfere with qRT-PCR results if RNA-specific primers/probes were not used. The three TRI-Reagent solutions co-isolated relatively low levels of DNA, with TRI-Reagent RT being the only RNA isolation method that successfully isolated high concentrations of RNA, as well as levels of DNA that fall below qRT-PCR background.

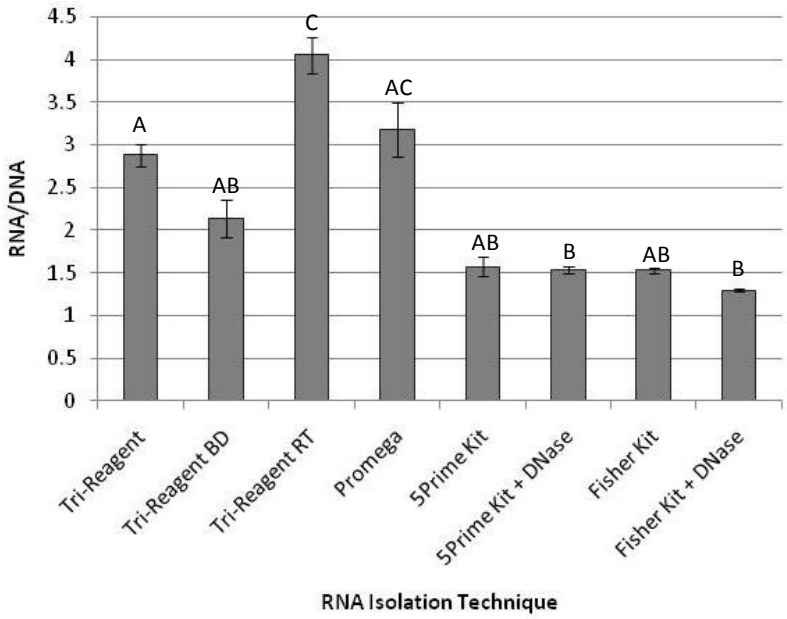

Figure 5: Average amount of RNA and DNA isolated from porcine dental pulp using various isolation methods. After converting raw data to 40 minus Ct values (40-Ct), the ratio of RNA/DNA was examined between RNA isolation techniques. A high value obtained by the ratio indicates high levels of isolated RNA with low levels of co-isolated DNA. Lower values indicate increased concentrations of DNA within the RNA isolates. A significant difference was found in the RNA/DNA ratio obtained among RNA isolation techniques ($F=10.4815$, $p=<0.001$). The error bars represent standard error where $n=24$. Means associated with the same letter are not significantly different (Tukey-Kramer HSD).

Discussion and Conclusions

The results from this study confirmed prior observations that DNase treatment of RNA isolates may affect the results of qRT-PCR (**Figure 4**). Although the first observation of decreased Ct value after DNase treatment occurred with RNA isolated from porcine dental pulp, we saw that this phenomenon is not tissue-specific. Ct values obtained from qRT-PCR of DNase-treated bloodstains were altered equally (**Figure 3**).

In both porcine dental pulp and human blood, when two differently sized amplicons are quantified in a multiplex qRT-PCR reaction after DNase treatment, the larger of the two amplicons is more degraded than the smaller. Although more degraded than the small amplicons (71 bp and 89 bp respectively), both large amplicons (301 bp each) were equally affected by treatment. The small amplicons, similar in length, were also equally affected, but less so than the larger amplicons. This result supports our earlier observations that larger regions of an mRNA molecule are more affected by environmental, degradative insults than smaller molecules, based merely on their size.

The observed loss of qRT-PCR signal upon DNase treatment is most likely due to residual DNase degrading cDNA and not to loss of RNA itself. The last step of Ambion's TURBO DNA-free DNase utilizes an inactivation reagent and room temperature incubation to prevent further activity of the enzyme. The DNase was almost certainly not being completely inactivated during the room temperature incubation period. DNase I has the ability to effectively degrade both single-stranded and double-stranded DNA, as well as RNA-DNA hybrids. Active DNase is most likely being transferred to the reverse transcription step of qRT-PCR, or even into the final Real-Time reaction, where it continued to degrade the DNA products that were created through these applications.

Multiplex reactions in which two RNAs are being compared to one another (where one of the assayed RNAs is used as the control to which to compare the other RNA) estimation of relative concentration is also of concern after DNase treatment. The use of Ambion's TURBO DNA-free DNase in this study showed a preferential degradation of larger amplicons compared to smaller amplicons in both tooth pulp and blood samples. Our results, using the ΔCt method of analysis, indicated that DNase treatment significantly increases the ΔCt values obtained. In the case of blood, it was found that a mean ΔCt of -1.099 from samples not treated with DNase was reported as 3.042 following DNase treatment; therefore, the differential degradation of a large amplicon compared to a smaller amplicon in multiplex reactions could lead to erroneous conclusions.

Although the results focus on multiplex qRT-PCR results, these are not the only type of analyses that could be affected. Singleplex qRT-PCR reactions, performed to determine RNA

concentration from a particular biological sample, may also be affected. This type of analysis is performed by comparing Ct values obtained from a sample of unknown RNA concentration to a standard curve created from known RNA concentrations. The results of this study show a significant increase in Ct value when certain DNase treatments are used to rid RNA isolates of contaminating DNA. If the sample of unknown RNA concentration had been treated with DNase and the RNA used to create the curve had not, it is possible to gravely underestimate the concentration of RNA in the sample. This underestimation could lead to skewed results of gene expression analyses, incorrect PMI estimates, or to misdiagnosis in the case of medical tests.

Caution is advised when working with new tissues or in this case, new DNase treatment protocols. The preferred solution to this problem would be to find a method of RNA isolation that isolates high quality, DNA-free RNA. If this can be accomplished, then a DNase treatment would not be necessary. In this study we focused our search for such an isolation protocol to monophase solutions and affinity-based spin column methods. The only isolation procedure that met our standards was that of TRI-Reagent RT. The amount of DNA detected within our pulp samples was extremely low and in fact, almost beyond detection by sensitive Real-Time techniques. The high Ct values produced in a screen for genomic DNA verified that as little as one to no copies of GAPDH existed in the samples isolated by this technique.

With a technique in which no DNA is co-isolated along with RNA, there is less need to design primers and/or probes to be RNA-specific. RNA-specific primers and probes are more difficult to design when the gene for an RNA target contains no introns, or the sequences at exon-exon boundaries cannot be used due to undesirable GC content or complex secondary structure. This isolation technique also eliminates the need to treat samples with DNase. By eliminating the requirement of a DNase treatment, as shown in this study, you can reduce the probability of degrading RNA within samples and thus have a better estimation of RNA concentration. Both accomplishments, better isolation technique and no use of DNase, can lead to a more accurate estimation of RNA quantity and analysis of results.

The results reported here, as well as observations by others in the Bishop laboratory, clearly indicate that DNase treatments should be avoided if at all possible. If such treatments are unavoidable, then great care must be taken to fully eliminate and/or inactivate the DNase prior to conversion of RNA to cDNA.

Chapter 3: Using a Porcine System to Develop a Molecular Approach for Estimating Postmortem Interval

Introduction

Estimation of postmortem interval (PMI), or time since death, is a common technique used in forensic science after the discovery of a corpse which can provide needed information in order to determine the timeline of events leading up to the death. Knowing when a suspicious death occurred can limit the number of potential suspects by excluding those with viable alibis for the time of the crime.

Modern techniques in the estimation of PMI predominantly utilize fluctuating variables, such as the concentration of biomolecules within bodily remains, that vary in relation to the length of time in which the body has been deceased or the temperature-dependent life cycles and seasonal succession of corpse-colonizing insects. These techniques include visual identification of the stages of tissue decomposition due to cell autolysis and putrification [72], temperature of the body at the time the body is recovered [28], the presence/absence of the stiffening of the limbs [29], decomposition chemistry within bodily remains [30, 32] such as potassium ion concentration changes within the vitreous humor of the eye [31], and the presence/absence of forensically significant insect species on or around the body.

All of the previously mentioned techniques, with the exception of forensic entomology, rely mainly upon predictable, physiological changes that occur within the body following death. These changes usually occur within a four day period postmortem, after which the methods can no longer provide an accurate estimate of PMI. To determine PMIs that are longer than roughly four days, investigators currently rely upon forensically significant insect species to formulate their estimates.

Forensic entomology is a technique that utilizes a combination of information regarding environmental conditions, the presence/absence of particular insect species attracted to a body depending on a corpse's stage of decay, along with life stage of those species present at the time a body is discovered. Although there are several forensically significant insect orders, the carrion flies of order Diptera are most often used for PMI estimation due to their rapid colonization of a corpse following death [37]. While it is possible for this method to be used to create carefully calculated estimates of PMI for extended time frames after death, it also has its limitations. Estimates using Diptera can only be made while there is flesh remaining on the corpse [38]. At skeletonization, the soft tissues used as a food source for developing Diptera larvae have either decomposed or have been completely consumed. Any remaining individuals in immature stages will either move on to find another food source in close proximity, go into stress-response pupariation [73], or parish. The technique is also limited by a multitude of

environmental and situational variables (similar to those that affect tissue decomposition), such as whether the corpse is in direct sunlight or in shade, above ground or buried below ground, and the amount of clothing the individual may have been wearing at the time of fatality [26]. Insects must have access to the corpse which becomes more difficult for certain species in the cases of burial. There is a need for expert knowledge of local insect fauna, and the developmental data for these insects at different temperatures must be known (which can make the technique geographically restricting). In addition, the hiring of an expert who also has expertise in testifying in court as a consultant can be expensive.

Previous studies have attempted to create novel and improved techniques for estimation of PMI. In cases where a body has been discovered in contact with soil or buried below ground, Benniger *et al.* [74] modified the approach taken to analyze biochemical changes that occur within tissues following death by examining fluctuations in soil elemental composition found underneath a decomposing body. Although the technique has low estimate resolution, it was found that by using the statistically significant increases in lipid-phosphorus, total nitrogen, and soil-extractable phosphorus from grave soil, a maximum PMI estimate of up to 100 days can be made. This surpasses current methods, including entomology, due to the pig carcasses in this study becoming fully skeletonized by day 14 [74]. A similar study has found that the increase of ninhydrin reactive hydrogen in the soil could also be used as a marker to estimate PMI up until day 97 [75]. Other recent attempts include the construction of a bioluminescent assay for microbial ATP. This assay can be used on external soft tissues, as well as internal organs, in order to find peaks of microbial activity that correlate with length of PMI up to 10 days [76]. Although these methods have potential, they lack needed estimate resolution and/or extension of time in which PMI estimates can be made in order to become common forensic practice.

Aiming to develop a more universal method for estimating time since death, we have applied a variation of our previous molecular-based method for estimating the age of a dried bloodstain [21, 22] to estimate the PMI of a corpse buried in a clandestine, shallow grave. In a process somewhat analogous to carbon-14 dating, where the ratio of radioactive carbon to non-radioactive carbon changes over time (due to radioactive decay of ^{14}C), the disappearance of a less stable molecule relative to the disappearance of a more stable molecule can be used to estimate the age of a specimen [39]. We have shown that differently sized segments of Ribonucleic Acids (RNAs) degrade at different rates in *ex vivo* blood samples [22], and as presented here, in postmortem tooth pulp. Longer RNAs degrade more rapidly than do shorter RNAs merely due to a function of their size. A larger RNA target has a higher probability of intercepting insults from the environment than does a small target. The differential rates of decay are used to calculate PMI, in this case, from tooth pulp. This tissue was chosen for study due to the morphology of mammalian teeth. Held within the protective outer enamel of the

tooth is found a soft tissue, tooth pulp, rich in genetic material. We theorized that the enamel of the tooth will act to maintain a fairly closed system and provide the RNA within the pulp protection from external elements: high humidity, exposure to direct sunlight, wet weather conditions, bacterial infestation, and potential insect or terrestrial scavengers.

Using quantitative Real-Time Reverse Transcription Polymerase Chain Reaction (qRT-PCR), we have determined the time-dependent change in the ratio between two differentially sized portions of β-actin mRNA molecules isolated from porcine tooth pulp. To better define the estimates produced with our method, a colorimetric analysis of pulp as it decays has also been performed. This technique does not rely upon visual analysis of the pulp, but rather on numeric values of color obtained from digital photographs of aging postmortem teeth. These two analyses can be used in combination to produce an estimate of PMI that furthers the range of time after death in which a reliable estimation can currently be made.

Most currently established indicators of PMI are influenced by environmental temperature. Taking accumulated temperature into account within our studies, as well as analysis of sample color, may lead to a more accurate and/or precise estimate of PMI. We hypothesize that RNA degradation should occur rapidly over summer months when temperatures are high; therefore winter months should show a decrease in such degradation. This measured degradation of RNA should therefore be more of a function of temperature than how long in absolute time, or time in days, a body has been deceased. Investigations to determine PMI from evidence provided by forensic entomology utilize the concept of accumulated degree days (ADD) or accumulated degree hours (ADH). Originally used by ecologists to describe levels of yearly plant growth in terms of exposure to varying air temperatures above 0^{o}C, ADD was first introduced in 1735 [77]. Entomologists apply accumulated degree days as a measure of the total amount of temperature (between an upper and lower insect viability threshold) to which a developing insect has been subjected, consequently leading to a particular point in an insect's life cycle. Between the threshold values, there is a linear relationship between temperature and developmental rate. For example, two days at 15^{o}C would be the equivalent of one day at 30^{o}C to reach the same stage of life for one particular species of insect. In the case of RNA degradation, ADD will be a sum of the total amount of temperature to which a body has been exposed in order to reach a particular degree of degradation of RNA.

The first objective of this study was to determine RNA degradation under environmental conditions that would most favor decay, the summer months. This is presented in Chapter 3.1 along with a statistical analysis of changes in color that occurred in the pulp as it aged postmortem. After this had been completed, RNA degradation and pulp coloration was monitored during the winter months to better understand the effect of temperature on these

values. Chapter 3.2 presents the findings of RNA degradation, along with color change, as a function of absolute time in days, as well as physiological time in the form of temperature units (ADD).

Methods

Burial Technique and Sample Collection

Pig heads were obtained from a local meat market, Emerick Meat & Packing (Hyndman, PA,). For the study held during the summer of 2008, 8 heads were acquired. The study held during the winter of 2008-2009 utilized 7 heads. The heads were transported to the West Virginia University Plant and Soil Sciences Farm where they were buried in a shaded area approximately 3 inches below the ground's surface in a shallow grave. Chicken wire was placed over the top of each grave and secured with tent pegs to protect samples from predation. Two teeth were randomly sampled from each pig on days 0, 7, 14, 21, 28, 42, 56, 70, 84, 98, 112, 126, and 140, as well as days 156 and 168 in the winter study. Teeth that were determined visually to be severely diseased were not collected for study.

RNA Extraction from Tooth Pulp

After extracting the teeth on the designated days, debris were washed away with cool water and antibacterial soap. The teeth were placed in a ceramic mortar, frozen with liquid nitrogen, and struck with a pestle to expose the pulp. RNA was extracted from small sections of tooth pulp using a mono-phase solution containing both phenol and guanidine thiocyanate, TRI-Reagent RT (Molecular Research Center, Cincinnati, OH). The pulp from each tooth was ground in a glass tissue grinder in the presence of 350 μl TRI-Reagent RT until no large pieces of pulp remained. The homogenate was then transferred to a 1.5 ml tube containing 650 μl of TRI-Reagent RT. After mixing by vortex, the samples were incubated at room temperature for 5 minutes. Centrifugation followed for 10 minutes. All centrifugations were performed at 12,000 x g at 4^{o}C. Approximately 950 μl of supernatant was decanted and placed into a new 1.5 ml tube. To each sample, 175 μl 1-bromo-3-chloropropane (Molecular Research Center) was added and the samples briefly mixed using a vortex. After centrifugation for 15 minutes, the aqueous phase of the samples was removed and placed in a new 1.5 ml tube. To each sample, 500 μl of cold isopropanol was added and the tubes inverted to mix. After room temperature incubation for 8 minutes, the samples were centrifuged for 5 minutes. The supernatant was removed and 1 ml of 75% ethanol was used to wash the remaining RNA pellet. The pellet was concentrated by centrifugation for 5 minutes. The ethanol was then decanted and the pellet air-dried in a fume hood for 5 minutes. To resuspend the pellet, 40 μl nuclease-free water (Fisher Scientific, Pittsburgh, PA) was added and the sample was heated for 10 minutes at 55^{o}C.

qRT-PCR Screen for Genomic DNA Contamination

DNA-specific primers and probes were designed to detect the presence of a non-transcribed portion of the porcine glyceraldehyde-3-phosphate dehydrogenase (GAPDH) gene. This screen allowed for measurement of any genomic DNA that may contaminate our RNA samples. All custom designed primer and probe combinations for Real-Time PCR were designed using Primer Express software version 3.0 and synthesized by Applied Biosystems (Foster City, CA). Primer and probe sequences can be found in **Table 2**. Two sets of primers/probes were created to amplify a 71 base pair and a separate 83 base pair region of the GAPDH gene. These amplicons were known as PGAP71 and PGAP83 respectively. Two sets of primers/probes were used so that any residual DNA found within the RNA isolates would be detected, even if a pig were polymorphic in the binding sites of one of the primers or fluorescently labeled probes. RNA samples (5μl) were run in a multiplex Real-Time PCR reaction with each of the previously mentioned primer/probe combinations in a PCR master mix having a final concentration of: 200 nM PGAP71 forward and reverse primer, 250 nM PGAP71 VIC-labeled probe, 500 nM PGAP83 forward and reverse primer, 250nM PGAP83 FAM-labeled probe, 12.5 μl of Applied Biosystems Universal PCR Master Mix, and nuclease-free water to bring the final volume of the mix to 20 μl. The Real-Time PCR reaction for each sample was run using an Applied Biosystems Prism 7300 Sequence Detection System under default conditions (1 cycle at 50^{o}C for 2 minutes, 1 cycle at 95^{o}C for 10 minutes, and 40 cycles of 95^{o}C for 15 seconds followed by 60^{o}C for 1 minute). A positive control was included in each run that contained 20 μl master mix and 5 μl porcine DNA. Negative controls were 20 μl master mix and 5 μl nuclease-free water, and 25 μl nuclease-free water. Amplification resulting in Ct values below 35 in our RNA isolates is indicative of residual DNA contamination.

Reverse Transcription

Reverse transcription of RNA samples to cDNA was accomplished through the use of Applied Biosystems' Taqman Gold Reverse RT-PCR kit. A reverse transcription master mix was created with final concentrations: 1X Taqman buffer A, 2.5 μM random hexamers, 5.5 mM magnesium chloride, and 500 μM each dATP, dCTP, dGTP, and dTTP. 57 μl of the reverse transcription mix was combined with 40 μl of RNA isolate, 2 μl of RNase inhibitor (0.8 U), and 2.5 μl of Multiscribe reverse transcriptase (3.25 U). The samples were then pulse centrifuged, placed into a Techne Touchgene Gradient thermocycler (Burlington, NJ), and run under the following conditions: 25^{o}C for 10 minutes, 48^{o}C for 30 minutes, 95^{o}C for 5 minutes.

qRT-PCR Quantification of RNA

Two sets of porcine-specific, RNA-specific primers and probes were created in order to amplify two separate, non-overlapping regions within β-actin mRNA. One set of primers, known as PBA71, amplifies a 71 base pair segment, while the other, PBA301, amplifies a 301 base pair segment of the same porcine β-actin mRNA molecule. Primer and probe sequences can be found in **Table 2**. The multiplex reaction was tested for efficiency using the guidelines and recommendations of Livak and Schittgen [40]. Each cDNA sample (5 μl) was run in multiplex with final master mix concentrations of: 100 nM PBA71 forward and reverse primer, 250 nM PBA71 VIC-labeled probe, 1100 nM PBA301 forward and reverse primer, 250nM PBA301 FAM-labeled probe, 12.5 μl of Applied Biosystems Universal PCR Master Mix, and nuclease-free water to bring the final volume of the mix to 20 μl. The Real-Time PCR reaction for each sample was run in duplicate using an Applied Biosystems Prism 7300 Sequence Detection System under the following conditions: 1 cycle at 50^{o}C for 2 minutes, 1 cycle at 95^{o}C for 10 minutes, and 40 cycles of 95^{o}C for 15 seconds followed by 60^{o}C for 3 minutes. A positive control was included in each run that contained 20 μl master mix and 5 μl porcine cDNA. Negative controls were 20 μl master mix and 5 μl nuclease-free water, and 25 μl nuclease-free water.

qRT-PCR Data Analysis

Cycle threshold (Ct) values were obtained by setting the Real-Time PCR baselines and thresholds according to Applied Biosystems' recommendations. These values were kept constant for all Real-Time PCR applications. Once Ct values were obtained for all samples, the data were imported into Microsoft Excel (Microsoft Corporation, Redman, WA). Applied Biosystems has determined that reported Ct values of 35 or higher are indicative of one-to-zero copies of the target RNA present in a sample [70, 71]. For this reason, any sample producing a Ct value of 35 or higher was removed from further analysis. All remaining Ct values were transformed using the $2^{-\Delta Ct}$ data conversion of Livak and Schittgen [40]. This conversion is necessitated by the fact that the Ct values are measured on a logarithmic scale. The conversion was calculated by subtracting the Ct value of the 71 bp region from the 301 bp region for all samples.

To determine statistical reasoning for the peak seen at day 21 within the resulting plot of $2^{-\Delta Ct}$ vs postmortem interval, the raw data were analyzed using a general linear mixed model appropriate to the repeated measures design from which the data were collected using JMP version 8. The factors included PMI; pig replicate, which was nested within PMI: pig (PMI); tooth, which was nested within pig replicate: (tooth (pig (PMI)); Ct values for both PBA301 and PBA71, which were both nested within tooth: (Ct (tooth (pig (PMI))); and the Ct value for either

PBA301 or PBA71 crossed with PMI: (Ct*PMI). An ANOVA of the model was performed and the multiple comparison procedure of orthogonal contrasts was used to sequentially determine if the ΔCt for any one day was significantly different from all other days as a group.

Table 2: Real-Time PCR primers and probes used to amplify porcine β-actin mRNA and GAPDH DNA.

Name	Size Amplified (bp)	Specificity	Primer/Probe Sequence
PGAP71	71	DNA-Specific	FP: 5'-GGCTGACTTGGACCAGGAAAG-3' RP: 5'-CCCTTCAAGTGAGCCTGCAG-3' Probe (VIC): 5'-AAGCCCGGGTGTCTGACTGCTCC-3'
PGAP83	83	DNA-Specific	FP: 5'-AAGTATGGAAGACGGAACCGG-3' RP: 5'-GGGACCACAGACCCAAGGT-3' Probe (FAM): 5'-AGGAGGTGGTGCTGGGACGGG -3'
PBA71	71	RNA-Specific	FP: 5'-TCGCCGCCGGTCTACA-3' RP: 5'-GCCGTTGTCGACCACGAG-3' Probe (VIC): 5'-CGCCATGGATGACGATATTGCTGC-3'
PBA301	301	RNA-Specific	FP: 5'-ACCGACTACCTCATGAAGATCCTG-3' RP: 5'-GCACTTCATGATGGAGTTGAAGG-3' Probe (FAM): 5'-CTGCCCGACGGCCAGGTCATC-3'

Colorimetric Analysis

Each tooth, once broken open, was photographed using a Leica MZ16 high-performance stereomicroscope and supporting Leica FireCam software version 1.9.1 (Bannockburn, IL). Parameters for each photo were are follows: exposure at 127 ma, gain at 3.1x, and saturation at 121%.

The coloration of exposed tooth pulp within the photos was analyzed using Adobe Photoshop version 7.0 (Adobe Systems Incorporated, San Jose, California) RGB mode. A standard for the colors red, green, and blue was photographed adjacent to each tooth to later correct for changes in indoor light intensity that may have occurred over the course of time in which the photographs were taken. Along with the 3 color standards, 3 points (pixels) were randomly selected on the exposed pulp in each photograph and color intensity values were recorded for the colors red (R), green (G), and blue (B). Pure red, green, or blue coloration of a pixel in Photoshop has an intensity value of 255 for its respective color while producing an intensity value of 0 for all others [78]. For example, the intensity values for pure red are R: 255,

B:0, and G:0. Each photograph was corrected for each color standard's deviation from pure red, green, and blue in order to standardize all photos.

Correction factors were determined by first calculating each color standard's deviation from pure red, green, or blue. For example, the standard for red (RS) in one photograph will yield three observed intensity values, one for red (RS_R), green (RS_G), and blue (RS_B) respectively. To determine the Red Correction Factors (RCFs), each color must be taken into consideration:

$$RCF_R = 255 - RS_R$$

$$RCF_G = 0 - RS_G$$

$$RCF_B = 0 - RS_B$$

The correction factors for green and blue were calculated in a similar manner where the standard being examined was always subtracted from 255 (intensity value for pure coloration) while others are subtracted from 0.

To obtain a corrected estimate of red coloration of a sample ($Sample_R$), the correction factors were added to the observed intensity value recorded for red (R_{obs}):

$$Sample_R = R_{obs} + RCF_R + RCF_G + RCF_B$$

This equation, yet again, was repeated for both observed green and blue coloration in each sample. Samples used for RNA degradation analyses were excluded from color analysis if no pulp remained to be photographed after RNA isolation procedures. The average values for each color, for each tooth, were analyzed using k-means cluster analysis (k=3). Cluster analysis was performed using JMP version 8 (SAS Institute Inc., Carry, N.C.) in order to determine statistical similarities in color between samples with varying PMIs.

ADD Analysis

In-grave temperature was recorded hourly by a PASCO Xplorer Datalogger (Roseville, CA). Ambient air temperature in the form of daily highs and lows were obtained from local weather station KMGW located approximately 1 mile from the field site at the Morgantown Municipal Airport, Morgantown, WV (**Figure 6**). All data were imported into Microsoft Excel for further analysis.

To better compare temperatures recorded within graves with those temperatures recorded from a nearby weather station, simple linear regression was utilized. The R^2 value found for both summer and winter studies allows for the calculation of the amount of variation in in-grave temperatures that can be explained by variation in ambient air temperature.

Average daily temperatures were calculated using ambient air temperatures as variables in the equation: (daily high – daily low)/2. In entomological studies, normally a base temperature (minimum threshold temperature) is subtracted from the equation above. There is a dispute among current literature as to what temperature bodily decomposition ceases to occur [79-81]. To remain as conservative as possible, a minimum threshold, or baseline, of 0°C was used. Therefore, nothing was subtracted from daily average temperatures. ADD was calculated for each sample by adding all positive values for the average daily temperatures recorded to which the samples were subjected before RNA isolation.

Figure 6: Map displaying the distance between field site and KMGW weather station. (http://maps.google.com) The location of the burial/field site at the West Virginia University Plant and Soil Sciences Farm is indicated by a red arrow (39.6447°N, 79.9349°W), while the location of the weather station that supplied environmental temperature is designated by a blue arrow (39.6420°N, 79.9163°W).

ADD Statistical Analysis

To determine whether the variables of RNA degradation ($2^{-\Delta Ct}$) and color (red, green, and blue) are more predictive of time in days or time in the form of ADD, the statistical analysis of multiple regression was performed. All statistical analysis was performed using JMP version 8. Factors in the model included: season; $2^{-\Delta Ct}$; red color; green color; blue color; pig nested within season: pig (season); tooth nested within pig: tooth (pig (season)); season crossed with

$2^{-\Delta Ct}$: (season*$2^{-\Delta Ct}$); season crossed with red color: (season*red color); season crossed with green color: (season*green color); and season crossed with blue color: (season*blue). All factors were deemed fixed, except the nested factors of pig and tooth, which were designated as random. This model was examined twice, once with the experimental variable being the PMI of samples in days and again with the experimental variable being ADD. The resulting multiple R^2 values were used to determine the variable best predicted by the model.

To formulate an equation into which known variables can be placed to determine the PMI of a particular sample, again multiple regression was utilized. Factors in the model include predictive x-variables $2^{-\Delta Ct}$, red, green, and blue, as well as the y-variable to be predicted: ADD. To better infer an estimate of PMI from collected data, two regressions were analyzed, one containing data from the summer study alone and one from winter data. Analysis of variance (ANOVA) statistics were used to determine the statistical significance of each model. The regression supplies a prediction estimate onto which a 95% confidence interval was also placed.

Chapter 3.1: Summer RNA Degradation and Color Analysis

Results

Multiplex qRT-PCR Primer/Probe Efficiency

An assumption of the $2^{-\Delta Ct}$ method (Livak and Schmittgen, 2001) of qRT-PCR analysis is that the efficiencies of the two primer/probe combinations (PBA301 and PBA71) are comparatively equal to one another in a multiplex reaction (one is not being preferentially amplified over another). Therefore, in order to obtain accurate results from qRT-PCR using this method, the efficiencies of the amplicons in multiplex were validated (slope = -0.0655) (**Figure 7**). Efficiency increases as the absolute value of the slope reaches zero.

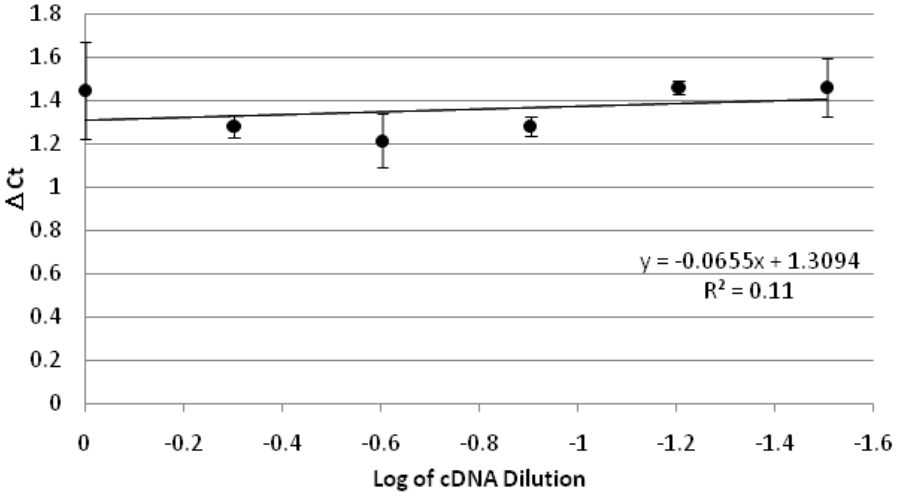

Figure 7: Multiplex qRT-PCR efficiency. To determine efficiency of the primer/probe multiplex combination of PBA301 and PBA71, the log of serial cDNA dilutions was plotted against the ΔCt (Ct_{PBA301}-Ct_{PBA71}). The absolute value of the slope determines the efficiency of amplification of each primer/probe combination during a multiplex Real-Time reaction. Bars represent standard errors where n=36.

Analysis of Genomic DNA within RNA Samples

Using two different sets of primers/probes for porcine GAPDH, genomic DNA contamination within RNA isolates was assessed. The RNA isolates from porcine dental pulp were considered to be free of residual DNA if the resulting Ct value from Real-Time PCR using DNA-specific primers and probes was 35 or above. Samples with Ct values above 35 would contain minute concentrations of DNA that are beyond the limits of detection of sensitive Real-

Time PCR technology [70, 71]. All isolated RNA samples were deemed clear of DNA (results not shown) and ready for downstream reverse transcription and subsequent Real-Time PCR applications.

Postmortem Pulp RNA Degradation

RNA degradation was determined with the use of qRT-PCR. The Ct values obtained from each sample were analyzed using the data conversion $2^{-\Delta Ct}$ (**Figure 8**). The higher the value of $2^{-\Delta Ct}$, the more alike the concentration of the small and large portion of β-actin mRNA in the samples for any given time point (known PMI) in the study. As this value decreases, differential degradation is seen where the large portion of the molecule is found in much lower quantities than the smaller, more stable portion of the RNA molecule.

Figure 8 illustrates a significant loss of the larger, 301 bp segment of β-actin mRNA over time in comparison to the smaller, 71 bp portion. Although samples were collected for 168 days postmortem, it was found that by using these particular primers/probes for multiplex qRT-PCR analysis, comparisons in degradation can be made for 84 days during the summer months in Morgantown, WV. After this time, the larger RNA target, the 301 bp portion of mRNA, was no longer present in concentrations great enough to be detected by Real-Time PCR.

The regression seen in **Figure 8** is interrupted at a PMI of 21 days. To better understand the occurrence of this peak, an ANOVA was run to determine statistical differences of the Ct values for each PBA301 and PBA71 over time. The results of the ANOVA suggest that the difference between Ct values was statistically significant for at least one day over the course of experimentation ($F = 119.6691$, $p = <0.0001$). A multiple comparison procedure in the form of orthogonal contrasts was used to determine that day 21 is statistically different from all other days as a group. Raw data (**Figure 9**) exhibited Ct values for PBA301 and PBA71 that began to separate from one another through days 0, 7, and 14. This can be seen as the larger, 301 bp region of β-actin degrades more quickly than the 71 bp region, represented by an increase in Ct value. As seen in **Figure 9**, between day 14 and 21, Ct values for PBA301 did not continue to rise as sharply as previously, while during this same time interval, Ct values for PBA71 suddenly started to increase. After day 21, Ct values for PBA301 yet again began to rise and further separate from PBA71 through day 84.

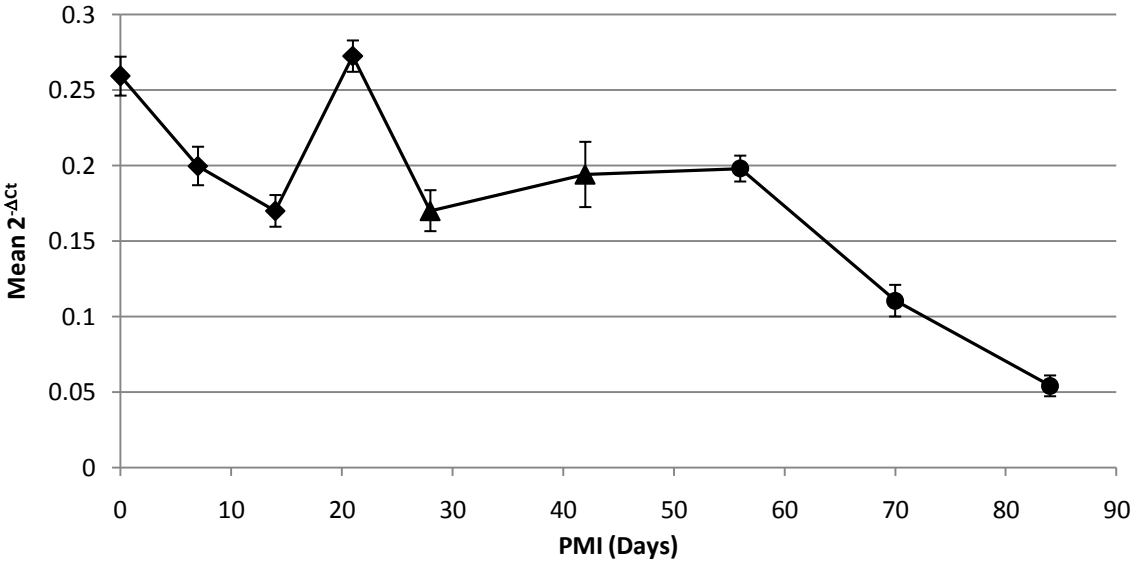

Figure 8: RNA degradation within aging postmortem dental pulp. Differential RNA degradation in dental pulp over time as shown after statistical analysis using the $2^{-\Delta Ct}$ conversion. The regression represents the differences in degradation of a 301 bp and a 71 bp region of porcine β-actin mRNA extracted from postmortem dental pulp over 84 days. Error bars represent standard error where n=192. Each point is represented by one of three different shapes determining if that particular age was later assigned to cluster #1(●), cluster #2 (◆), or cluster #3 (▲) during multivariate k-means cluster analysis of color.

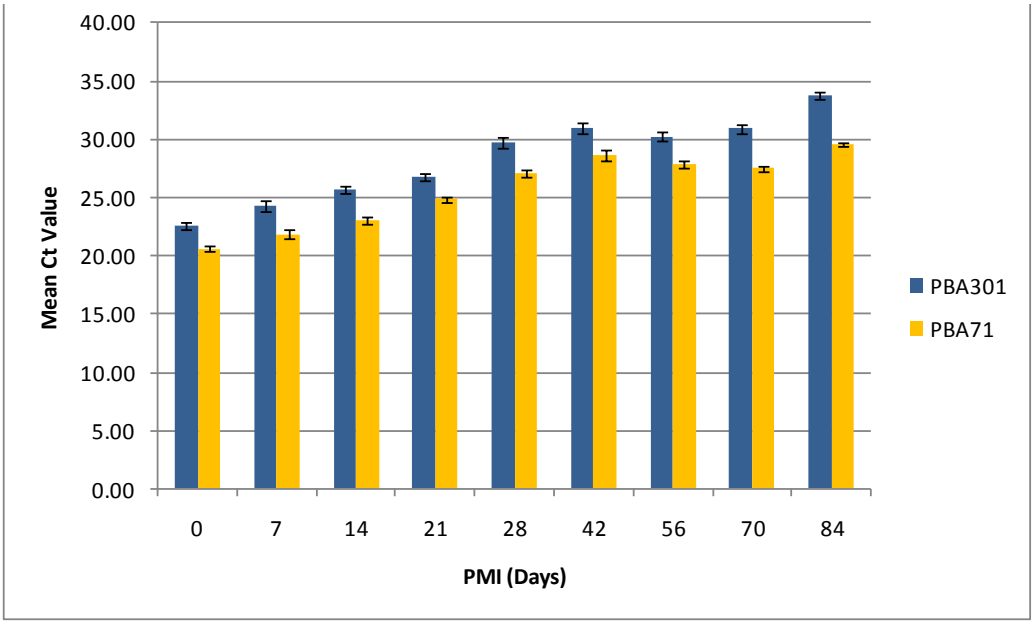

Figure 9: Fluctuation of small and large amplicons within postmortem tooth pulp. To better compare rates of degradation, mean Ct values for both the 301 bp (large) segment and the 71 bp (small) segment of porcine β-actin mRNA are presented. Error bars show standard error where n=192.

Colorimetric Analysis of Pulp Decomposition

Using the PBA301 and PBA71 set of Real-Time PCR primers/probes, there was reduced resolution between days 14, 28, 42, and 56 (**Figure 8**). This is noticeable in the flattened area of the regression. Upon revealing the pulp from each tooth for isolation of RNA, morphological changes in the pulp as it aged was observed. Some of these changes in pulp coloration and/or texture correspond to the aforementioned interruptions and flattened areas seen in the regression. In order to determine if a correlation exists between increasing PMI and morphological changes within the pulp as it ages, an analysis of aging pulp color was performed.

Visual analysis of the dental pulp recovered from aging teeth revealed four morphological stages. These stages were similar to those seen and described previously by Duffy *et al*. [82]. In the early stages of the study, the pulp was deep red in coloration and its texture was rubbery. As the pulp aged, it began to lighten in color and became more semi-solid in nature. This occurred by day 21 of the study. By day 42, pulp lost coloration (became white) and became more powder-like. In the later stages of our study (days 70 and beyond), the pulp became yellow/brown and was a hard solid that adhered to the inner canal of the tooth. This visual analysis of pulp morphology and color is a subjective measure. To obtain a quantitative measurement of color, digital photographs of the pulp from each tooth were taken and analyzed under the RGB setting of Adobe Photoshop.

A quantitative measure of color was obtained for red, green, and blue from three randomly selected pixels of the photographed pulp of each sampled tooth. The mean corrected color values for each tooth at varying ages postmortem was then subjected to k-means cluster analysis. Three clusters were found with means presented in **Table 3**. From this table, we see that samples that have a low value of red and intermediate values of green and blue were placed into cluster #1. Cluster #2 consisted of samples with an intermediate value of red, and low values of green and blue. Finally, samples with high values for all color measures were placed into cluster #3.

Table 3: Mean color values for each cluster determined by k-means cluster analysis. Three pixels from the photograph for each aging tooth's pulp were analyzed for a numerical value of color using RGB mode in Adobe PhotoShop. The values for each color (red, green, or blue) were averaged together for each tooth. These values, after being subjected to multivariate cluster analysis using k-means lead to the division of the data into three clusters of color. The means of the clusters are presented, along with cluster standard deviations in parentheses, where n=114.

Cluster	Red	Green	Blue
1	236.841 (SD 16.919)	202.159 (SD 16.113)	156.841 (SD 30.093)
2	243.696 (SD 9.044)	151.933 (SD 16.198)	120.993 (SD 25.321)
3	268.148 (SD 17.506)	245.049 (SD 19.391)	221.099 (SD 33.925)

The ages of pulp samples that fell into each cluster based on color is shown in **Table 4**. As mentioned previously, the pulp of samples collected at early stages postmortem were deep red in coloration. This is statistically shown as the majority of samples (71%) from days 0, 7, 14, and 21 fall into cluster #2 with a high degree of red compared to green and blue. The next stage of visual decomposition began when pulp lost coloration and became pink-to-white. This describes cluster #3. Cluster #3 includes 78% of samples from days 28 and 42. At later stages of decomposition, pulp became more yellow to brown in coloration. This is shown in cluster #1, where the lowest values of red and blue are present. This final cluster included the majority of samples (64%) taken from pulp with a PMI of days 56, 70, and 84.

Table 4: Contingency table - Teeth by age sorted into clusters using multivariate k-means cluster analysis. After sorting dental pulp samples into color clusters, the ages of the samples falling into each cluster was analyzed. The number of teeth from each age group (PMI) that fall into each of the three identified color clusters is presented. Italicized numbers are those samples correctly placed into a specific cluster.

	PMI								
Cluster	**0**	**7**	**14**	**21**	**28**	**42**	**56**	**70**	**84**
1	2	1	4	3	2	3	*9*	*10*	*8*
2	*12*	*13*	*7*	*7*	4	0	1	1	0
3	2	0	0	0	*5*	*11*	6	1	2
TOTAL	16	14	11	10	11	14	16	12	10

Discussion and Conclusions

The results of the presented study show measurable changes that occur within postmortem dental pulp that correlate with length of time following death. Evidence as to the predictable nature of mRNA degradation within the pulp as it ages was exhibited. Further analysis of morphological changes that occur within the pulp, color variation in particular, was also shown to be measurable and vary as experimental samples age. Further research will be required for a better understanding of RNA degradation over time, but this preliminary study has provided results that can be strengthened as more experimental variables are examined. Although not always completely discriminatory, both RNA degradation and pulp color showed constant variation over the duration of the study. This led us to believe that these variables have value in the determination of PMI for extended periods of time.

As mentioned previously, current PMI indicators are useful for no longer than a period of approximately four days, with the exception of forensic entomology. The use of entomology within our study would have provided estimates for a longer period of time than other currently accepted methods utilizing biochemistry, but would have decreased in its power of estimation after day 28 when the pig heads became completely skeletonized. At this stage of decomposition, insect activity drops significantly [38]. The primers/probes utilized here for qRT-PCR allowed for quantification of two differently sized regions of the same β-actin mRNA molecule for 84 days. The use of RNA degradation analysis of dental pulp in this study tripled the amount of time in which a reliable estimate of PMI could be calculated.

The regression seen in **Figure 8** is interrupted by a peak that presented itself at day 21. This peak in particular occurred at a morphological transitional stage in the coloration and texture of the aging dental pulp. As to the exact reason that Ct values changed at this point postmortem, we can only speculate at this time. Perhaps it was brought about by a change in the enzymes being released by the decomposing tissue or by other chemical products of degradation that were not present up until this point. An influx in bacterial load within the pulp could also play a role in RNA degradation at this point in time.

To determine how closely changes in morphology are related to RNA degradation in postmortem dental pulp, a color analysis was performed. Morphological changes in the pulp as it ages have been observed in the past, but only as a qualitative measure [82]. We have provided a means of obtaining a quantitative, numerical value for color observation. These values can be analyzed in a short amount of time and can be used to partition the results of RNA degradation analysis (**Figure 8**). Not all samples were placed into their correct cluster based on color alone (between 64% and 78% were placed correctly), demonstrating that this type of colorimetric assay does not have a sufficient power of discrimination to determine PMI on its own. The combination of the results from these two experimental variables (RNA

degradation and colorimetric analysis) can be used together to produce a more precise estimate of PMI that neither could provide if used alone.

This preliminary study can be expanded upon to further increase the accuracy of an estimate of PMI made by this method. Further experimental variables that the authors would like to pursue include analysis of the effect of temperature on the degradation of RNA in dental pulp. This would include adding an accumulated degree day model to additional summer studies, along with corresponding studies for the winter months. Another variable of interest includes RNA degradation analysis of different types of RNA, including ribosomal RNAs. In previous studies presented by our laboratory to determine the time since deposition of bloodstains, we have shown that 18s ribosomal RNA is more stable than labile β-actin messenger RNA [21, 22]. If these two species of RNA were to be used in combination in the detection of RNA degradation within postmortem dental pulp, it is hypothesized that the span of time following death in which an estimate of PMI could be made would be greatly extended.

In conclusion, although this method of PMI estimation is in its early stages, we foresee several advantages over existing and previously proposed techniques, the strongest estimator being entomology. Advantages of our method include that it remains viable long after the flesh of a body has been consumed and can be used on specimens collected anywhere in the world. These improvements give our technique an advantage over entomological practices where knowledge of local insect fauna and these species' growth curves as a function of temperature is a necessity. The proposed method is not subject to environmental limitations to the degree of current estimators. Being as close to a closed system within mammals that can be re-sampled without compromising the RNA-rich tissue inside, dental pulp is protected from many external conditions such as high humidity and insect scavengers. In addition, processing of samples is less expensive than hiring a board certified forensic entomologist.

Chapter 3.2: Summer and Winter RNA Degradation, Color, and ADD Analysis

Results

Comparison of Environmental Versus In-Grave Temperature for the Calculation of ADD

To better understand the relationship between environmental temperature readings and the actual temperature below ground in the shallow graves of our subjects, a simple linear regression analysis was performed (**Figure 10**). In-grave temperature was much more predictable in summer months (**Figure 10A**), where approximately 76.6% of the variation in temperatures below ground can be explained by fluctuations in environmental temperature. Below ground temperatures were much less predictable in the winter (**Figure 10B**). In the winter months, a positive relationship still existed between environmental temperature recordings and in-grave temperature, but variation in ground temperature was explained to lesser degree (only 19.4%).

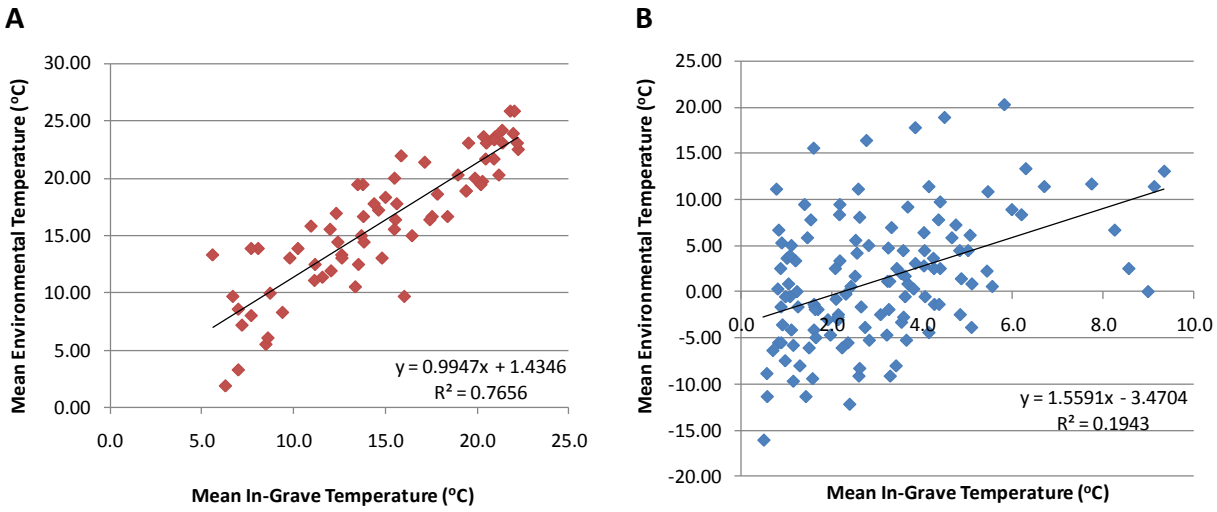

Figure 10: Regression of environmental temperature and in-grave temperature by study season. To determine the degree of association between temperature measurements collected from a local weather station and those obtained from in-ground dataloggers, linear regression analysis was employed. Environmental temperatures during the (A) summer months (R^2=0.7656) were more predictive of actual ground temperatures than those recorded during the (B) winter months (R^2=0.1943).

RNA Degradation as a Function of Time in Days or Temperature in ADD

RNA degradation was hypothesized to be better described as a function of the amount of temperature to which a sample was exposed than to the amount of time that has passed since death. Although the best source to calculate ADD for these studies was most likely in-grave temperature that has accumulated since the time of death/burial, this type of data will not be readily available to crime scene authorities at the time a body is discovered. Data in the form of past temperatures from local weather stations will be more likely. ADD calculated from ambient air temperatures recorded one mile from our field site was used as an alternative for grave temperatures. RNA degradation is shown in **Figure 11** as a function of either PMI calculated in days (**A**) or PMI calculated in ADD (**B**). It should be noted that RNA concentration was no longer measurable in the summer study after 84 days, or 1,377.5 ADD, due to complete loss of the large, 301 bp fragment. The winter study ended at day 126, or 407.8 ADD, not due to RNA loss, but because all teeth from all pigs had been extracted by this date. In **Figure 11A**, it is apparent that RNA degradation, displayed in units of $2^{-\Delta Ct}$, can be measured for longer periods of absolute time in the winter than during the summer months. The low value of RNA degradation seen in the summer at day 84 was never reached in the winter study, even though RNA degradation had been measured until day 126. When RNA decay was plotted against time in ADD (**Figure 11B**), patterns of degradation align. The same approximate amount of RNA degradation is reached by both sets of pigs, summer and winter, after reaching approximately 400 degree days.

To statistically determine if RNA degradation and color analysis better describe time in days or ADD, a multiple regression analysis was performed. The resulting multiple R^2 values of the model were higher when ADD was used as the variable to be predicted (R^2=0.7759), than when time in days were predicted (R^2=0.5066). The higher R^2 designates which of the two variables were better explained by the known numerical values of RNA decay and color.

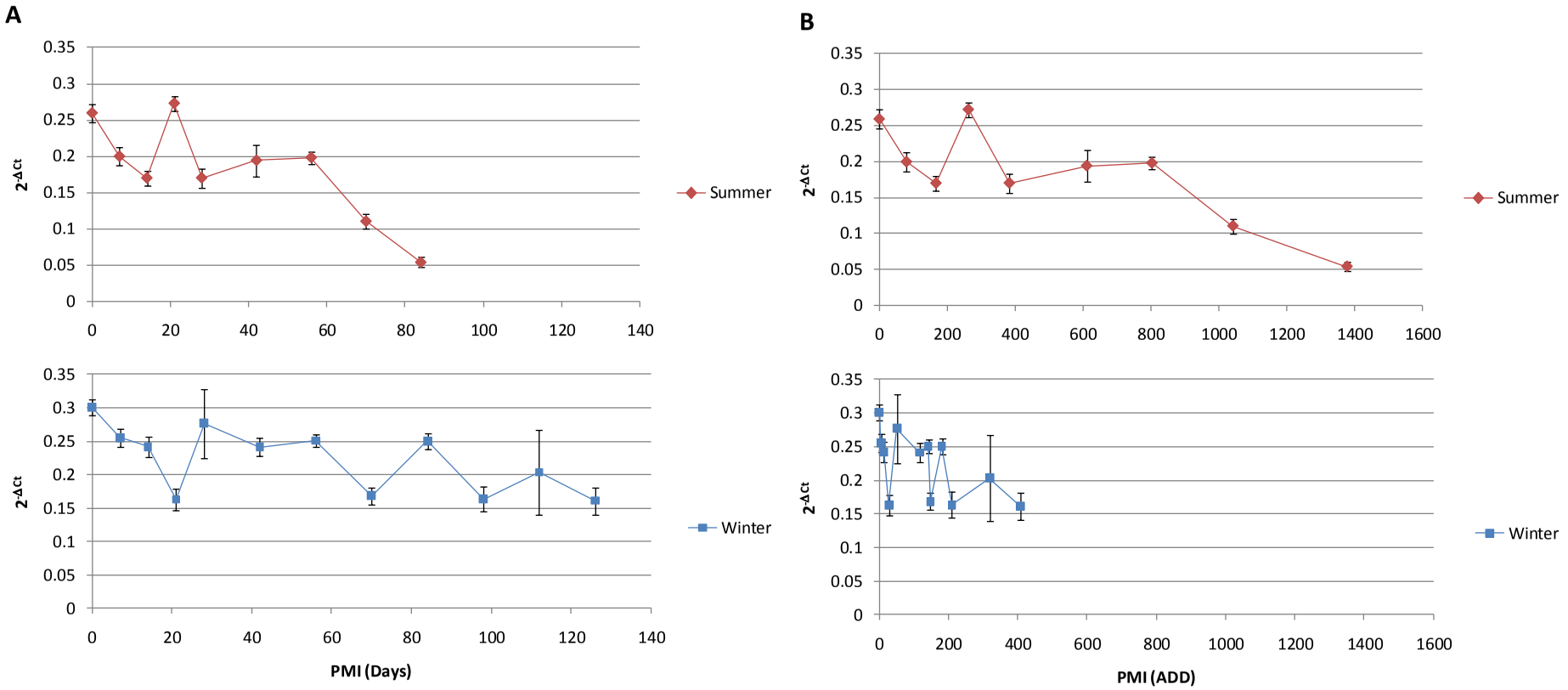

Figure 11: RNA degradation by season as a function of time in days as compared to accumulated degree days. Differential RNA degradation of a 301 bp and a 71 bp region of porcine β-actin mRNA from postmortem dental pulp after $2^{-\Delta Ct}$ conversion is displayed. RNA degradation data are plotted by (A) absolute time in days, as well as by (B) physiological time in ADD. Error bars represent standard error where n=192 for the summer study and n=288 for the winter study.

Constructing an Equation to Estimate PMI from RNA Degradation and Analysis of Color from Postmortem Tooth Pulp

To prepare an equation for the prediction of PMI in the form of ADD using our method, multiple regression was employed. Due to the variation that has been identified between environmental and ground temperature during the winter season, two different predictive equations for PMI were formulated: one for bodies discovered during the summer months, one for winter months. A 95% confidence interval was fitted to each equation. **Figure 12** shows the JMP output for each model, **(A)** summer and **(B)** winter, along with corresponding ANOVA tables.

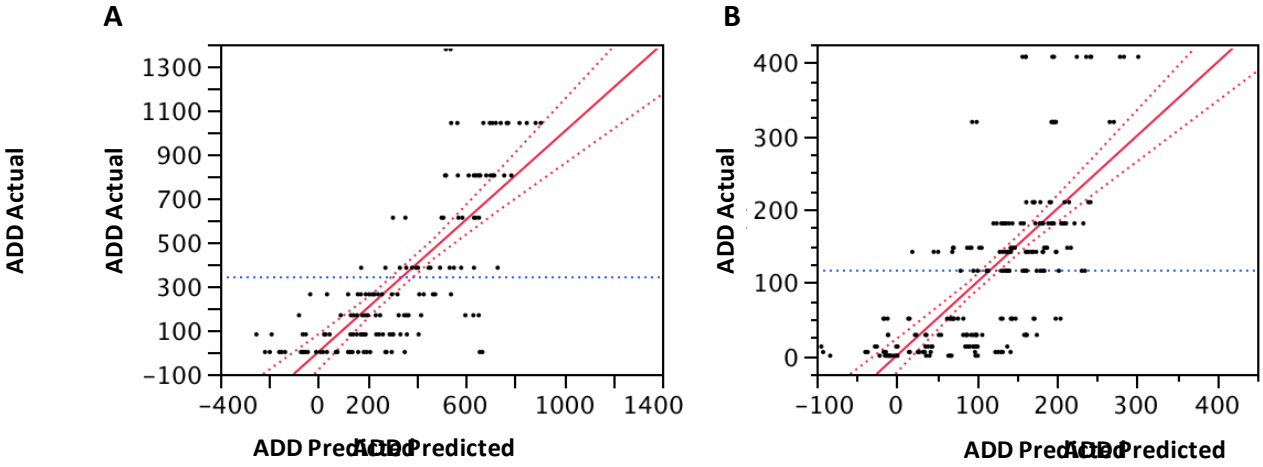

Source of Variation	df	Sum of Squares	F	p
$2^{-\Delta Ct}$	1	1,676,970.5	31.9653	<0.0001
Red Color	1	2,569,049.5	48.9695	<0.0001
Green Color	1	3,919,053	74.7024	<0.0001
Blue Color	1	266,457.6	5.0790	0.0256
Error	153	8,026,718		

Source of Variation	df	Sum of Squares	F	p
$2^{-\Delta Ct}$	1	12179.2	1.9035	0.1688
Red Color	1	15222.6	2.3791	0.1241
Green Color	1	1067268	166.8001	<0.0001
Blue Color	1	3000.1	0.4689	0.4941
Error	275	1759583.1		

Figure 12: JMP multiple regression analysis and corresponding ANOVA table for models predicting ADD. To construct predictive equations to estimate ADD from the known variables of RNA degradation and color, multiple regression analysis was performed in JMP. Results for each model, (A) summer and (B) winter, are shown. The horizontal blue line indicates the mean of actual ADD measurements for all samples within the model. The solid red line in each graph represents the modeled space where predicted ADD and actual ADD are equal. Dashed red lines indicate confidence limits. Below each graphical representation are the ANOVA results for each factor within the model. Factors were considered to significantly affect the prediction of ADD if p-values of less than 0.05 were reported.

It can be seen from the ANOVA table in **Figure 12A** that each factor played a significant role in the statistical model to predict ADD during the summer months, as each had a p-value below 0.05. The predictive power of the model, the R^2 value, for the summer equation is 0.5876. In the predictive model for winter months (**Figure 12B**), only one variable was considered to be significant in explaining ADD. For our winter model, the main predictive variable was green coloration of the pulp as it ages. All other factors are considered non-significant, yet were kept in the predictive equation due to the very small amount of variation that they explain. Using only green coloration in the model predicting ADD in the winter provided a multiple R^2 of 0.5064. By including RNA degradation, the R^2 value of the model increased marginally to 0.5095. By adding the red and blue coloration as well, the R^2 value increased to 0.5141.

In the summer months, the following equation was produced to predict the ADD that a sample must have been subjected to in order to reach the observed level of RNA degradation and coloration:

$$ADD = (1395.729 + (-1375.106*2^{-\Delta Ct}) + (-9.033*Red) + (8.094*Green) + (-1.747*Blue)) \pm 456.238$$

When a body is found in the winter months, ADD can be calculated for a particular PMI through the use of the following equation:

$$ADD = (-131.455 + (-49.563*2^{-\Delta Ct}) + (-0.346*Red) + (1.788*Green) + (0.089*Blue)) \pm 158.453$$

To determine PMI from the calculated value of ADD, a temperature history of the site in which the body was found is needed. Starting with the day the body was found, add daily average temperatures from previous day until the calculated ADD of the lower 95% confidence interval is reached. This provides lower limit of the PMI estimation range. The process is repeated for the calculated ADD of the upper 95% confidence limit. This value will give the upper limit of the estimated range of PMI. **Tables 5** and **6** hold estimates of PMI calculated using the provided equations for summer and winter respectfully.

Table 5: Estimates of ADD and PMI for randomly selected samples obtained during summer analyses

Subject	Actual ADD	Predicted ADD	Actual Date of Death	Predicted Date of Death Lower 95%	Predicted Date of Death Upper 95%
1	0	-216.87	3/25/2008	2/2/2008	3/25/2008
2	167.22	-82.89	3/25/2008	2/4/2008	4/8/2008
3	803.06	520.41	3/25/2008	2/9/2008	5/15/2008
4	803.06	516.33	3/25/2008	2/20/2008	5/16/2008
5	1041.67	672.36	3/25/2008	3/10/2008	5/23/2008

Table 6: Estimates of ADD and PMI for randomly selected samples obtained during winter analyses

Subject	Actual ADD	Predicted ADD	Actual Date of Death	Predicted Date of Death Lower 95%	Predicted Date of Death Upper 95%
1	5.0	-91.72	11/18/2008	11/2/2008	11/25/2008
2	12.5	36.08	11/18/2008	10/30/2008	12/2/2008
3	12.5	-93.94	11/18/2008	11/5/2008	12/18/2008
4	115.83	138.74	11/18/2008	10/30/2008	12/20/2008
5	147.22	217.49	11/18/2008	10/7/2008	12/27/2008

The large values used to place a 95% confidence interval around estimates do at times make for rather large approximations of PMI. This of course depends on the magnitude of daily temperatures recorded for the days prior to the discovery of a body.

Discussion and Conclusions

The results of this study show that measureable changes in postmortem tooth pulp can be used to estimate PMI. They also describe the significant effect of temperature on the predictive values of RNA degradation and colorimetric analysis.

Temperature was thought to play a significant role in the degradation of RNA in porcine tooth pulp. Before analyses could be run to determine if RNA degradation and color analysis would better predict time in days or time in the form of accumulated temperature, we were interested in determining which type of measure of temperature should be considered for ADD analysis, in-grave temperature or environmental air temperatures. Although the use of in-grave temperatures for analysis would most likely produce more accurate estimates of PMI, they are not measurements that would be readily available to those processing the crime scene. The most common form of past weather recordings are those of environmental air temperatures, which can be easily obtained from local weather stations. The results of comparisons of recorded in-grave temperature and environmental temperature show a close relation of these two variables during the summer months (R^2=0.7656). The use of ambient air temperature to calculate ADD for estimations of PMI should produce estimates of actual PMI that are rather accurate during the summer. This relationship is very different during the winter (R^2=0.1943), which may be due to freezing of the topsoil at some time during these months. Once the ground has frozen, it is likely that grave temperatures will not fluctuate with minor changes in environmental temperature to the same degree in which was seen during the summer. The authors recognize that this phenomenon may negatively affect the precision of estimates of ADD made with ambient air temperatures in the winter, but have chosen this measurement for ease of acquiring information over exactitude at this time.

When tracking RNA decay over time, two differently sized portions of the same β-actin mRNA were analyzed. Although samples were collected from pigs in the summer study for 140 days, the larger portion (301 bp) of RNA could no longer be amplified by Real-Time PCR after day 84 in the summer, making calculation of $2^{-\Delta Ct}$ impossible after this point in time. Winter studies were completed on day 126 after all teeth had been sampled. The level of RNA degradation seen in the summer study was never reached in the winter. It is feasible to speculate that RNA would still have been detected in samples older than day 126 in winter, if teeth had still been present to sample. The vast differences in RNA degradation between seasons, based on time in days, leads us to believe that temperature plays a major role in the degradation of RNA in postmortem pulp. When the same RNA degradation measurement, $2^{-\Delta Ct}$, is plotted by ADD, in place of time in days, it can be seen that although the winter study occurred over a longer period of absolute time, it did not contain the range of ADD covered in the summer study. In fact, at approximately 400 degree days, both studies had reached the same the level of RNA degradation. These results, along with results of multiple regression

analysis, gave evidence that PMI estimations made using our technique should utilize time in the form of temperature, not time in the form of days.

The models into which the preceding data were fit allowed for the creation of predictive equations to derive ADD. Upon further analysis of the ANOVA accompanying each model, it can be seen that numerical values of color are significant indicators, as well as RNA degradation, to the prediction of ADD in summer months. This is intuitive as all four measurable variables ($2^{-\Delta Ct}$, red color, green color, and blue color), vary throughout the tooth pulp degradation process. In the winter study, the only variable of significance is green color. As very little measurable changes occur in pulp at relatively low temperatures, it is understandable that RNA degradation was not considered to be significant. Through visual analysis alone, the red color of pulp at early ages did not seem to differ greatly from pulp of older ages as well. All factors remained within the equation for estimation of PMI in the winter, regardless of significance level reported from the ANOVA, in hopes that what little variation they could explain would be helpful to the predictive power of the model.

Upon the discovery of a corpse within a shallow grave, PMI can be estimated using the described method by measuring two factors: RNA decay and the quantification of color from postmortem tooth pulp. Results from qRT-PCR would be in the form of $2^{-\Delta Ct}$. Color values can be obtained from a digital photograph of the same tooth sampled from the body for RNA analysis. These values would then be inserted into one of two equations based on the time of year the body was unearthed. The resulting values are the amount of time in temperature needed to reach this sample's specific stage of decomposition. Starting with the calendar date of the body's discovery, adding all positive daily average temperatures of the past days, until the value determined by the equation is met, will provide the estimate of PMI. By determining the upper and lower confidence limits provided by the equation, the estimate provided is expected to be accurate 95% of the time it is utilized.

Some estimates of PMI using this method will be more precise than others. Higher temperatures of the days prior to the estimates make for smaller values of ADD needed to satisfy confidence intervals. There are other ways in which the authors feel that estimates can be made more precise. The presented study utilized one pair of RNAs to compare by $2^{-\Delta Ct}$. By developing multiple sets of primers to detect other differently sized pairs of RNAs to add to the prediction model, this may produce estimates with smaller confidence intervals. We have shown in the past that portions of RNA of longer lengths degrade more quickly than shorter sections of RNA. In bloodstains, we have shown that different species of RNAs degrade at different rates, 18s rRNA being more stable than β-actin mRNA [22]. By creating different combinations of RNA species of various lengths for study, then incorporating the results into the model, it is possible to better estimate time since death.

This study has characterized the effect of temperature on postmortem changes in RNA degradation and coloration of porcine dental pulp in order to estimate PMI. By studies performed at both high and low environmental temperatures, it has been determined that temperature plays a major role in either progressing or retarding the stages of RNA decomposition and the morphology of tooth pulp. These observed changes are more related to temperature, than to absolute time in days. With a better understanding of the stages of decomposition of RNA and coloration that occur in postmortem tooth pulp, an assay to estimate the accumulated temperature to which samples had been exposed in the form of ADD has been illustrated. By estimating ADD, this can be used to determine the PMI of a certain individual. Although information can be gained through the use of this analysis in temperate regions, where estimates can be made for longer periods of time than present estimators, its best use at this time may be in locations in which warm ambient temperatures dominate the climate.

Chapter 4: On-Site Body Fluid Identification to Reduce DNA Backlog

Introduction

Due to the popularity of forensic-based television programs, the general public has come to hold several misconceptions about the way forensic evidence is collected, processed, and delivered in court. Many believe that physical evidence, including DNA evidence will be found at every crime scene. Also, the amount of time required to process physical evidence is gravely underestimated. These misconceptions become problematic when those who believe these falsities as fact are called upon to serve jury duty. If DNA evidence is not presented, or presented in a form that jurors do not expect (for example, "inconclusive"), confusion arises. This "CSI effect" among jurors, combined with technological advances that allow for DNA to be extracted from decreasingly small samples of biological evidence, has inadvertently affected the way crime scenes are processed [83]. In hopes of providing jurors with concrete DNA evidence, the number of items that are being collected as potential evidence is increasing, which in turn, has added to the predicament of DNA evidence backlog among crime laboratories.

The National Institute of Justice (NIJ) has recently published a special report in order to better inform the forensic community of an exact definition of case/evidence "backlog", as well as to provide an explanation of how the problem is evolving. According to NIJ, a backlogged case is "one that has not been tested 30 days after submission to the crime laboratory" [84]. A figure within this report, **Figure 13**, shows that the number of cases completed by crime laboratories annually has been increasing since 2005. The general problem is that the number of cases presented to crime laboratories each year is also rising. Although more cases are being completed, there is still an increasing number of new cases remaining unfinished that are carried on to the next year as backlog [84].

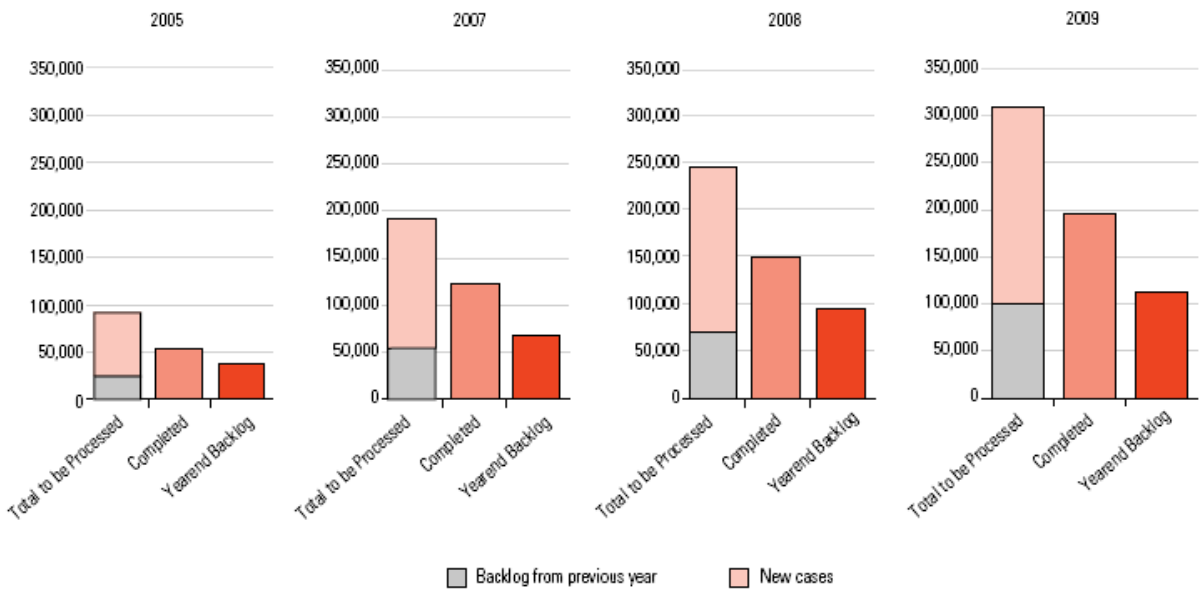

Figure 13: DNA casework trends: supply, demand, backlogs (Nelson, 2011). The number of cases presented to participating United States' crime laboratories each year from 2005 to 2009 is shown. Excess cases that fail to be processed are carried over into the following years as backlog.

One way to reduce the amount of annual backlog is to decrease the number of pieces of potential evidence that are collected at crime scenes. If it were possible to definitively establish which evidence was of biological nature, as well as what body fluid is present, while still at the scene, this information could drastically reduce the amount of evidence that is taken to the crime laboratories for further processing. At present, there is one presumptive test that can identify the possible presence of blood, saliva and/or semen (the three most common biological fluids found at the scene of a crime): an alternative light source. Multiple confirmatory tests exist for both blood and semen, but these techniques usually utilize methods that cannot be performed until samples have reached a fully equipped laboratory. Confirmatory tests for blood include identification of blood cells under a microscope [41], crystal tests such as the Teichman and Takayama tests [41, 44], and ultraviolet absorption tests [43]. Semen is usually confirmed by either the presence of Christmas Tree stained sperm cells in the sample [45] or by the presence of prostate-specific antigen (PSA), which will provide a positive result even with aspermatic males [46]. Saliva, at this time, does not have a reliable test for confirmation. The total number of presumptive and confirmatory tests presently available can be found in **Table 7**. While most presumptive tests can be performed while at the crime scene, confirmation that a piece of potential evidence is biological in nature, along with determination of exact tissue-type of origin is usually performed within a laboratory setting.

Table 7: Number of presumptive and confirmatory tests for the three most common types of biological stains found at the scene of violent crimes (As reviewed in Virkler and Lednev, 2009). Presumptive tests allow for crime scene investigators to determine if biological fluids are present at a crime scene. Absolute identification of a particular type of fluid is then performed using a battery of confirmatory tests.

Body Fluid	# Presumptive Tests	# Confirmatory Tests
Blood	14	8
Semen	20	8
Saliva	9	0

Here, we describe a novel method for the confirmation of body fluid from forensic evidence that has the potential to be made portable to the scene of a crime. It consists of one assay that detects tissue-specific RNAs with the use of fluorescently-labeled probes known as molecular beacons (MBs). Due to an additional probe for human-specificity, this method can help crime scene technicians judge whether a particular piece of potential evidence should be collected or if it is not pertinent to the crime at hand.

We are not the first to propose the use of tissue-specific RNAs in the identification of body fluid. Many have attempted to use mRNAs specific to blood [12, 13, 16, 17], semen [12, 13, 17], saliva [12, 13, 16, 17], menstrual blood [11, 12, 17], and vaginal secretions [13, 17] in order to provide a means of confirmation of the presence of these bodily fluids. More recently, Hanson *et al.* has proposed the use of micro-RNAs for the identification of each of the aforementioned body fluids in forensic evidence [18]. Although promising, the one common characteristic among these techniques is the use of Reverse Transcription Real-Time PCR (qRT-PCR). qRT-PCR is an extremely sensitive technique for RNA detection, however, with current technology, also confines these assays to a laboratory. Our presented technique is distinctive in that it requires no PCR of any kind. After identification of a piece of potential evidence, RNA is obtained by means of an isolation technique that requires less than 15 minutes to perform. The extracted RNA is directly combined with the MB probes in which an increase in fluorescence should occur in the presence of one specific RNA only. The emitted fluorescence is detected by a portable fluorospectrometer no larger than a tissue box and powered by a USB connection to a laptop computer. Resulting fluorescent peaks indicate which fluid(s) is present in a sample.

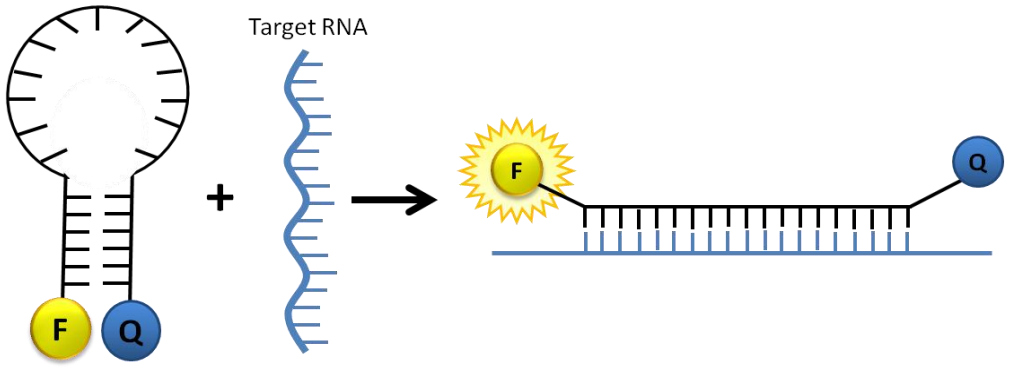

Figure 14: Structure and fluorescence of a MB in a "closed" and "open" conformation. When a MB is not in the presence of its target nucleic acid, it maintains a "closed" hairpin conformation in which the fluorophore (F) is being quenched by the close proximity of the quencher molecule (Q). Upon introduction of the target nucleic acid, here an RNA with a complementary nucleic acid sequence, the MB probe "opens" and binds to the target. Upon binding, the distance between the fluorophore and the quencher is great enough that increased fluorescence can be detected.

MBs are single-stranded nucleic acid probes that possess a hairpin shape (**Figure 14**) [54]. The probe portion of the MB is composed of bases that are complementary to a nucleic acid target, but that also do not form a complex secondary structure of their own. The stem of the MB is made up of 5-7 nucleotides of complementary sequence designed to flank either end of the probe sequence. The 5' end of the MB is linked to a fluorophore, while on the 3' end, a quencher molecule is attached. As long as the MB remains in a closed conformation, emission from the fluorophore is quenched; therefore minimal fluorescence is detected. This "closed" conformation changes when the probe is in the presence of its complementary nucleic acid target, here our tissue-specific RNA. The probe will "open" to bind to its target, which provides adequate distance between the fluorophore and quencher for increased fluorescence to be detected.

To avoid PCR, the fluorophore linked to MBs needs to be exceptionally intense. To fulfill this requirement, the fluorophore chosen was that of a Quantum Dot (QD) attached to the probe through biotin-streptavidin interactions. A QD (**Figure 15A**) is a commercially available nanocrystal composed of a core of CdSe molecules contained within a ZnS shell. These nanocrystals have a wide absorption wavelength, fluorescing under a wide range of light sources. The emission wavelengths are extremely narrow and are tunable based on the size of the CdSe core [63]. Small QDs fluoresce at low wavelengths, while increasing the size of the QD increases the emission wavelength (**Figure 15B**). This tunability allows for QDs of various diameters to emit different wavelengths, providing multiple fluorophores to later be used in

multiplex reactions (one wavelength per blood MB, saliva MB, semen MB, and human MB). As previously stated, the intensity of QDs surpasses most other commonly used fluorophores. **Table 8** presents the extinction coefficients (used to determine intensity of a fluorophore) of two common fluorophores compared to two QDs with varying emission wavelengths. QDs are much brighter, but are still quenchable within in the MB form.

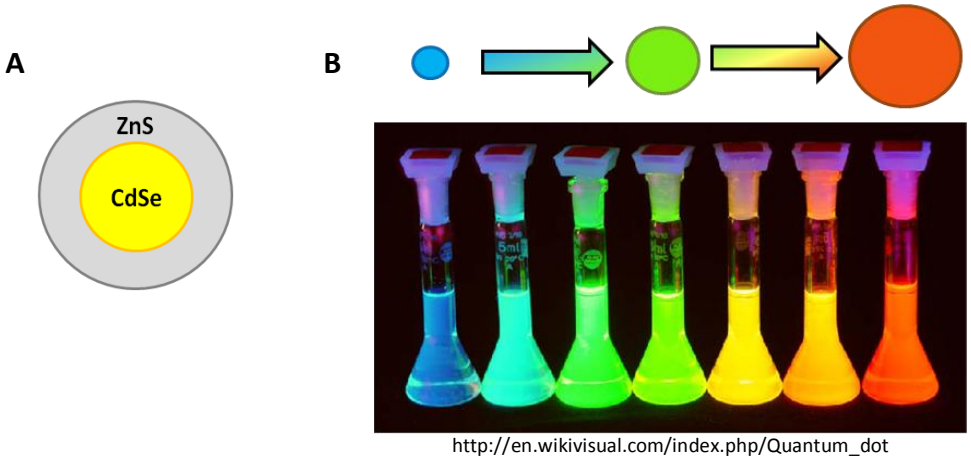

http://en.wikivisual.com/index.php/Quantum_dot

Figure 15: Structure and tunability of quantum dot nanocrystals. (A) The basic structure of a cadmium selenide QD is composed of a core of several CdSe molecules surrounded by a thin ZnS shell. The core the QD gives these fluorophores the majority of their photo-physical properties, while the shell lends towards the QD's stability. (B) [Adapted from 86] The more confined the space in which the core CdSe molecules are held, the lower the emission wavelength. Increasing the diameter of the core also increases the emission wavelength, which provides multiple fluorophores with a large Stokes shift (distance between optimal absorbance and optimal emission wavelengths).

Table 8: Comparison of fluorophore intensity. Extinction Coefficients are listed for two common fluorescent molecules, FAM and Texas Red, as well as two QDs, one from each the upper and lower range of emission wavelengths. Commercially available QDs are anywhere from 5- to 168-fold more intense than many traditional fluorophores.

Fluorophore	Emission Wavelength (nm)	Extinction Coefficient ($M^{-1}cm^{-1}$)
FAM[64]	525	74,850
Texas Red[64]	583	136,000
QD525[65]	525	710,000
QD800[65]	800	12,600,000

The objective of this series of experiments is to produce a collection of QDMBs that detect tissue-specific RNA from blood, saliva, and semen, as well as a human-specific probe that can be used in an assay to confirm the identity of the type of body fluid found in evidentiary samples at crime scenes. For the purpose of this paper, the term "tissue-specific" will be used to describe any RNA found within, or probe that detects, only one of the three tissues tested. The authors recognize that the tissue-specificity of certain RNAs or probes could change upon further experimentation with additional tissue types. Candidate RNAs are either alternatively spliced or are tissue-specific due to epigenetic factors. Once RNA candidates are determined, the assay should have the potential to be used without PCR amplification of samples, to be multiplexed, and to be made portable to the scene of a crime. The main goal for the completion of such an assay is to provide more information to a crime scene technician so that better judgment can be used as to whether a piece of potential evidence should be collected or not. This, in turn, should help to reduce the number of samples collected at crime scenes, as well as reduce the sample load of backlogged crime laboratories.

Methods

Exploration and Rationale for Tissue-Specific RNA Candidates

To determine which RNAs should be tested for tissue-specificity, a literature search was performed. Multiple potential RNA candidates for blood, saliva, and semen were determined. Candidate RNAs were established based on the criteria that each is highly expressed in a tissue of interest, is not expressed in any other tissue or tissues of forensic significance, is not a known marker for disease, and that each are either alternatively spliced or harbor introns. Alternative splice sites provide a target area for the downstream creation of a MB probe that is tissue-specific based on splice pattern. If an alternatively spliced RNA could not be found, an RNA sequence that spans an exon-exon boundary can be used to make the MB RNA-specific. To determine if a suspected biological stain is human in origin, a control RNA that would be found in all three tissue types, and in which a species-specific region could be targeted, was also sought. For this purpose, β-actin mRNA was candidate.

The candidate tissue-specific RNAs featured in this manuscript were found in literature that utilized microarray or northern blot technology. The mRNA candidate thought to be specific to blood, erythrocyte membrane protein band 4.1 (4.1R), was chosen from the work of Yamamoto *et al*., in which microarray assays were used to illustrate the presence of certain alternatively spliced 4.1R mRNAs at various times during the lifespan of an erythrocyte [87]. As for the saliva-specific mRNA candidate, epithelial membrane protein 1 (EMP1), Hu *et al*. employed mass spectroscopy and microarrays to try to characterize the diversity of RNA and proteins found in saliva [88]. From their supplementary data, multiple candidates, including EMP1, were examined for tissue-specificity. Finally, hexokinase 1 (hHK1) was selected as a semen-specific mRNA due to the work of Mori *et al.*, who used PCR-based screens and northern blots to investigate the sequence conservation across species of alternatively spliced type 1 hexokinase mRNAs thought to be testes-specific [89].

PCR-Based Screening of RNA Candidates for Tissue-Specificity

To investigate the tissue specificity of the selected target RNA molecules, a set of PCR primers was developed for each. The forward primer of each set was designed to bind to the RNA candidate at the site of the alternative splicing event that was thought to be the reason for the RNA's tissue-specificity. If the RNA was not alternatively spliced, the forward primer would span the boundary of two exons, thus reducing the chance that any residual DNA in the RNA isolates would also be a target for amplification. The β-actin forward primer spans an area of the RNA in which the sequence is less conserved across species. All primer sequences used for PCR were designed using Applied Biosystems Primer Express Software version 3.0 (Foster City,

CA). The sequences for these primers and the RNAs that they detect within each bodily fluid can be found in **Table 9**.

Total RNA was extracted from 15 μl blood, 30 μl saliva, and 30 μl semen sample aliquots using the SurePrep TrueTotal RNA Purification Kit (Fisher Scientific, Pittsburgh, PA) according to the manufacturer's protocol for each type of bodily fluid. All biological samples were obtained with a protocol approved by the West Virginia University Institutional Review Board for Protection of Human Research Subjects. The RNA isolates were reverse transcribed to cDNA for downstream PCR applications through the use of Applied Biosystems' Taqman Gold Reverse RT-PCR kit. A reverse transcription master mix was created with final concentrations: 1X Taqman buffer A, 2.5 μM random hexamers, 5.5 mM magnesium chloride, and 500 μM each dATP, dCTP, dGTP, and dTTP. 57 μl of the reverse transcription master mix was combined with 40 μl of the extracted RNA, 2 μl of RNase inhibitor (0.8 U), and 2.5 μl of Multiscribe reverse transcriptase (3.25 U). The samples were then pulse centrifuged, placed into a Techne Touchgene Gradient thermocycler (Burlington, NJ), and run under the following conditions: 25^{o}C for 10 minutes, 48^{o}C for 30 minutes, 95^{o}C for 5 minutes.

cDNA from each of the tissues of interest was used as the template material for PCR reactions with each of the previously described primer pairs. Five microliters of cDNA was added to a PCR master mix with the final concentrations: 1 μM forward primer, 1 μM reverse primer, 12.5 μl of Applied Biosystems Universal PCR Master Mix, and nuclease-free water to bring the final volume of the mix to 20 μl. The samples were pulse centrifuged, placed into a Techne Touchgene Gradient thermocycler, and run under the following conditions: 1 cycle of 94^{o}C for 5 minutes; 40 cycles of 95^{o}C for 1 minute, 54^{o}C for 30 seconds, and 72^{o}C for 1 minute; 1 cycle of 72^{o}C for 5 minutes. A negative control was also prepared for each PCR master mix which consisted of 20 μl master mix and 5 μl nuclease-free water.

PCR products and negative controls underwent agarose gel electrophoresis to observe the presence/absence of amplified bands for each tissue type. A 30 ml 1.5% agarose gel containing 1 μl 5mg/ml ethidium bromide was prepared for each primer set. Five microliters of PCR product was added to 5 μl water and 2 μl New England Biolabs Inc. Gel Loading Dye, Blue 6x (Ipswich, MA). Ten microliters of this mixture was added to each well. A 100 bp DNA ladder (New England Biolabs Inc.) was used as a reference. Gels were run in 0.5X TBE at 80V for 1.25 hours. Gels were visualized and photographed under a UV light source.

Table 9: PCR primer sequences used to detect presence/absence of RNAs from blood, saliva, and semen to evaluate tissue-specificity.

Bodily Fluid	RNA	RNA Alternatively Spliced?	Primer Sequence
Blood	4.1R	Yes	FP: 5'- AGCATGGAAGAAAAAGAGAGAAAGA -3' RP: 5'- TCTTCACCAGGGGAGGTCCT -3'
Saliva	EMP1	No	FP: 5'- ACCCTTCAGAACTCTCTTTGCTCA -3' RP: 5'- AACGCCGATGATGAAGCTG -3'
Semen	hHK1	Yes	FP: 5'- GCAAGGACAGTGCGTTCAAGA -3' RP: 5'- CCGCATGGCATAGAGATACTTG -3'
Blood/Saliva/Semen (Human-Specific)	β-actin	No	FP: 5'- CCATCCATGTACGTTGCTATCCAGGCTGT -3' RP: 5'- GCAGCCGTGGCCATCTC -3'

Synthesis of Quantum Dot-Conjugated Molecular Beacons

Molecular beacons were synthesized according to established protocols for streptavidin-biotin-linked MBs [90] with few modifications. 2'-O-Methyl-RNA oligonucleotides modified with an Iowa Black quencher on the 3' end and a 5' biotin linker were obtained from Integrated DNA Technologies (Coralville, IA). The sequence of each oligonucleotide was designed to incorporate the complementary sequence of the forward primer used in the previous PCR-based screen. Six nucleotides of complementary sequence were designed to flank either end of the oligonucleotide to create the stem portion of the MB. Streptavidin-coated QDs were obtained from Invitrogen Corp. (Carlsbad, CA). The sequence for each MB oligo, the emission wavelengths of the QD label, and the corresponding quencher molecule used for each body fluid can be found in **Table 10**. To link the QDs to the MBs, 100 pmol of streptavidin-coated QDs, 1 nmol of biotinylated oligonucleotide, and 40 μl 10mg/ml BSA (New England Biolabs Inc.) were combined in a 1.5 ml eppendorf tube. Phosphate-buffered saline (PBS) was used to bring the volume to 400 μl. The reaction mixture was allowed to incubate at room temperature for one hour. Linked QD-modified MBs (QDMBs) were separated from unbound oligonucleotides and QDs using a 50kDal Amicon Ultra spin filtration system (Millipore Corporation, Billerica, MA). All centrifugations were performed at room temperature at 7,000 x g unless otherwise noted. The membrane of the Amicon spin column was first prepared by the addition of 100 μl of PBS and centrifugation for one minute. The reaction mixture was then added to the spin column and centrifuged for 5 minutes. The flow-through was discarded as the QDMBs were retained on the filter membrane. The column was washed twice by the addition of 400 μl PBS and centrifugation for 5 minutes. The QDMBs were removed from the membrane by placing the spin column upside-down in a collection tube and centrifuging for 2 minutes at 1,000 x g. The final concentrate was resuspended in 400 μl PBS.

A modification of the original protocol was used in which the QDMBs were then filtered through a 100kDal Amicon Ultra (Millipore Corporation) using the manufacturer's protocol to further remove any unbound reactants. The final product was then further concentrated by one 10 minute spin at 14,000 x g in a new 50kDal Amicon Ultra. The final retainate was brought to a total volume of 100 μl and stored at 4°C until further use.

Table 10: 2'-O-Methyl-RNA oligonucleotide sequences including the QD and Iowa Black Quencher to which it was conjugated. Underlined portions of MB sequences represent the complementary nucleotides that will form the stem of the MB in secondary structure.

RNA	QD	Iowa Black Quencher	MB Oligonucleotide Sequence
4.1R	585 nm	FQ	5'- CCCGGAUCUUUCUCUCUUUUUCUUCCAUGCUUCCGGG -3'
EMP1	525 nm	FQ	5'- CCCGGAUGAGCAAAGAGAGUUCUGAAGGGUUCCGGG - 3'
hHK1	655 nm	RQ	5'- CCCGGAUCUUGAACGCACUGUCCUUGCUCCGGG - 3'
β-actin	565 nm	FQ	5'- CCCGGAACAGCCUGGAUAGCAACGUACAUGGCUGGUCCGGG - 3'

Effective Coupling and Quenching of QDMBs

To determine the proper linkage of the QD to the 2'-O-Methyl-RNA oligonucleotides containing the quencher molecule, the fluorescence of the QDMBs were measured and compared to the intensity of QDs alone. Fluorescence in the form of Relative Fluorescence Units (RFU) was quantified using a NanoDrop 3300 (ThermoFisher Scientific, Pittsburgh, PA) fluorospectrometer. A standard curve was first created with 2 μl PBS as the 0 μM standard and 2 μl streptavidin-modified QD as the 1 μM standard. A negative control measuring RFU of 2 μl of PBS was also included. A blank was created containing 2 μl of PBS. Next, the RFU of 2 μl of each QD was measured and recorded at the appropriate emission wavelength for each. The fluorescence of each QDMB at 2 μl was also measured. A comparison of RFU between QD and QDMB should show a reduction in fluorescence of the QDMB if successfully conjugated.

QDMB Specificity Assay – RNA Extracts from Biological Fluids

Proper and specific binding of QDMBs to target RNAs was determined by combining the probes with RNA extracted from fresh blood, saliva, and semen samples. RNA was isolated from biological fluids using the SurePrep TrueTotal RNA Purification Kit according to the manufacturer's protocol for each type of fluid. Again, 15 μl blood and 30 μl saliva and semen

aliquots were used for isolation. Six microliters of QDMB was transferred to three 0.5 ml tubes. Eight microliters of RNA extracted from blood, saliva, or semen were placed into one of each tubes respectively. After a 10 minute incubation period at room temperature, 2 μl of each RNA-QDMB mixture was read to determine fluorescence in RFU on the NanoDrop 3300. The previously mentioned standard curve was again utilized. The blank for each measurement was composed of 2 μl solution of a 3:4 ratio of each QDMB to PBS. Positive controls consisted of measuring RFU values of 2 μl unlinked QDs and 2 μl QDMBs after blanking the fluorospectrometer with 2 μl PBS. A negative control measured RFU of 2 μl PBS.

Human-Specificity of β-actin QDMB

To determine the human-specificity of the β-actin MB, first an NCBI Blast search [91] was performed on the RNA sequence complementary to the probe portion of the MB oligonucleotide. Search parameters were set to megablast highly similar reference RNA sequences from all species, except *Homo sapiens*. The resulting Taxonomy Report was examined to find taxa that may provide a source of contaminating RNAs at a crime scene: dog, *Canis lupus familiaris* (NM_001195845.1); mouse, *Mus musculus* (NM_007393.3); rat, *Rattus norvegicus* (NM_031144.2); and pig, *Sus scrofa* (AY550069.1). The RNAs detected were of the β-actin gene for each respective taxa. Other taxa were chosen beyond the Blast search as possible sources of RNA from either pets or food items: cat, *Felis catus* (GQ848333.1); chicken, *Gallus gallus* (NM_205518.1); cow, *Bos Taurus* (NM_173979.3); lamb, *Ovis aries* (NM_001009784.1); and salmon, *Salmo salar* (NM_001123525.1). Human β-actin mRNA sequence data was also obtained from NCBI: *Homo sapiens* (NM_001101.3).

RNA sequence data was aligned using the online multiple sequence alignment software ClustalW2 (European Molecular Biology Laboratory – European Bioinformatics Institute, Hinxton, England). Species-specific nucleotide polymorphisms were detected between the β-actin RNA sequence from humans and other taxa of interest.

For better prediction of the thermodynamics of the β-actin QDMB probe-RNA hybrids, the estimated melting temperature (T_m) of the QD and each double-stranded hybrid was determined by the DINAMelt Web Server [92, 93]. The Quikfold application provided the T_m of the QDMB. After providing the RNA sequence, all parameters were set to default, except the "Energy Rules" option was altered to reflect "RNA." The Two State Melting (Hybridization) application provided the T_m of the double-stranded QDMB-RNA hybrids. Again, the only parameter not set to default was "Energy Rules," which was set to "RNA." A high T_m shows thermodynamically stable bonds between two nucleic acid stands. These strands are less likely to disassociate from one another at lower temperatures. To provide a measure of stability of

the bonds between the β-actin QDMB and the RNA from each non-human taxa, a measurement of ΔT_m is calculated, in which the T_m of the hybrid of RNA from non-human taxa and the β-actin MB is subtracted from the T_m of the hybrid of RNA from human β-actin and its QDMB ($T_{m(\text{Human RNA:MB})} - T_{m(\text{Non-Human RNA:MB})}$). The higher the value of ΔT_m, the less thermodynamically stable the double-stranded non-human hybrid is when compared to the human hybrid.

Results

PCR Screen of Tissue-Specific RNA Candidates

Candidate RNAs were preliminarily screened for specificity using PCR. The forward primer was designed to span the nucleotide sequence that was believed to make each RNA tissue-specific. Total RNA extracted from blood, saliva, and semen, after reverse transcription, was PCR amplified using each primer set. Results of the PCR products run on agarose gels for three candidate tissue-specific RNAs, along with a candidate human-specific RNA, are found in **Figure 16**. Primers for 4.1R mRNA were designed to amplify a 266 bp region thought to be specific to blood. Results of gel electrophoresis display a single band when these primers were used in a reaction containing cDNA from blood. Amplification did not occur when 4.1R primers were used in PCR with cDNA from saliva or semen. Similar results were seen with primers designed to amplify EMP1 and hHK1 mRNAs. EMP1 produced the expected 498 bp band only in saliva, while hHK1 shows a 186 bp product only in semen. β-actin, the speculated human-specific primer pair, produced a 500 bp band of amplified product from cDNAs from all three tissue types as expected. Negative controls, in which nuclease-free water was substituted for cDNA, did not produce a band for any of the primers tested.

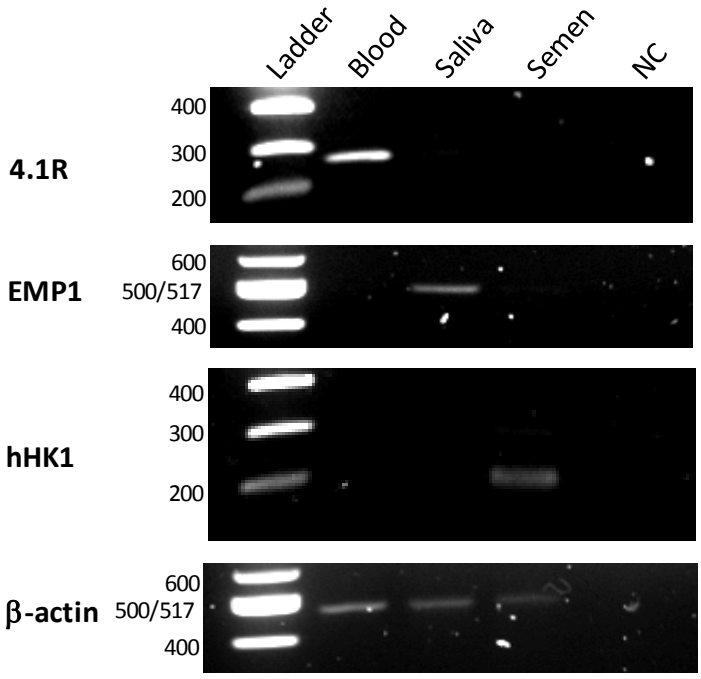

Figure 16: Tissue-specific RNAs as determined through a PCR screen. Total RNA extracted from blood, saliva, and semen was reverse transcribed. Resulting cDNAs were used as the template material for PCR amplification with primers designed to amplify possible tissue-specific regions of candidate RNAs. For the tissue-specific RNA candidates shown to the left, each band is of the expected length and amplifies RNAs found in only one of the three biological fluids tested. The β-actin primers were designed to be human-specific and were found in all three tested fluids. A negative control (NC) for each PCR reaction yielded no amplified product.

Effective Coupling of QD and MB

After linking the streptavidin-coated QD to the biotinylated oligonucleotide sequence containing an Iowa Black quencher molecule, the amount of fluorescence the QDMB exhibits should decrease. Effective coupling of QDs and MB oligonucleotides is demonstrated in **Figure 17**. Levels of QD quenching vary, with the greatest decrease in fluorescence, 97.4%, displayed by the QDMB for 4.1R RNA for detection of blood (**Figure 17C**). The QDMB designed to detect EMP1 in saliva (**Figure 17A**) is the least quenched with a 48.3% reduction in fluorescent signal. The remaining QDMBs for human-specificity (**Figure 17B**), targeting β-actin, and for semen (**Figure 17D**), targeting hHK1 RNA, show a reduction in signal of 74.3% and 83% respectively.

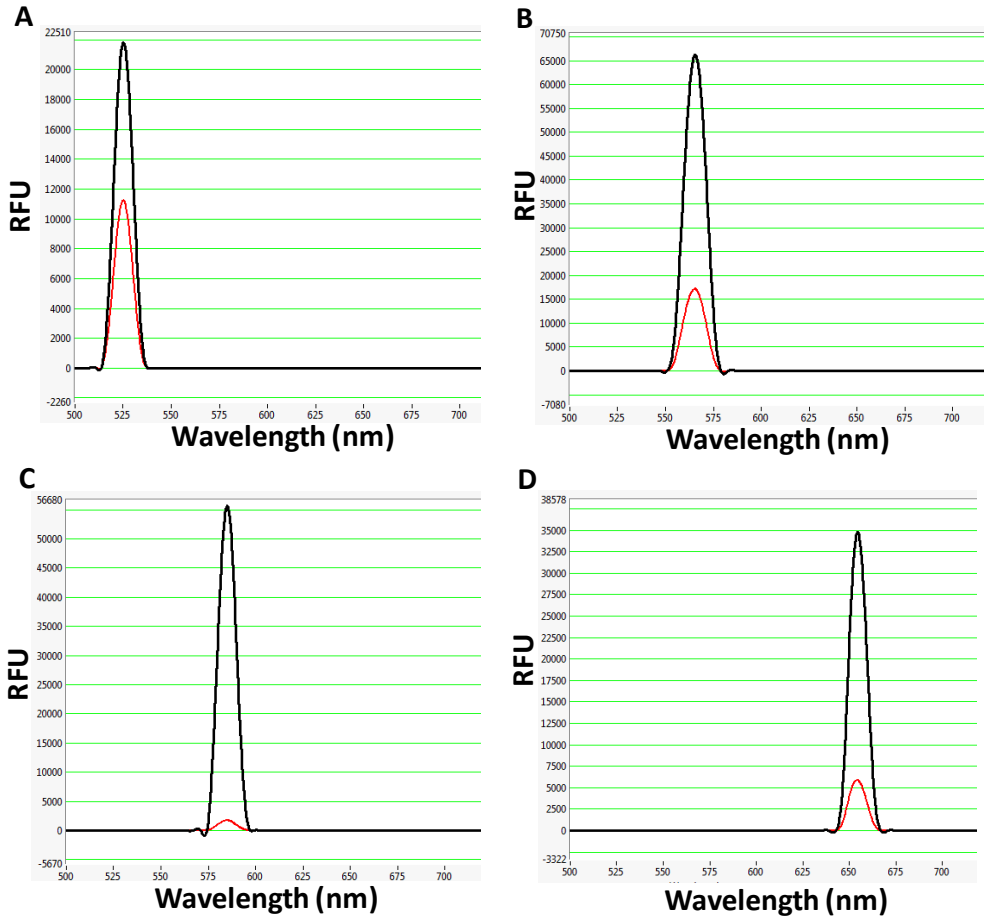

Figure 17: Quantified RFU of each QD versus QDMB. The RFU values of each QD (shown in black) are compared to the RFU of the same QD once linked to form a QDMB (shown in red). QDMBs were designed to detect the presence of the candidate tissue- or human-specific RNAs (A) EMP1, (B) β-actin, (C) 4.1R, and (D) hHK1.

Specificity of Tissue-Specific QDMBs

QDMBs were tested for specificity by combining each with RNA extracted from blood, saliva, and semen samples (**Figure 18**). An increase in fluorescence was seen when each tissue-specific QDMB was in the presence of RNA from only one biological material. β-actin QDMBs, as expected, showed an increase in fluorescence when combined with RNA from all three tissue types. This illustrates proper function of the probes in which a conformational change is possible when the target RNA is present. When in the presence of RNAs from other sources, an increase in fluorescence was not detected. These results demonstrate that the QDMBs will not open in the presence of merely any RNA, but only when the target RNA is present.

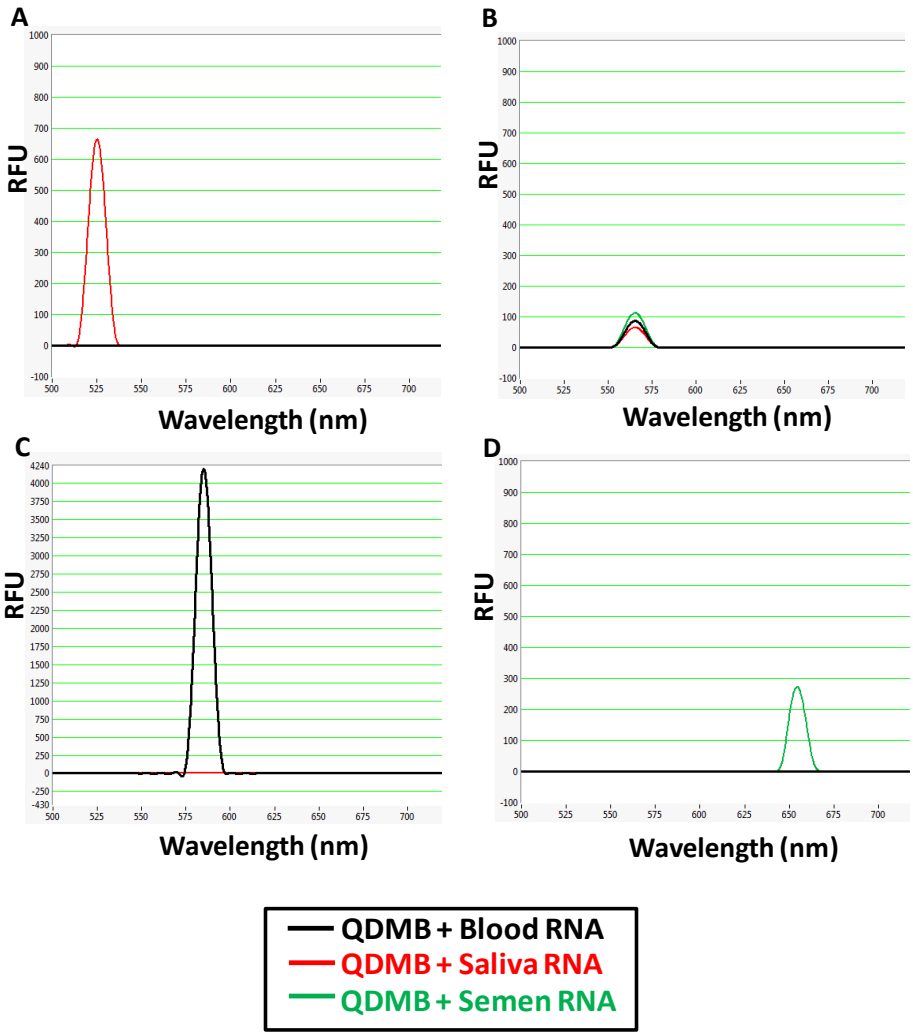

Figure 18: QDMB detection of RNA extracted from fresh biological samples. RNA extracted from blood, saliva, and semen was combined with QDMBs designed to detect human- or tissue-specific mRNAs (A) EMP1, (B) β-actin, (C) 4.1R, and (D) hHK1. A peak is indicative of QDMB conformational change in the presence of complementary nucleic acid sequences.

Specificity of β-actin QDMB

To better estimate the specificity of the β-actin QDMB, the human RNA complement sequence of the probe was compared to similar sequences of species possibly present at a crime scene. These similar sequences were determined by the results of an NCBI Blast search. Among the most highly similar sequences was the RNA of several taxa's β-actin gene. The alignment of all sequences, including the messenger RNA (mRNA) sequence of human β-actin, is shown in **Figure 19**. It was observed that the sequence of human β-actin mRNA differs from all other taxa at nucleotide positions 15 and 18. The salmon species β-actin RNA sequence differs most from human with a total of 4 mismatches, while the taxa of dog, mouse, and cat differ the least with 2 mismatched bases. The remaining taxa differ in sequence at 3 nucleotide positions, although the position of each base discrepancy is not the same in each taxa. For example, chicken is the only taxa in which position 12 differs from the human sequence.

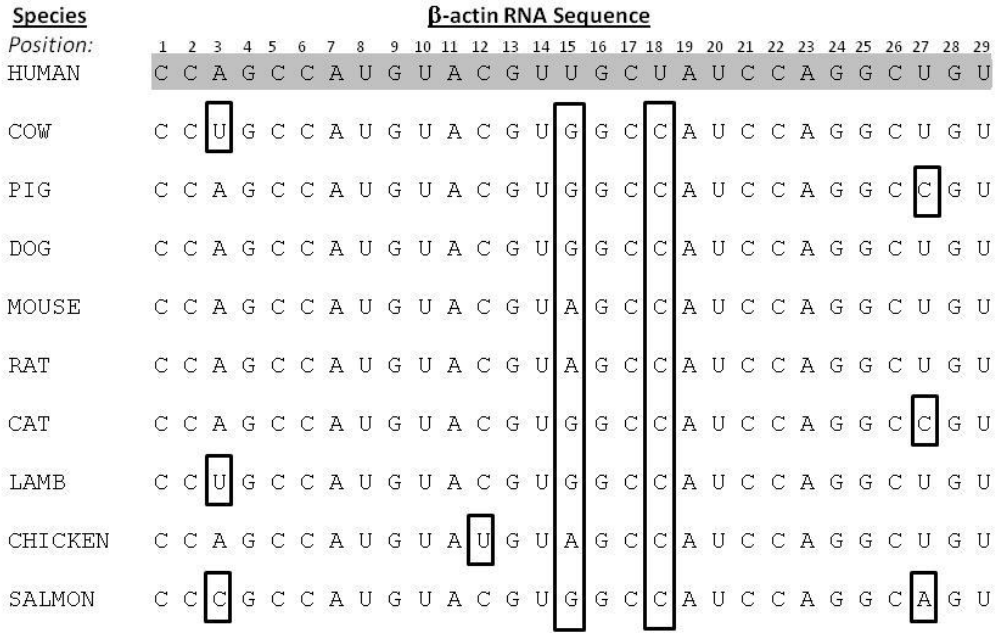

Figure 19: Sequence alignment of β-actin mRNA from multiple taxa. To determine species-specific sequence polymorphisms, the β-actin mRNA sequences of 9 taxa that may provide a source of contaminating RNA at crime scenes were aligned. All non-human taxa sequences were compared to human (highlighted in grey). Sequence aberrations from human are held within boxes. Each base is given a numerical nucleotide position to better reference its location.

Although MBs have been found to provide complete discrimination between sequences that contain as few as one single nucleotide polymorphism [94-96], the potential of the possible human-specific QDMB to bind to similar, yet non-complementary sequences was further

investigated. The estimated T_m of each RNA-QDMB hybrid is provided in **Table 11**. The estimated T_m of the β-actin QDMB in secondary structure was found to be 87.4 ^oC. The T_m of the double-stranded hybrid of human β-actin RNA and the β-actin QDMB was found to be 96.9 ^oC. Linear nucleic acid probes that have the ability to discriminate between sequences with only one base difference usually have at least a 1-2 ^oC ΔT_m [97]. According to the expected melting point measurements, the β-actin QDMB should be rather discriminatory against RNA extracted from those species that contain 3 or 4 sequence aberrations (with high values for ΔT_m). As for the β-actin RNA sequences for dog, mouse, and rat, the ΔT_m is lower than the other organisms (3.1 ^oC), but still higher than those expected from a discriminatory linear probe.

Table 11: Comparison of melting temperature between RNA-QDMB hybrids. The measure of ΔT_m provides the difference in T_m between perfectly matched complementary sequences (human RNA-β-actin QDMB RNA hybrid) and those sequences that differ at 2-4 nucleotide locations (non-human taxa RNA-β-actin QDMB RNA hybrids).

Number of Mismatches Compared to Human Sequence	Organism RNA-QDMB Hybrid	T_m (^oC)	ΔT_m (^oC)
-----	Human	96.9	0
2	Dog Mouse Rat	93.8	3.1
3	Cow Pig Cat Lamb Chicken	91.0	5.9
4	Salmon	87.9	9.0

Discussion and Conclusions

The purpose of this study was to provide the forensic community with novel probes for later use to confirm the presence of biological fluids in potential evidence found at crime scenes. Knowing if a stain is biological in nature, as well as determining exact tissue-type, while still at the scene can help to reduce the number of items collected by crime scene technicians. The results of this study confirm that tissue-specific RNAs can be targeted to determine the biological make-up of a stain without the use of PCR. The presented method, once optimized in multiplex, may help to reduce the amount of backlog that is currently plaguing crime laboratories nation-wide.

Multiple tissue-specific RNA candidates where sought in the literature. After testing 36 candidates, three RNAs were preliminarily determined to be specific to one of three fluids, blood, saliva, or semen, through the use of a PCR-based screen. A potential human-specific region of β-actin mRNA was present in all three tissue types. Although all candidate RNAs selected using this method did provide QDMBs that were tissue-specific, this assay was merely for preliminary purposes to screen possible QDMB sequences for further analysis.

The forward primer of the PCR-based screen was used as a template for the design of MB probes. The MB oligonucleotides were linked to their fluorophores, QDs, using biotin-streptavidin interactions. The QDMBs were tested for proper conjugation using an assay in which quenching of the fluorophore was measured. It was determined that all MB oligonucleotides containing a quencher molecule had been correctly coupled to the corresponding QD. The fluorescence of certain QDMBs was more highly quenched than others, exhibiting a range of 97.4% to 48.3% reduction in fluorescence. Although QDMBs for EMP1 and β-actin showed the least reduction in quenching, further optimization can be managed. Using a lower concentration of QD and/or higher concentration of MB oligonucleotide with attached quencher in initial linkage reactions may help to further reduce the RFU of the "closed" QDMB. Both of these actions would provide QDs conjoined to multiple oligonucleotides, and therefore multiple quencher molecules. Although we have simplified the appearance of a MB in **Figure 14**, depending on the concentrations of the components used for coupling, the QDMB produced most likely takes the form of the probe seen in **Figure 20**. Streptavidin proteins coat the entire outer surface of the QD. Depending on the ratio of concentration of QDs to MB oligonucleotides in the initial reaction, several oligonucleotides could potentially bind to the QD, quenching the fluorophore further. This enhanced quenching will lead to an increase in the fluorescence detected when the QDMB is in the presence of its target RNA.

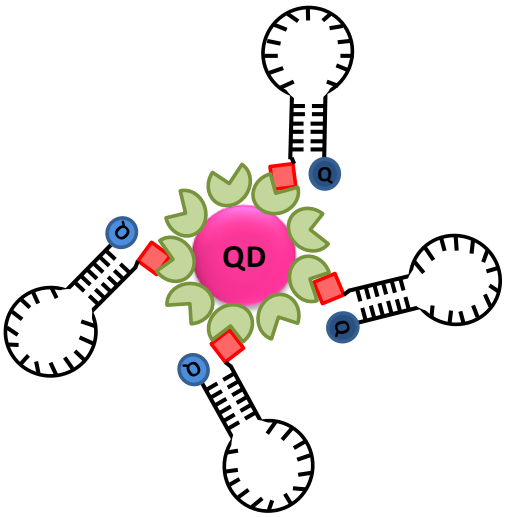

Figure 20: A more realistic View of QDMBs produced through biotin-streptavidin coupling. Streptavidin proteins, shown in green, coat the surface of the QD. One biotin protein, shown in red, is attached to the 5' end of the MB oligonucleotide. The concentration of QD and MB oligonucleotide can be modified to maximize the number of oligonucleotides coupled to each QD. The more oligonucleotides attached, the further bright QDs will be quenched.

Although the proposed tissue-specific QDMBs were found to be specific to the RNAs isolated from only one type of bodily fluid and the QDMB targeting β-actin recognized all three human tissues, the amount of fluorescence detected in RFU differ between each QDMB. This is most likely due to the concentration of each RNA in the body fluid tested. Increased signals can be obtained by optimizing the amount of QDMB and isolated RNA used in each reaction. Further reduction of the fluorescence of the "closed" QDMB, by increasing the number of quencher molecules attached to each QD as previously described, may also increase the signal produced by the QDMB when in the "open" conformation. Furthermore, this difference in fluorescent signal strength may indicate that increased biological sample sizes of more than 30 μl of semen and saliva should be used for analysis. These variations of the original protocol should be the focus of future experimentation.

Although how a probe works in singleplex is important, the final goal of experimentation is to provide one, multiplex assay to detect the presence of all three of these fluids in one sample, as well as to determine if that sample is human in origin. Singleplex reactions provide some information on how these probes will work in multiplex, but much optimization will need to be performed in order for all of the probes to function at an optimal level once combined in multiplex.

The human-specificity of the QDMB for β-actin was examined by means of computer software analysis. A Blast search revealed several similar sequences from animals that could potentially provide a source of contamination at a crime scene. All of these sequences were of β-actin RNA. After sequence alignment, it was discovered that many of the animal β-actin RNA sequences differed from human by 2-4 nucleotide bases. Estimated melting temperatures of each double-stranded non-human RNA-QDMB hybrid was compared to the melting

temperature of the double-stranded complete complement: the human RNA-QDMB hybrid. It was determined that the β-actin QDMB should have little difficulty selecting its target complement over the other sequences. As mentioned previously, MBs are usually much better than traditional linear nucleic acid probes at distinguishing single nucleotide differences between target molecules. This is due to the increased ΔT_m of MBs compared to linear probes, which is attributed to the thermodynamic properties of stem portion of the MB [97]. It is also believed that 2'-O-methyl RNA MBs possess a superior affinity for RNA targets [98, 99]. 2'-O-methyl RNA MBs will bind more quickly to an RNA target than to a DNA target. Those nucleic acid probes that have even less binding affinity than any 2'-O-methyl version are simple RNA:RNA or DNA:DNA hybrids. To be absolutely certain that the QDMB for β-actin will only target human RNA, the only reliable test is to use the probe in reactions with RNA isolated from each of the animals examined, or at least those most similar to the human sequence. If RNA from dog, mouse, or rat does not elicit a fluorescent response, it is not likely that RNA from any of the other animals will as well.

Once optimized in a multiplex reaction, further experimentation will be needed to determine the age of samples, or longest time since deposition, that can be detected using our assay. It is also of interest to determine the smallest volume of biological fluid required for proper confirmation of presence. Furthermore, it may be possible to remove the use of an RNA isolation technique that requires a centrifuge. The probes were composed of 2'-O-Methyl-RNA oligonucleotides. These bases are highly resistant to enzymatic degradation [98] and may allow for an assay somewhat similar to that used for in situ hybridization studies. A biological sample would be collected and then combined with a lysis reagent to break open cells and release the RNA held within. The lysed cellular components would then be added to the QDMBs, where RNA is targeted and increases in fluorescence read directly from the tissue lysates. This type of RNA "isolation" procedure would significantly reduce total assay time, as well as eliminate the need of a portable centrifuge. Removing the need of a centrifuge improves the ease of portability.

We believe that this technique will have multiple advantages over currently available presumptive and confirmatory tests for biological evidence. First, our technique has a short assay time, in which multiple samples can be processed in less than an hour. Without the requirement of PCR, this method features a reduced assay time, as well as reduced cost. Current technology utilizing qRT-PCR can cost $25 per sample. Our assay, at this time, with small scale production of QDMBs, would cost approximately $10 per sample to complete. This cost is of a multiplex reaction, where any of the three biological fluids tested can be determined along with human origin, as well as the possible determination of the components of mixtures. Currently, at least two different tests performed in the laboratory would be needed to acquire both pieces of information. Although more tissues of forensic importance need to be tested for

certainty, this technique has the potential to be the first reliable confirmatory test for saliva. Finally, the possibility for portability to the scene of a crime is high. Only a limited number of items are needed to run the assay and each is of small size and weight.

This preliminary study provides proof of concept for the use of QDMBs for tissue-specific RNAs in the confirmation of body fluids from potential evidence. Although further experimentation will be required before use on forensic samples, the presented method holds multiple advantages over current techniques. The advantages of time and cost alone would allow for our assay to replace current techniques in the laboratory if portability were to be deemed too cumbersome.

Chapter 5: Conclusions

As a whole, these studies were focused on the use of RNA to provide the forensic community with improved techniques for processing biological evidence. RNA, although holding many of the key characteristics that should make it an attractive candidate for study, has been largely ignored by the field of forensic science until recent years. It was thought to degrade too quickly within biological evidence to be of any use. The results of the experiments presented here show that RNA does degrade over time, but that this degradation, based on size of the molecule examined, is predictable. The ability to predict RNA decay of large versus small segments of RNA extracted from different biological samples can be manipulated to determine time since death. The lack of rapid degradation of very small portions of RNA allow for the detection of tissue-specific RNAs that can determine the type of bodily fluids present in biological evidence found at a crime scene.

The conclusions of the presented work have augmented the current knowledge of the capabilities of the use RNA within our field. We were not the first to propose the use of RNA in PMI estimation or in the detection of biological material as evidence. We are, however, the first to present a working model of estimating PMI that uses a molecular approach to exploit predictable RNA degradation. We have also presented a new technique for quantifying and documenting what was once a qualitative measure, color changes that occur within decomposing tissues. Technological advances have allowed us to be the first to promote the use of MB probes as a way to detect novel tissue-specific RNAs while still at a crime scene.

The implications of this work have the potential to be far reaching. Understanding the damaging effects of DNase on RNA to be used in qRT-PCR applications, both singleplex and multiplex, can help to make the results of experimentation using this technique more reliable. This work has also shed light on the need to find the best isolation technique when working with RNA from new tissues, such as tooth pulp, as not all tissues yield DNA-free RNA in a similar manner. Once the proper isolation technique is determined, the comparison of RNA segments of different sizes can lead to an estimation of time since death. The PMI estimates produced by our method utilizing β-actin RNA from tooth pulp and color analysis, although sometimes broad, have extended the period of time following death in which current estimators are reliable. This technique is affected by environmental temperature, but due to the protective enamel of a tooth, is not as affected by many of the other factors that must be taken into consideration when using other methods of estimation such as humidity, insect scavengers, containers such as body bags, or local knowledge of forensically significant insect species. An analyst need not have any specialized knowledge, except for the laboratory techniques of RNA extraction, reverse transcription, and Real-Time PCR. This work may also be inspiration to find other quantitative means of measuring what were once seen as qualitative characteristics that are used in the field of forensic science. The use of new probes, such as MBs, may increase as a

means to provide more reliable information about the evidence collected at crime scenes. The technique presented for the confirmation of biological tissues in forensic evidence, once completed, may provide a means to significantly reduce the number of items submitted to crime laboratories. With fewer pieces of evidence, that simultaneously provide more relevant information, crime laboratories may become more efficient at fighting the plaguing issue of backlog. Finally, the projects elaborated upon in this dissertation are not the only uses for RNA in forensic science. Once the value of this molecule is established, new techniques can be devised that use RNA to solve other forensic-related issues.

The experimentation begun here has presented the opportunity for further studies. Our estimates of PMI, in some cases, span extended ranges of time. To make more precise estimates, the degradation patterns of additional RNAs can be assessed. The degradation of different combinations of RNA species, including rRNA, and multiple sizes/lengths of these species should be determined. Adding this information into our equation may allow for more precise estimates of PMI to be determined. Besides RNA degradation, a change in model species should also be considered. Although pigs have many molecular similarities to humans, using these assays on cadavers would make the conclusions drawn from this research more sound.

As for the continuation of MBs used as confirmatory tests for blood, saliva, and semen, there is more work to be completed. The QDMBs will need to be tested in the presence of multiple tissues, as well as with RNA extracted from more than three individuals. Also, the amount of fluorescence that can be detected from biological samples of varying ages, as well as on samples of different volumes will need to be assessed. This technique can be evaluated on stains recovered from different substrates, such as tile, wood, and drywall. Novel RNAs that are specific for other forensically relevant body fluids may also be sought and MBs designed for the detection of these as well.

The work presented in this dissertation has provided a new role for the use of RNA in the processing of biological evidence. Although more experimentation should be completed before these techniques are put to use in the forensic community, the results have provided a foundation of techniques, which when fully developed, will provide the forensic community with more reliable techniques to be used in the processing of forensic evidence.

Appendix A: Free Radical Accumulation in Dried Bloodstains as a Possible Source of RNA Degradation

Introduction

To estimate time since deposition, previous studies with our laboratory have recorded the rates of RNA decay within dried blood samples [21, 22], but have not studied the source of the observed degradation. As mentioned previously in Chapter 1, *in vivo* degradation of RNA within the body is an enzymatic process that occurs within an aqueous environment; therefore another source of degradation must be functioning in dehydrated samples. We hypothesize that one degradative force acting upon the RNA of such samples is that of free radical formation. Free radical formation, and subsequent accumulation, can occur without the presence of water and has been known to cause damage to nucleic acids [9, 100]. Due to the high oxygen content of blood, one group of free radicals, reactive oxygen species (ROS), are known to be constantly produced in red blood cells [10].

In order to determine the role of free radicals in the degradation of RNA within dried bloodstains, we must first determine the base level of radical production in newly created stains and then how this production/accumulation changes over time. We hypothesize that free radicals will increase in concentration as the stains age, until a certain unknown threshold is met, providing the mechanism for RNA degradation in a relatively anhydrous environment.

The technique chosen to measure free radicals within a bloodstain is known as Electron Paramagnetic Resonance (EPR). This technique has the ability to both determine what radicals are present in a sample while simultaneously quantifying the production of radicals at one specific moment in time. Most free radicals are short-lived. In order to quantify the concentration of radicals present at any one moment in time, a spin trap is incorporated into the reaction. The spin trap, DMPO (5,5-dimethyl-l-pyrroline-N-oxide), undergoes chemical bonding with the radicals present creating a second radical (a radical adduct) with greater stability. The radical-spin trap adduct is then introduced to a magnetic field within which the radical will align itself and cause interference. This interference is caused by the movement of the radical's unpaired electrons from lower to higher energy states. This release of energy can then be detected and recorded by an EPR spectrometer as a spectrum (**Figure 21**). The height of the peaks seen in the resulting spectrum is indicative of the radical's concentration within a sample. The number and height of each peak in relation to one another allow for identification of what radical is present.

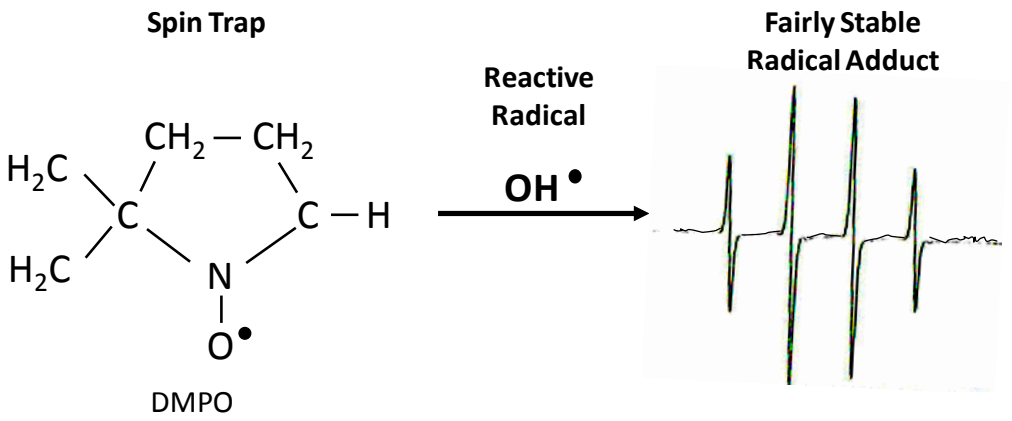

Figure 21: EPR Simplified. Due to the short lifespan of most reactive radicals, when introduced to a magnetic field alone, a steady spectrum would not be produced. To create a radical that is stable for a longer period of time, a spin-trap is utilized. The spin trap, here DMPO, is also a radical. When in the presence of a short-lived reactive radical, a chemical reaction occurs in which the product is a new radical species that is relatively stable. This more stable radical will last long enough within the magnetic field of EPR to produce a reliable spectrum. The more of the same radical present, the larger the peaks will be in the resulting spectrum.

Methods

Acquiring and Aging Bloodstains

Blood samples were obtained from three individuals by pricking their finger with a sterile lancet. Blood samples were obtained with a protocol approved by the West Virginia University Institutional Review Board for Protection of Human Research Subjects. The blood was deposited in 100 μl aliquots onto sterile Petri plates and stored at ambient temperature and humidity to dry and age. Once bloodstains had reached the ages of 0, 0.5, 1, 5, 10, 20, 35, 50, 65, and 80 days, the dried bloodstains were removed from the surface of the Petri dish and placed into 1.5 ml Eppendorf tubes.

Electron Paramagnetic Resonance for Free Radical Detection in Bloodstains

The blood samples, once contained in 1.5 ml tubes, were rehydrated with 500 μl phosphate buffered saline (PBS). To combine radical with spin trap, reagents were added to a glass test tube in the following order: 325 μl PBS, 100 μl 1M DMPO, 25 μl resuspended blood, and 50 μl 100mM H_2O_2. The contents were mixed briefly by vortex. Five-hundred microliters of the reaction mixture was transferred to a glass flat cell, which was immediately aligned within a Bruker-EMX-300 EPR Spectrometer (Bruker Daltonics Inc., Billerica, MA). Attenuation was set to 5 and the number of cycles of the x-axis set to 1. Results were analyzed using WinEPR Acquisition Software (Bruker Daltonics Inc.). Each sample was assayed by EPR in triplicate. The positive control for EPR analysis was a simple Fenton reaction, where 25 μl 10mM $FeSO_4$ was used in the place of blood to form a hydroxyl radical. A negative control consisting of PBS and DMPO, but no resuspended blood, was also assayed.

Data Analysis

Peak height of each resultant peak was manually measured in cm from printed spectra. The measurements were corrected based on the Y-axis scale of each spectrum. Data were entered into Microsoft Excel (Microsoft Corporation, Redman, WA), where means and standard errors for samples were calculated.

Statistical Analysis

A one-way analysis of variance (ANOVA) and a subsequent Tukey-Kramer HSD multiple comparison procedure were used to determine statistical differences in free radical accumulation over time. Experimental units, height of peak 2 in cm, were compared and the level of significance was determined using α=0.05.

Results

As seen in **Figure 22**, an unknown radical, or group of radicals, appears in bloodstains as early as one day after deposition. Although present, the peaks are not distinct enough for measurement until at least 5 days after deposition. These same peaks are detected in older bloodstains as well (days 10 and 20), yet accumulation of radicals is seen in the increase of peak height over time.

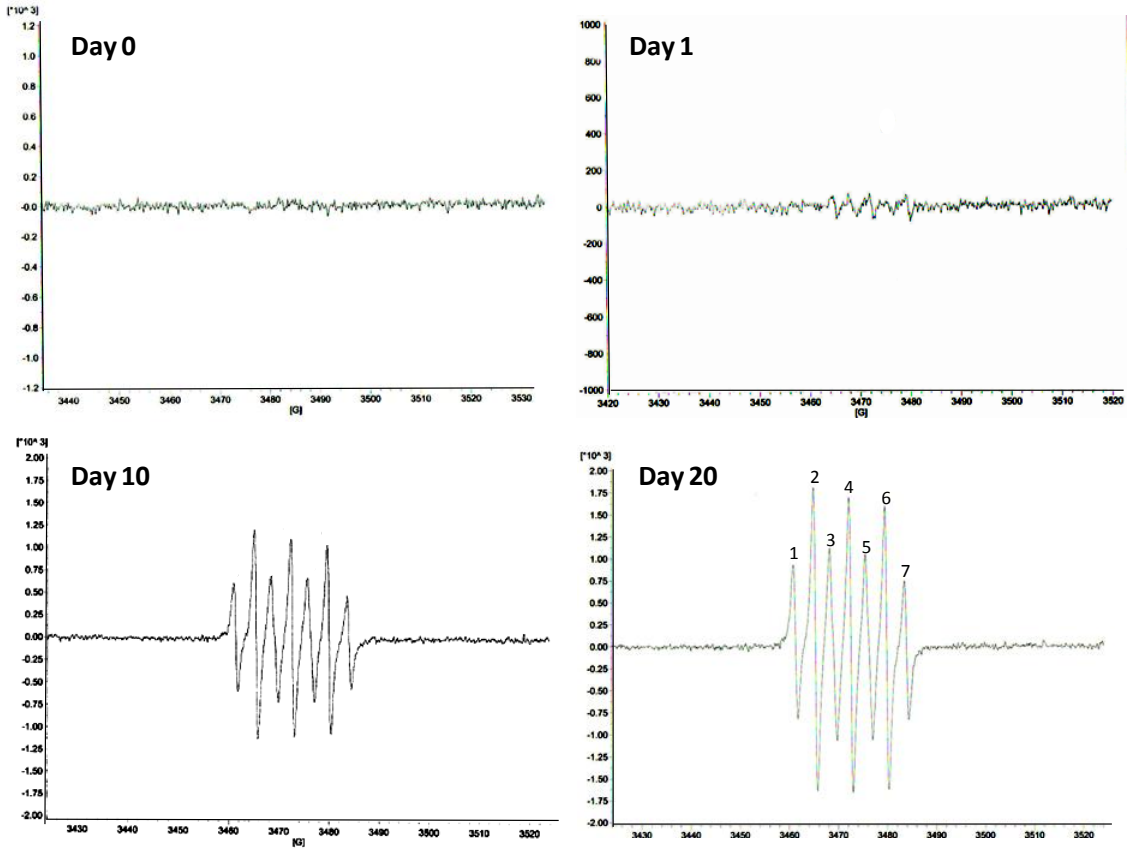

Figure 22: EPR of 100 μl bloodstains over time. Bloodstains from the same subject were aged on plastic Petri plates. The same radical(s) is present at all time points after day 0, but as shown by the scale in each spectrum, this radical is found in increasing quantities as the stains age. Peaks of day 20 are labeled by number for use in further analysis.

Figure 23 depicts the peak height for each of the 7 peaks that continually arise in our analysis of dried bloodstains. All peaks show a rise in the accumulation of radicals through day 20. Over time, the height of each peak, used as a measure of free radical concentration within samples, follows the same pattern. As hypothesized, this increase in free radical formation cannot continue infinitely, where after a steady increase through day 20, peak heights decline through day 80. These trends are also seen in **Figure 24**, where the mean peak height of peak 2 from the aged bloodstains of three donors is depicted. There are significant differences in the

amount of free radicals that accumulate in dried bloodstains as they age (F=34.1333, p=<0.0001).

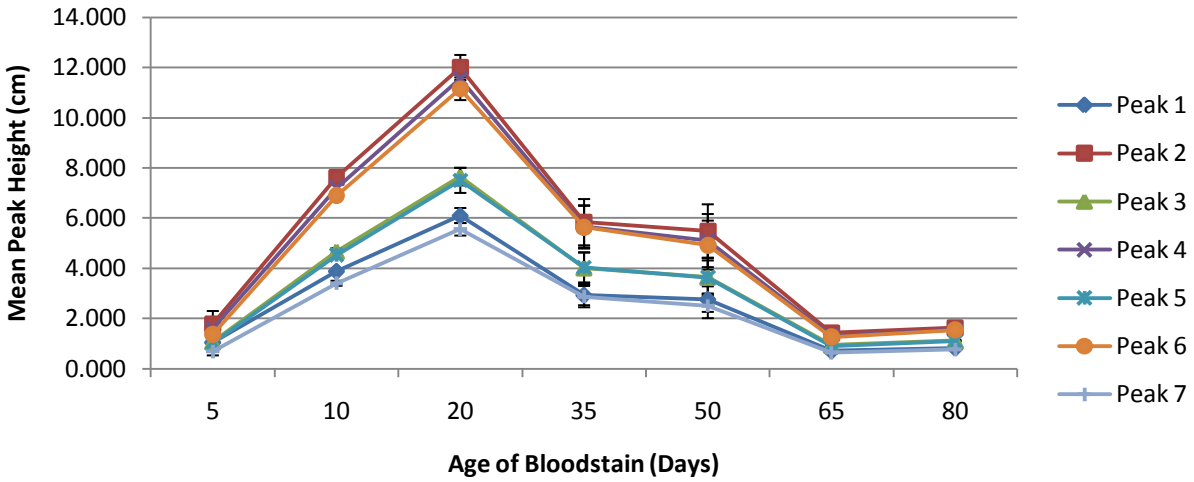

Figure 23: Individual peak height of EPR spectra as bloodstains age. Bloodstains aged on plastic petri plates at ambient temperature and humidity for 5 through 80 days underwent EPR analysis. The day of blood deposition (day 0), as well as day 0.5 and day 1 were also analyzed using EPR, although peak heights were too indiscrete to be measured at these time points. The error bars indicate standard error where n=63.

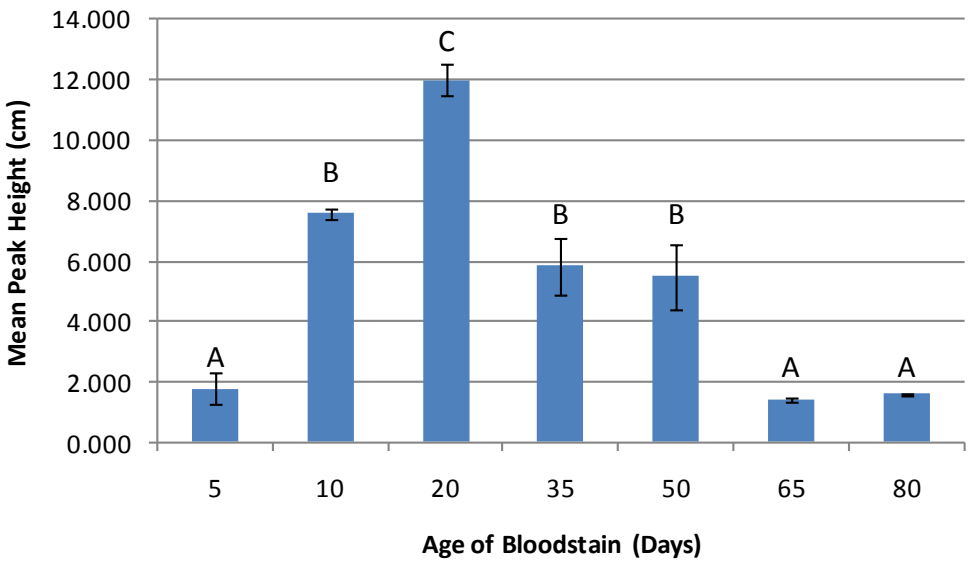

Figure 24: ANOVA of EPR spectra peak 2 height from three subjects. The accumulation of the visible radical(s) is compared as bloodstains age. The error bars indicate standard error where n=63. Means associated with the same letter are not statistically different (Tukey-Kramer HSD).

Due to blood being a complex mixture of multiple components, the "radical" observed is most likely a combination of radicals that are simultaneously being scavenged by the spin trap DMPO. Based upon the shape of the EPR spectra (number of peaks and height of peaks in relation to one another), we hypothesize that at least two radicals are present in our preliminary results. The two radicals mostly likely present are a hydroxyl radical ($OH^{\bullet}$), along with a form of reactive nitrogen species (such as $NO^{\bullet}$) (**Figure 25**).

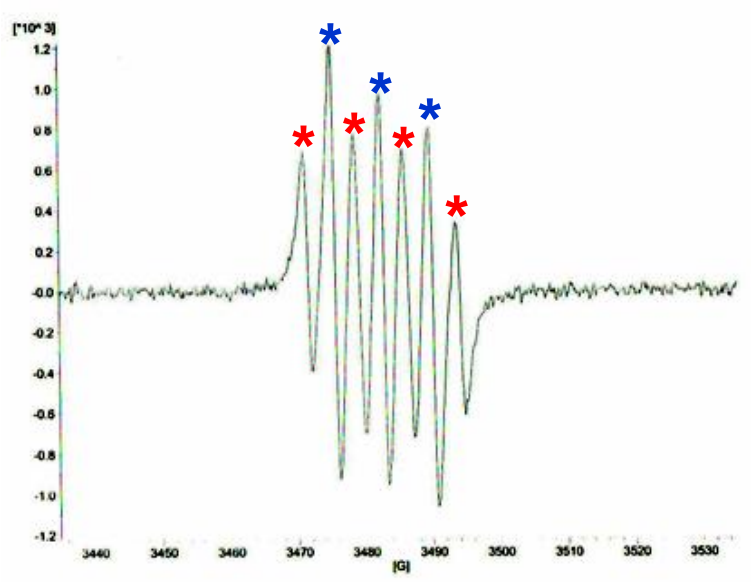

Figure 25: EPR spectra of a dried bloodstain aged 14 days. Peaks thought to belong to hydroxyl radicals are marked with red asterisks, while radicals hypothesized to belong to nitroxide radicals are marked with blue.

Further evidence that these two radicals exist in our samples is seen in **Figure 23**, where peaks 2, 4, and 6, thought to belong to hydroxyl radicals, group together very closely and change in relation to one another over time. The remaining peaks (1, 3, 5, and 7), also group together rather closely with one another and are thought together to form the spectrum of a nitroxide radicals.

Discussion and Conclusions

Preliminary studies show that free radical accumulation does occur and significantly changes as bloodstain samples age. Furthermore, the same radical, or group of radicals, was detected in multiple bloodstains of varying ages using EPR spectroscopy. Assays of samples that were fresh or that were only one half day old fail to detect the presence of any radical. Low levels of accumulated radicals can be detected in samples that have aged for one day, although the concentration of such radicals is immeasurable. After radical concentration peaks at 20 days, a decline in radical concentration is seen. This may be due to the loss over time of whichever molecule the radicals are using as a "reactant" for chemical reactions that occur within a bloodstain. Once the concentration of reactant molecules is decreased, radical concentrations would decline.

The changes in height of spectral peaks, along with the shape and size of peaks in relation to one another, give evidence that the two radicals present in our samples are hydroxyl and nitroxide radicals. This is not surprising, as hydroxyl radicals are found within the group known as ROS radicals, which as previously stated, are major cellular components of red blood cells [10].

It was hypothesized that free radicals, due to their deleterious effects on nucleic acids, may play a role in the degradation of RNA in biological stains, in this scenario, blood. These preliminary studies show that an increase in free radical concentration does occur over time in aging bloodstains, but further experimentation is needed to directly identify these radicals as the source of RNA degradation in anhydrous biological evidence. A free radical knock-down experiment could show a correlation between free radical accumulation and RNA degradation. It would be possible to lower free radical concentration by the addition of an antioxidant in liquid form to bloodstains before completely dry. It is hypothesized that a decrease in free radicals within a sample would lead to a decrease in RNA degradation. This information would strengthen the preliminary results seen here as to the effect of radicals on RNA degradation within dried bloodstains.

References

1. Jeffreys, A.J., Allen, M., Hagelberg, E., Sonnberg, A., *Identification of the Skeletal Remains of Joseph Mengele by DNA Analysis*. Forensic Science International, 1992. **56**: 65-76.

2. Green R.E., Krause J.K., Ptak S.E., Briggs, A.W., Ronan, M.T., Simons, J.F., Du, L., Eghold, M., Rothberg, J.M., Paunovic, M., Pääbo, S., *Analysis of one million base pairs of Neanderthal DNA*. Nature, 2006. **444:** 330–336.

3. Noonan, J.P., Coop, G., Kudaravalli, S., Smith, D., Krause, J., Alessi, J., Chen, F., Platt, D., Pääbo, S., Pritchard, J.K., Rubin, E.M., *Sequencing and analysis of Neanderthal genomic DNA*. Science, 2006. **314**: 1113–1118.

4. Hagelberg, E. & Sykes, B., *Ancient bone DNA amplified*. Nature, 1989. **342**: 485.

5. Hagelberg, E., Thomas, M.G., Sher, A.V., Baryshnikov, G.F., Lister, A.M., *DNA from ancient mammoth bones.* Nature, 1994. **370**: 333-334.

6. Chromczynski, P. & Sacchi, N., *Single-step method of RNA isolation by acid guanidinium thiocyanate-phenol-chloroform extraction.* Analytical Biochemistry, 1987. **162**: 156-159.

7. Chromczynski, P. & Sacchi, N., *The single-step method of RNA isolation by acid guanidinium thiocyanate-phenol-chloroform extraction: twenty-something years on*. Nature Protocols, 2006. **1**: 581-585.

8. Scholes, G. & Weiss, J., *Chemical action of X-rays on nucleic acids and related substances in aqueous systems:1. Degradation of nucleic acids, purines, pyrimidines, nucleosides, and sucleotides by X-rays and by free radicals produced chemically*. Biochemical Journal, 1953. **53**: 567-578.

9. Adelman, R., Saul, R.L., Ames, B.N., *Oxidative damage to DNA: Relation to species metabolic rate and life span*. Genetics, 1988. **85**: 2706-2708.

10. Burak Çimen, M.Y., *Free radical metabolism in human erythrocytes*. Clinica Chimica Acta, 2008. **390**: 1-11.

11. Bauer, M. & Patzelt, D. *Evaluation of mRNA markers for the identification of menstral blood.* Journal of Forensic Science, 2002. **47**: 1278-1282.

12. Juusola, J. & Ballantyne, J., *Messenger RNA profiling: a prototype method to supplant conventional methods for body fluid identification*. Forensic Science International, 2003. **135**: 85-96.

13. Nussbaumer, C., Gharehbaghi-Schnell, E., Korschineck, I., *Messenger RNA profiling: A novel method for body fluid identification by Real-Time PCR*. Forensic Science International, 2006. **157**: 181-186.

14. Zubakov, D., Hanekamp, E., Kokshoorn, M., van IJcken, W., Kayser, M., *Stable RNA markers for identification of blood and saliva stains revealed from whole genome expression analysis of time-wise degraded samples*. International Journal of Legal Medicine, 2008. **122**: 135-142.

15. Setzer, M., Juusola, J., Ballantyne, J., *Recovery and Stability of RNA in Vaginal Swabs and Blood, Semen, and Saliva Stains*. Journal of Forensic Science, 2008. **53**: 296-305.

16. Zubakov, D., Kokshoorn, M., Kloosterman, A., Kayser, M., *New markers for old stains: stable mRNA markers for blood and saliva identification from up to 16-year-old stains*. International Journal of Legal Medicine, 2009. **123**: 71-74.

17. Haas, C., Klesser, B., Maake, C., Baer, W., & Kratzer, A., *mRNA profiling for body fluid identification by reverse transcription endpoint PCR and realtime PCR*. Forensic Science International – Genetics, 2009. **3**: 80-88.

18. Hanson, E.K., Lubenow, H., & Ballantyne, J., *Identification of forensically relevant body fluids using a panel of differentially expressed microRNAs*. Analytical Biochemistry, 2009. **387**: 303-314.

19. Sakurada, K., Ikegaya, H., Fukushima, H. Akutsu, T., Watanabe, K., & Yoshino, M., *Evaluation of mRNA-based approach for identification of saliva and semen*. Legal Medicine, 2009. **11**: 125-128.

20. Bauer, M., Polzin, S., Patzelt, D., *Quantification of RNA degradation by semi-quantitative duplex RT-PCR: a possible indicator of the age of bloodstains?* Forensic Science International, 2003. **138**: 94-103.

21. Anderson, S., Howard, B., Hobbs, G., Bishop, C., *A method for determining the age of a bloodstain.* Forensic Science International, 2005. **148**: 191-198.

22. Anderson, S., Howard, B., Hobbs, G.R., Bishop, C.P., *Multivariate Analysis for Estimating the Age of a Bloodstain*. Journal of Forensic Science, 2011. **56**: 186-193.

23. Alvarez, M. & Ballantyne, J., *The identification of newborns using messenger RNA profiling analysis*. Analytical Biochemistry, 2006. **357**: 21-34.

24. Bauer, M. Polzen, S., Gramlich, I., Patzelt, D., *Quantification of mRNA degradation as possible indicator of postmortem interval – a pilot study.* Legal Medicine, 2003. **5**: 220-227.

25. Miller, C.L., Diglisic, S., Leister, F., Webster, M., Yolken, R.H., *Evaluating RNA status for RT-PCR in extracts of postmortem human brain tissue*. Biotechniques, 2004. **36**: 628-633.

26. Mann, R.W., Bass, W.M., and Meadows, L., *Time since death and decomposition of the human body: variables and observations in case and experimental field studies*. Journal of Forensic Science, 1990. **33**: 102-111.

27. Rodriguez, W.C., III & Bass, W.M., *Decomposition of buried bodies and methods that may aid in their location*. Journal of Forensic Science, 1985. **30**: 836-852.

28. Patten, T.D., *A percentage method for representing the fall in body temperature after death. Its use in estimating the time of death. With a statement of theoretical basis of the percentage model*. Journal of Forensic Medicine, 1958. **5**: 2-15.

29. Clark, M.A., Worrell, M.B., Pless J.E., *Postmortem changes in soft tissues*. In: *Forensic taphonomy: the postmortem fate of human remains*. Haglund, W.D., Sorg, M.H. Editors. 1997, CRC Press: Boca Raton, FL. p. 151-160.

30. Vass, A.A., Barshick, S.A., Sega G., Caton, J., Skeen, J.T., Love, J.C., Synstelien, J.A., *Decomposition chemistry of human remains: a new methodology for determining the postmorterm interval*. Journal of Forensic Science, 2002. **47**: 542–553.

31. Sturner, W.Q., *The vitreous humour: postmortem potassium changes*. The Lancet, 1963. **1**: 807-808.

32. Coe, J.I., *Postmortem chemistries on human vitreous humor*. American Journal of Clinical Pathology, 1969. **51**: 741-750.

33. Madea, B., Henssge, C., Honig, W., & Gerbracht, A., *References for determining the time of death by potassium in vitreous humor*. Forensic Science International, 1989. **40**: 231-243.

34. Muñoz, J.I., Suárez-Peñaranda, J.M., Otero, X.L., Rodríguez-Calvo, M.S., Costas, E., Miguéns, X., Concheiro, L., *A new perspective in the estimation of postmortem interval (PMI) based on vitreous [K^+]*. Journal of Forensic Science, 2001. **46**: 209-214.

35. Madea, B. & Rödig, A., *Time of death dependent criteria in vitreous humor – accuracy of estimating the time since death*. Forensic Science International, 2006. **164**: 87-92.

36. Jashnani, K.D., Kale, S.A., Rupani, A.B., *Vitreous Humor: Biochemical Constituents in Estimation of Postmortem Interval.* Journal of Forensic Science, 2010. **55**: 1523-1527.

37. Hall, R.D. & Haskell, N.H., *Forensic entomology – Applications in Medicolegal Investigations.* In: *Forensic Sciences*. Wecht C., Editor. 1995, Matthew Bender: New York, NY.

38. Rodriguez, W.C., III & Bass, W.M., *Insect activity and its relationship to decay rates of human cadavers in east Tennessee*. Journal of Forensic Science, 1983. **28**: 423-432.

39. Libby, W.F., Anderson, E.C., Arnold, J.R., *Age Determination by Radiocarbon Content: World-Wide Assay of Natural Radiocarbon*. Science, 1949. **109**: 227-228.

40. Livak K.J. & Schmittgen T.D., *Analysis of relative gene expression data using real-time quantitative PCR and the $2^{-\Delta\Delta CT}$ method*. Methods, 2001. **25**: 402-408.

41. Shaler, R.C., *Modern forensic biology*, in: *Forensic Science Handbook*. Saferstein, R. Editor. 2002, Prentice Hall: Upper Saddle River, NJ. p. 529-546.

42. Sensabaugh, G.F., *Isozymes in forensic science*, in: *Isozymes: Current Topics in Biological and Medical Research*. Rattazzi, M.C., Scandalios, J.G., Whitt, G.S. Editors. 1982, Alan R. Liss Inc.: New York, NY. p. 247-260.

43. Gaensslen, R.E., *Sourcebook in Forensic Serology, Immunology, and Biochemistry*, 1983. U.S. Department of Justice: Washington, D.C.

44. Spalding, R.P., *Identification and characterization of blood and bloodstains*, in: *Forensic Science: an Introduction to Scientific and Investigative Techniques*. James, S.H., Nordby, J.J. Editors. 2003, CRC Press: Boca Raton, FL. p. 181-201.

45. Watson, N., *The Analysis of Body Fluids, Crime Scene to Court; the Essentials of Forensic Science*. 2004. Royal Society of Chemist: Cambridge, UK. p. 377-413.

46. Greenfield, A. & Solan, M.A., *Identification of biological fluids and stains*, in: *Forensic Science: an Introduction to Scientific and Investigative Techniques*. James, S.H., Nordby, J.J. Editors. 2003, CRC Press: Boca Raton, FL. p. 181-201.

47. Venter *et al*., *The sequence of the human genome*. Science, 2001. **291**: 1304-1351.

48. Gilbert, W., *Why genes in pieces?* Nature, 1978. **271**: 501.

49. Johnson, J.M., Castle, J., Garrett-Engele, P., Kan, Z., Loerch, P.M., Armour, C.D., Santos, R., Schadt, E.E., Stoughton, R., Shoemaker, D.D., *Genome-Wide Survey of Human Alternative Pre-mRNA Splicing with Exon Junction Microarrays*. Nature, 2003. **302**: 2141-2144.

50. Xu, Q., Modrek, B., Lee, C., *Genome-Wide detection of tissue-specific alternative splicing in the human transcriptome.* Nucleic Acids Research, 2002. **30**: 3754-3766.

51. de la Grange, P., Dutertre, M., Martin, N, Auboeuf, D., *FAST DB: a website resource for the study of the expression regulation of human gene products*. Nucleic Acids Research, 2005. **33**: 4276-4284.

52. de la Grange, P., Dutertre, M., Correa, M., Auboeuf, D., *A new advance in alternative splicing databases: from catalogue to detailed analysis of regulation of expression and function of human alternative splicing variants*. BMC Bioinformatics, 2007. **8**: 180.

53. Leipzig J., Pevzner P., Heber S., *The Alternative Splicing Gallery (ASG): bridging the gap between genome and transcriptome*. Nucleic Acids Research, 2004. **32**: 3977-3983.

54. Tyagi, S. & Kramer, F.R., *Molecular Beacons: Probes that Fluoresce upon Hybridization.* Nature Biotechnology, 1996. **14**: 303-308.

55. Sokol, D.L., Zhang, X., Lu, P., Gewirtz, A.M., *Real time detection of DNA-RNA hybridization in living cells*. PNAS, 1998. **95**: 11538-11543.

56. Bratu, D.P., Cha, B., Mhlanga, M.M., Kramer, F.R., Tyagi, S., *Visualizing the distribution and transport of mRNAs in living cells*. PNAS, 2003. **100**: 13308-13313.

57. Santangelo, P.J., Nix, B., Tsourkas, A., Bao, G., *Dual FRET molecular beacon for mRNA detection in living cells*. Nucleic Acids Research, 2004. **32**: e57.

58. Nitin, N., Santangelo, P.J., Kim, G., Nie, S., Bao, G., *Peptide-linked molecular beacons for efficient delivery and rapid mRNA detection in living cells*. Nucleic Acids Research, 2004. **32**: e58.

59. Medley, C.D., Drake, T.J., Tomasini, J.M., Rogers, R.J., Tan, W., *Simultaneous Monitoring of the Expression of Genes Inside of Single Breast Carcinoma Cells*. Analytical Chemistry, 2005. **77**: 4713-4718.

60. Kim, J.H., Morikis, D., Ozkan, M., *Adaptation of inorganic quantum dots for stable molecular beacons*. Sensors and Actuators B, 2004. **102**: 315-319.

61. Yang, C.J., Medley, C.D., Tan, W., *Monitoring Nucleic Acids Using Molecular Beacons.* Current Pharmaceutical Biotechnology, 2005. **6**: 445-452.

62. Ekimov, A.I. & Onushchenko, A.A., *Size quantization of the electron energy spectrum in a microscopic semiconductor crystal*. Letters to Journal of Experimental and Theoretical Physics, 1984. **40**: 1136-1139.

63. Alivisatos, A.P., *Persepectives on the Physical Chemistry of Semiconductor Nanocrystals*. Journal of Physical Chemistry, 1996. **100**: 13226-13239.

64. Gene Link. *Fluorescent Molecular Probes Product Profile*. 2011.

65. Invitrogen. *The future of fluorescence: Qdot nanocrystal technology*. 2008.

66. Bruchez, M., Moronne, M., Gin, P., Weiss, S., Alivisatos, A.P., *Semiconductor Nanocrystals as Fluorescent Biological Labels*. Science, New Series, 1998. **281**: 2013-2016.

67. Li, Y., St. John, M.A.R., Zhou, X., Kim, Y., Sinha, U., Jordan, R.C.K., Eisele, D., Abemayor, E., Elashoff, D., Park, N., Wong, D., *Salivary transcriptome diagnostics for oral cancer detection*. Clinical Cancer Research, 2004. **10**: 8442-8450.

68. Quintela-Fandino, M., López, J.M., Hitt, R., Gamarra, S., Jimeno, A., Ayala, R., Hornedo, J., Guzman, C., Gilsanz, F., Cortés-Funes, H., *Breast Cancer-Specific mRNA Transcripts Presence in Peripheral Blood After Adjuvant Chemotherapy Predicts Poor Survival Among High-Risk Breast Cancer Patients Treated With High-Dose Chemotherapy With Peripheral Blood Stem Cell Support*. Journal of Clinical Oncology, 2006. **24**: 3611-3618.

69. Hershey, A.D., Tang, Y., Powers, S.W., Kabbouche, M.A., Gilbert, D.L., Glauser, T.A., Sharp, F.R., *Genomic Abnormalities in Patients with Migraine and Chronic Migraine: Preliminary Blood Gene Expression Suggests Platelet Abnormalities*. Headache, 2004. **44**: 994-1004.

70. Applied Biosystems. *Guide to Performing Relative Quantitation of Gene Expression Using Real-Time Quantitative PCR*. 2008.

71. Applied Biosystems. *Real-Time PCR: Understanding CT. Application Note*. 2008.

72. Gill-King, H., *Chemical and ultrastuctural aspects of decomposition*, In: *Forensic taphonomy: the postmortem fate of human remains*. Haglund, W.D., Sorg, M.H. Editors. 1997, CRC Press: Boca Raton, FL. p. 93-104.

73. Collins, N.C., *Developmental responses to food limitation as indicators of environmental conditions for* Ephydra cinerea *Jones (Diptera*). Ecology, 1980. **61**: 650-661.

74. Benninger, L.A., Carter, D.O., Forbes, S.L., *The biochemical alteration of soil beneath a decomposing carcass*. Forensic Science International, 2008. **180**: 70-75.

75. Van Belle, L.E., Carter, D.O., Forbes, S.L., *Measurement of ninhydrin reactive nitrogen influx into gravesoil during aboveground and belowground carcass (*Sus domesticus*) decomposition*. Forensic Science International, 2009. **193**: 37-41.

76. Liu, Q ., Sun, Q., Liu, Y., Zhou, L., Zheng, N., Liu, L., *Bioluminescent assay of microbial ATP in postmortem tissues for the estimation of postmortem interval*. Journal of Huazhong University of Science and Technology-Medical Sciences, 2009. **29**: 679-683.

77. Réaumur, R.A.F. de, *Observation du thérmomètre, faites à Paris pendant l'année 1735, comparées avec celles qui ont été faites sous la ligne, à l'Isle de France, à Alger et ae quelques-unes de nos isles de l'Amérique.* Mém Acad des *Sci Paris, France*. 1735.

78. Adobe Systems Incorporated, *RGB Mode: Specifying a color using numeric values*. Adobe Photoshop 7.0 Help Manual, 2002.

79. Polson, C.J., Gee, D.J., Knight, B., *The Essentials of Forensic Medicine, 4th edition.* 1985, Pergamon Press: Oxford, p. 20-39.

80. Micozzi, M., *Postmortem change in human and animal remains*. 1991, Charles C. Thomas: Springfield, IL.

81. Vass, A.A., Bass, W.M., Wolt, J., Foss, J., Ammons, J., *Time since death determinations of human cadavers using soil solution*. Journal of Forensic Science, 1992. **37**: 1236-1253.

82. Duffy, J.B., Skinner, M.F., Waterfield, J.D., *Rates of Putrefaction of Dental Pulp in the Northwest Coast Environment*. Journal of Forensic Science, 1991. **36**: 1492–1502.

83. Durnal, E.W., *Crime scene investigation (as seen on TV)*. Forensic Science International, 2010. **199**: 1-5.

84. Nelson, M., *Making Sense of DNA Backlogs, 2010 — Myths vs. Reality*. NIJ Special Report., 2011. 1-10.

85. Virkler, K. & Lednev, I.K., *Analysis of body fluids for forensic purposes: From laboratory testing to non-destructive rapid confirmatory identification at a crime scene*. Forensic Science International, 2009. **188**, 1-17.

86. Zrazhevskiy, P., Sena, M., Gao, X., *Designing multifunctional quantum dots for bioimaging, detection, and drug delivery*. Chemical Society Reviews, 2010. **39**: 4326-4354.

87. Yamamoto, M.L., Clark, T.A., Gee, S.L., Kang, J., Schweitzer, A.C., Wickrema, A., Conboy, J.G., *Alternative pre-mRNA splicing switches modulate gene expression in late erythropoiesis*. Blood, 2009. **113**, 3363-3370.

88. Hu, S., Li, Y., Wang, J., Xie, Y., Tjon, K., Wolinsky, L., Loo, R.R.O., Loo, J.A., Wong, D.T., *Human Saliva Proteome and Transcriptome*. Journal of Dental Research, 2006. **85**: 1129-1133.

89. Mori, C., Nakamura, N., Welch, J.E., Shiota, K., Eddy, E.M., *Testis-Specific Expression of mRNAs for a Unique Human Type 1 Hexokinase Lacking the Porin-Binding Domain.* Molecular Reproduction and Development, 1996. **44**: 14-22.

90. Cady, N.C., Strickland, A.D., Batt, C.A., *Optimized linkage strategies for quantum dot molecular beacons*. Molecular and Cellular Probes, 2007. **21**: 116-124.

91. Chenna, R., Sugawara, H., Koike,T., Lopez, R., Gibson, T.J., Higgins, D.G., Thompson, J.D., *Multiple sequence alignment with the Clustal series of programs*. Nucleic Acids Research, 2003. **31**: 3497-3500.

92. Markham, N. R. & Zuker, M., *DINAMelt web server for nucleic acid melting prediction*. Nucleic Acids Research, 2005. **33**: W577-W581.

93. Markham, N. R. & Zuker, M., *UNAFold: software for nucleic acid folding and hybriziation*. In: *Bioinformatics, Volume II. Structure, Function and Applications*. Keith, J.M., Editor. 2008, Humana Press: Totowa, NJ. p. 3–31.

94. Chakravorty, S., Aladegbami, B., Motiwala, A.S., Dai, Y., Safi, H., Brimacombe, M., Helb, D., Alland, D*., Rifampin Resistance, Beijing-W Clade-Single Nucleotide Polymorphism Cluster Group 2 Phylogeny, and the Rv2629 191-C Allele in* Mycobacterium tuberculosis *Strains*. Journal of Clinical Microbiology, 2008. **46**: 2555-2560.

95. He, Y., Zeng, K., Gurung, A.S., Baloda, M., Xu, H., Zhang, X., Lui, G., *Visual Detection of Single-Nucleotide Polymorphism with Hairpin Oligonucleotide-Functionalized Gold Nanoparticles*. Analytical Chemistry, 2010. **82**: 7169-7177.

96. Li, Y., Guan, L., Wang, J., Zhang, H., Chen, J., Lin, S., Chen, W., Zhao, Y., *Simultaneous detection of dual single-base mutations by capillary electrophoresis using quantum dot-molecular probe*. Biosensors and Bioelectronics, 2011. **26**: 2317-2322.

97. Farjami, E., Clima, L., Gothelf, K., Ferpapontova, E.E., *"Off-On" Electrochemical Hairpin-DNA-Based Genosenor for Cancer Diagnostics*. Anal Chem, 2011. **83**: 1594-1602. Nucleic Acids Research, 1995. **23**: 2019-2024.

98. Cummins, L.L., Owens, S.R., Risen, L.M., Lesnik, E.A., Freier, S.M., McGee, D., Guinosso, C.J., Cook, P.D., *Characterization of fully 2'-modified oligoribonucleotide hetero- and homoduplex hybridization and nuclease sensitivity*. Nucleic Acids Research, 1995. **23**: 2019-2024.

99. Tsourkas, A., Behlke, M.A., Bao, G., *Hybridization of 2'-O-methyl and 2'-deoxy molecular beacons to RNA and DNA targets*. Nucleic Acids Research, 2002. **30**: 5168-5174.

100. Scholes, G. & Weiss, J., *Chemical action of X-rays on nucleic acids and related substances in aqueous systems:1. Degradation of nucleic acids, purines, pyrimidines, nucleosides, and sucleotides by X-rays and by free radicals produced chemically*. Biochemical Journal, 1953. **53**: 567-578.